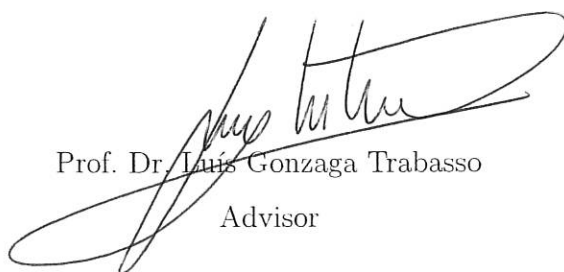


Thesis presented to the Instituto Tecnológico de Aeronáutica, in partial fulfillment of the requirements for the degree of Doctor of Science in the Program of Mechanical and Aeronautical Engineering, Field of Mechatronics and Aerospace Systems.

Douglas Coimbra de Andrade

**A METHODOLOGY FOR ROBUST OPTICAL
MARKER RECOGNITION IN OUTDOOR
ENVIRONMENTS**

Thesis approved in its final version by signatories below:



Prof. Dr. Luís Gonzaga Trabasso
Advisor

Prof. Dr. Luiz Carlos Sandoval Góes
Prorector of Graduate Studies and Research

Campo Montenegro
São José dos Campos, SP - Brazil
2017

**Cataloging-in Publication Data
Documentation and Information Division**

Andrade, Douglas Coimbra de
A Methodology for Robust Optical Marker Recognition in Outdoor Environments / Douglas
Coimbra de Andrade.
São José dos Campos, 2017.
122f.

Thesis of Doctor of Science – Course of Mechanical and Aeronautical Engineering. Area of
Mechatronics and Aerospace Systems – Instituto Tecnológico de Aeronáutica, 2017. Advisor:
Prof. Dr. Luís Gonzaga Trabasso.

1. Optical Marker Recognition. 2. Heterogeneous Computing. 3. Robotics. I. Instituto
Tecnológico de Aeronáutica.

BIBLIOGRAPHIC REFERENCE

ANDRADE, Douglas Coimbra de. **A Methodology for Robust Optical Marker
Recognition in Outdoor Environments**. 2017. 122f. Thesis of Doctor of Science –
Instituto Tecnológico de Aeronáutica, São José dos Campos.

CESSION OF RIGHTS

AUTHOR'S NAME: Douglas Coimbra de Andrade

PUBLICATION TITLE: A Methodology for Robust Optical Marker Recognition in
Outdoor Environments.

PUBLICATION KIND/YEAR: Thesis / 2017

It is granted to Instituto Tecnológico de Aeronáutica permission to reproduce copies of
this thesis and to only loan or to sell copies for academic and scientific purposes. The
author reserves other publication rights and no part of this thesis can be reproduced
without the authorization of the author.

Douglas Coimbra de Andrade
Rua Oscar Reinaldo, 661
36.400-000 – Conselheiro Lafaiete–MG

RESTRICTED ACCESS - The information contained in this document is confidential as
defined by law. Its contents may not be disclosed without approval by Petrobras.

A METHODOLOGY FOR ROBUST OPTICAL MARKER RECOGNITION IN OUTDOOR ENVIRONMENTS

Douglas Coimbra de Andrade

Thesis Committee Composition:

Profa. Dra.	Emília Villani	President	-	ITA
Prof. Dr.	Luís Gonzaga Trabasso	Advisor	-	ITA
Prof. Dr.	Carlos Henrique Quartucci Forster	Internal Member	-	ITA
Prof. Dr.	Mário Fernando Montenegro Campos	External Member	-	UFMG
Prof. Dr.	Walter Antonio Kapp	External Member	-	UFPR

ITA

This work is dedicated to my family and
all professors, teachers and friends.

Acknowledgments

I would like to thank every single person that helped me to become who I am.

To my parents and all professors, teachers and friends without whom this work would never exist.

Special thanks to Petróleo Brasileiro SA (Petrobras) and Agência Nacional do Petróleo (ANP) for making this development possible and funding this research.

*"Man surprised me most about humanity.
Because he sacrifices his health in order to make money.
Then he sacrifices money to recuperate his health.
And then he is so anxious about the future that he does not enjoy the present;
the result being that he does not live in the present or the future;
he lives as if he is never going to die, and then dies having never really lived."*

— DALAI LAMA

Resumo

Equipamentos industriais de grande porte, tais como tanques de armazenamento, dutos e vasos de pressão, são essenciais para a infraestrutura energética de qualquer país. No Brasil, em particular, tendo em vista a grande quantidade de óleo e gás esperados na camada pré-sal, será necessário construir novas embarcações e plataformas e, consequentemente, muitos desses equipamentos. Ao contrário de fábricas de veículos, nesses casos é a linha de montagem que se move, e não o produto final.

Os métodos atuais de construção e montagem (C&M) usam, em sua maior parte, trabalho manual para identificar, reconhecer e rastrear objetos, o que resulta em exposição de pessoal a situações de risco. O uso de robótica pode melhorar os métodos atuais de construção e montagem, que usam, em sua maior parte, procedimentos de posicionamento que dependem de operadores.

Este trabalho apresenta uma metodologia robusta para reconhecimento óptico de marcadores em ambiente externo com relação a iluminação, oclusão parcial, tipo de câmera e perspectiva. Marcadores óticos são uma ferramenta simples que, acoplada a sistemas de visão computacional, podem fornecer feedback para sistemas robóticos. Essa ferramenta pode ser usada para automatizar o rastreamento de posição e orientação de grandes componentes, tais como placas, vigas, válvulas e tubos usando marcadores óticos e sistemas de câmeras. Sua implementação tem potencial de reduzir custo, tempo e retrabalho pelo uso de melhor rastreamento e posicionamento desses componentes e menor exposição de pessoal a situações de risco.

Abstract

Large industrial equipments, such as storage tanks, pipelines, and pressure vessels, are essential for the energy infrastructure of any country. Particularly in Brazil, in view of the large amounts of oil and gas expected to be extracted from the pre-salt layer, it will be necessary to build new ships and platforms and, in turn, many of these equipments. Unlike vehicle production factories, the assembly line is the one that moves and not the final product.

Current construction and assembly (C&A) methods use mostly manual labor to identify, recognize and track objects, which results in exposure of personnel to risk. The use of robotics is expected to improve current construction processes which, for the most part, rely on positioning procedures that require operators.

This work presents a robust methodology for optical marker recognition (OMR) in outdoor environments with regards to lighting, partial occlusion, camera brand and perspective. Optical markers are a cheap technique which, coupled with computer vision systems, can provide position feedback for robotic systems. This tool can be used to automate tracking of position and orientation of large components, such as plates, beams, valves and tubes using optical markers and camera systems. Its implementation should result in cost, time and rework reduction through better tracking and positioning of these components, as well as reduced exposure of personnel to hazardous situations.

List of Figures

FIGURE 1.1 – Large equipments for product storage. Left: storage tanks. Middle: low pressure tanks. Right: pressure vessel (LPG sphere). Extracted from (BARROS, 2013)	23
FIGURE 1.2 – Usual product lifecycle for large equipments.	24
FIGURE 1.3 – Proposed product lifecycle for large equipments. The contribution of this work, a robust methodology for outdoor OMR, improves the C&A process.	25
FIGURE 2.1 – Typical planning and management chart.	31
FIGURE 2.2 – Detailed time location chart planning of a pipeline project (appropriate for reading in A0 paper size print). From (TILOS, 2016) . . .	32
FIGURE 2.3 – Rudimentary identification on top of concrete coating. The handwritten text is not well suited for automatic identification.	33
FIGURE 2.4 – Stored valves. No evident part identification.	34
FIGURE 2.5 – General overview of storage tank construction stages. From (PETROBRAS, 2016)	35
FIGURE 2.6 – Conventional positioning of plates. From (PETROBRAS, 2016) . . .	36
FIGURE 2.7 – Bent plates used to construct storage tanks. From (PETROBRAS, 2016)	36
FIGURE 2.8 – Auxiliary devices used to aid positioning. From (BARROS, 2013) . .	37
FIGURE 2.9 – Scaffoldings built during storage tank construction. From (PETROBRAS, 2016)	37
FIGURE 2.10 –Storage tank hydrostatic testing. From (PETROBRAS, 2016)	38
FIGURE 2.11 –Storage tank painting. From (PETROBRAS, 2016)	38
FIGURE 2.12 –LPG sphere supporting structure. From (PETROBRAS, 2016)	39

FIGURE 2.13 –LPG sphere scaffolding setup. From (PETROBRAS, 2016)	39
FIGURE 2.14 –Positioning LPG sphere plates. Accessories must be welded to the plate to allow crane grasp. From (PETROBRAS, 2016)	40
FIGURE 2.15 –Auxiliary devices used to aid positioning. From (PETROBRAS, 2016) .	40
FIGURE 2.16 –NDT testing in welded regions (penetrant liquid testing). From (PETROBRAS, 2016)	41
FIGURE 2.17 –LPG sphere after removal of auxiliary devices. Each region must be inspected using penetrant testing. From (PETROBRAS, 2016)	41
FIGURE 2.18 –Painting LPG spheres. From (PETROBRAS, 2016)	42
FIGURE 2.19 –Final painting for identification in LPG spheres. From (PETROBRAS, 2016)	42
FIGURE 2.20 –Pipeline time location chart for C&A management.	43
FIGURE 2.21 –Pipes laid on the right of way.	43
FIGURE 2.22 –Pipe being positioned prior to welding.	44
FIGURE 2.23 –Pipe welding in the field.	44
FIGURE 2.24 –Ultrasound inspection of welded joint.	45
FIGURE 2.25 –Welded pipeline column.	45
FIGURE 2.26 –Thermo contractile coating in welded region.	46
FIGURE 2.27 –Pipeline being positioned inside trench.	46
FIGURE 2.28 –Pipeline being buried after being positioned inside trench.	47
FIGURE 3.1 – NVidia’s Kepler architecture. From (NVIDIA, 2012b)	49
FIGURE 3.2 – CPU vs. GPU theoretical peak performance. From (BADGUJAR, 2013)	51
FIGURE 3.3 – Heterogeneous computing model.	51
FIGURE 3.4 – Robust calibration pattern proposed by (KANG; JEONG, 2008).	60
FIGURE 3.5 – Otsu binarization of source image, as obtained by (KANG; JEONG, 2008).	60
FIGURE 3.6 – Calibration pattern by (KANG; JEONG, 2008) processed using the proposed methodology.	61

FIGURE 3.7 – Comparison of proposed algorithm to OpenCV using the same input image from (RUFLI <i>et al.</i> , 2008). Red crosses: OpenCV output. Green circles: output of proposed algorithm.	62
FIGURE 4.1 – Robust Outdoor OMR Structure. Original contributions of this work are highlighted in orange.	64
FIGURE 4.2 – Performance comparison of Gaussian and median filters show very small difference in tested settings. Identified borders in yellow. Left: original image. Center: Gaussian filter result. Right: Median filter result.	65
FIGURE 4.3 – Example image in gray and unique color map initialization.	67
FIGURE 4.4 – Border map and first left-to-right sweep.	67
FIGURE 4.5 – First right-to-left and top-to-bottom sweeps.	68
FIGURE 4.6 – First bottom-to-top and second left-to-right sweep.	68
FIGURE 4.7 – Second right-to-left and top-to-bottom sweeps.	69
FIGURE 4.8 – Final configuration and visual identification of contiguous regions. .	69
FIGURE 4.9 – Contiguous color region in the shape of an annulus with mean distance to center r and width w	71
FIGURE 4.10 – Visualization of neighboring regions. Regularity analysis proposed in this work allows recognizing the bottom image as a checkerboard. .	72
FIGURE 4.11 – Checkerboard false positives.	74
FIGURE 4.12 – Checkerboard structure. Left: valid checkerboard. Right: invalid checkerboard.	74
FIGURE 4.13 – Assignment of checkerboard positions to each color region. Number of squares is identified automatically.	76
FIGURE 4.14 – Automatic identification of checkerboard sizes inside image. Number of squares: 15x7, 7x11, 7x7 and 7x5.	77
FIGURE 4.15 – Robust checkerboard identification under occlusion. Dimensions are identified automatically. Corner squares must be visible for proper identification.	78
FIGURE 4.16 – Identified targets with proper label. Left: cropped picture Right: identified contiguous color regions. GWBWP and RWPWG are target color label strings, denoting the sequence of colors from the inside out.	80

FIGURE 4.17 – Picture from (JIANG; QUAN, 2005) processed by our methodology. The middle circle was edited to remove its marks.	80
FIGURE 4.18 – Partially identified targets. Chromatic variations impair proper color classification. Left: cropped picture Right: identified contiguous color regions.	80
FIGURE 4.19 – Region filling image for runtime comparison purposes.	82
FIGURE 4.20 – Extracted images containing samples of the environment.	83
FIGURE 4.21 – Extracted images containing samples of optical markers (checkerboards) in the presence of non-uniform lighting and perspective.	84
FIGURE 4.22 – Left: Plates aligned using robotic systems, aided by optical markers. Right: visual identification feedback in the identification system. From CCM-LAM digital database.	85
FIGURE 4.23 – Automatic positioning of plates with robots using optical marker feedback. From CCM-LAM digital database.	85
FIGURE 4.24 – Combination of optical markers for recognition and QR codes for information retrieval. From CCM-LAM digital database.	86
FIGURE 5.1 – ARToolKit OMR. Left: identified optical marker (rectangle with text “Hiro”). Center: slight occlusion prevents marker identification. Right: slight variation in lighting prevents marker identification.	87
FIGURE 5.2 – Proposed robust OMR methodology. Left: identified optical markers (checkerboards). Center: robustness to occlusion. Right: robustness to variation in lighting.	88
FIGURE 5.3 – OMR in storage tank plates. Left: detail of simulated camera input. Right: desired recognition software output.	88
FIGURE 5.4 – Simultaneous multiple checkerboard identification under highly variable lighting and orientation settings.	89
FIGURE 5.5 – Checkerboard and target patterns used to test robustness of proposed methodology.	90
FIGURE 5.6 – Sample test image: Sony Cybershot DSC-WX7 camera, outdoor environment, frontal pose, uniform shadow.	92
FIGURE 5.7 – Sample test image: Fuji W1 camera, outdoor environment, skewed pose, hard shadow.	92

FIGURE 5.8 – Identification detail: Fuji W1 camera, outdoor environment, skewed perspective, hard shadow.	93
FIGURE 5.9 – Simulated hard shadow. Identification is impaired when shadow intensity exceeds threshold of 0.8.	96
FIGURE 5.10 –Simulated soft shadow - shadow beginning and end separated by 133 pixels . Identification is impaired when shadow intensity exceeds threshold of 0.8.	96
FIGURE 5.11 –Correct identification results in simulated perspective for $\phi = 70^\circ$	97
FIGURE 5.12 –Optical markers placed in simulated industrial environment at Petrobras' Research Center (CENPES). Left: Storage tank. Center: Pressure vessel. Right: Heat exchanger. Note that the identification is robust even when placed in a curved surface.	98
FIGURE 5.13 –Correct marker identification in a heat exchanger.	98
FIGURE 5.14 –Detail of identification of optical marker in the presence of shadow cast by the equipment.	99
FIGURE 5.15 –Top: marker not identified due to severe occlusion. Bottom: marker recognized in the presence of partial occlusion.	99
FIGURE 5.16 –Correct identification of optical markers in a curved surface, subject to shadow and exposed to light.	100
FIGURE 5.17 –Details of correct OMR when marker is exposed to light, soft shadow and object curvature.	100
FIGURE 5.18 –Algorithm limitations. Left: harsh light → shadow transitions impair checkerboard identification. Right: glare impairs target identification.	101
FIGURE 5.19 –False negatives color region analysis. Left: edges were not properly identified. Right: light reflex impairs edge detection.	101
FIGURE 6.1 – Possible location of cameras for part tracking in shipyards; pipes and spools that could be identified using optical markers.	105
FIGURE 6.2 – Possible location of cameras for part tracking in shipyards; boxes and their contents can carry optical markers.	106
FIGURE 6.3 – Identification of checkerboard inside checkerboard. The inner checkerboard may be exchanged for other markers.	107

FIGURE 6.4 – Optical marker composed of random shapes and positions. The proposed region grouping algorithm identifies that the contiguous regions of the marker are similar enough to belong to the same group.	107
FIGURE 6.5 – Robust OMR and tracking: the combination of a slow cycle, using the proposed OMR methodology, and a fast tracking cycle will improve system performance and allow for optical marker persistency when temporarily occluded by a moving object. Blue: slow cycle. Orange: fast cycle.	108
FIGURE A.1 – Test pictures thumbnails: Apple iPad 3 camera.	119
FIGURE A.2 – Test pictures thumbnails: Fuji W1 3D camera.	119
FIGURE A.3 – Test pictures thumbnails: Sony Cybershot DSC-WX7.	120
FIGURE A.4 – Detail of checkerboard true positive.	120
FIGURE A.5 – Detail of target true positive. Notice both target identification and color sequence labels are correct.	121
FIGURE A.6 – Detail of checkerboard and target false negative.	122
FIGURE A.7 – Detail of cluttered regions that may be identified as checkerboards. Limiting the methodology to only search for checkerboards with 5x7 number of squares solves this issue.	122

List of Tables

TABLE 1.1 – Desired characteristics of acquisition systems using the proposed OMR methodology compared to available technologies for site data acquisition (adapted from (OMAR; NEHDI, 2016))	26
TABLE 1.2 – Approaches for OMR in outdoor environments	27
TABLE 3.1 – Benefits of adopting the parallel paradigm	50
TABLE 3.2 – Typical modern GPU parameters relevant to heterogeneous computing	52
TABLE 3.3 – OpenCL memory types	52
TABLE 3.4 – CUDA vs. OpenCL comparison chart. Desired property in bold . .	54
TABLE 3.5 – Parallel programming best practices. Comments on NVidia’s recommendations	54
TABLE 4.1 – Region data properties computed in the proposed method	70
TABLE 4.2 – Approximation of annulus properties using computed region data . .	70
TABLE 4.3 – Criteria for robust identification of adjacent regions	72
TABLE 4.4 – Criteria for robust identification of targets	79
TABLE 4.5 – Algorithm runtime for processing full HD (1920x1080) images. Times in seconds. Average values - 10 runs.	81
TABLE 5.1 – Relevant parameters for outdoor optical mark recognition	90
TABLE 5.2 – Field lighting conditions	91
TABLE 5.3 – Performance criteria for the proposed identification algorithm	91
TABLE 5.4 – Summary of identification performance of proposed algorithm. Results were computed using 90 images and criteria shown in Table 5.3	93

List of Abbreviations and Acronyms

ANOVA	Analisis of Variance
API	American Petroleum Institute
AR	Augmented reality
ARToolKit	Augmented Reality Toolkit
ASME	American Society of Mechanical Engineers
BLAS	Basic linear algebra subprograms
C&A	Construction and assembly
CCD	Charged Coupled Device
CMOS	Complementary Metal Oxide Semiconductor
CPU	Central Processing Unit
CUDA	Compute unified device architecture (NVidia)
DDP&T	Petrobras' Development of Production and Technology Section
DSP	Digital Signal Processor
ELM	Extreme Learning Machine
FCAW	Flux cored arc welding
FHPP	Friction Hydro Pillar Processing
FPGA	Field-programmable gate array
FPSO	Floating production, storage and offload unit
FSW	Friction Stir Welding
GDDR5	Graphics DDR SDRAM 5
GMAW	Gas metal arc welding (also known as MIG/MAG welding)
GPGPU	General purpose computing on GPUs
GPS	Global positioning system
GPU	Graphics Processing Unit
GTAW	Gas tungsten arc welding (also known as TIG welding)
HLAW	Hybrid laser arc welding
iGPS	Indoor global positioning system
IT	Information Technology
LNG	Liquefied natural gas
LoG	Laplacian of Gaussian edge extractor

LPG	Liquefied petroleum gas
MIMD	Multiple Instruction Multiple Data
NDT	Non destructive testing
OCR	Optical character recognition
OMR	Optical mark recognition
OpenCL	Open computing language (Khronos Group)
PDCA	Plan do check act
QR Code	Quick Response code
RFID	Radio Frequency Identification
RGB	Red, green and blue
SDRAM	Synchronous dynamic random-access memory
SIMD	Single Instruction Multiple Data
SMAW	Shield metal arc welding

List of Symbols

G	Total estimated Sobel edge intensity
G_x	Gradient estimator in X direction
G_y	Gradient estimator in Y direction
\mathbf{T}	ELM training set
$\mathbf{W_0}$	ELM connection weights from input to hidden layer
$\mathbf{W_1}$	ELM connection weights from hidden layer to output

Contents

1	INTRODUCTION	22
1.1	Motivation	22
1.1.1	Large Equipments	22
1.2	Objectives	23
1.3	Contribution of this Work	27
1.4	Presentation Structure	28
2	CURRENT C&A METHODS	30
2.1	Design	30
2.2	Management	31
2.2.1	Planning	31
2.2.2	Part Identification	31
2.3	Construction	32
2.3.1	Example: Storage Tanks	32
2.3.2	Example: LPG Container Spheres	33
2.3.3	Example: Pipelines	34
3	THEORETICAL FOUNDATION	48
3.1	Heterogeneous Computing	48
3.1.1	Motivation	49
3.1.2	Platform Model	50
3.1.3	CUDA vs. OpenCL	53
3.1.4	Capabilities and Limitations	54
3.2	Computer Vision	55

3.2.1	Edge Detection	55
3.2.2	Optical Mark Recognition	56
3.3	Extreme Learning Machine	57
3.4	Related Work	58
4	METHODOLOGY FOR OMR IN OUTDOOR ENVIRONMENTS	63
4.1	Structure	63
4.2	Identification of Contiguous Color Regions	64
4.2.1	Image Filtering	64
4.2.2	Edge Detection	65
4.2.3	Region Filling	66
4.2.4	Region Identification	70
4.3	Extraction of High Level Region Information	70
4.3.1	Circular and Concentric Regions	70
4.3.2	Neighboring Regions	71
4.4	Recognition of Specific Optical Marks	73
4.4.1	Checkerboards	73
4.4.2	Targets	77
4.5	Considerations About Running Time	81
4.5.1	Preliminary Optical Marker Detection	82
4.6	Identification Layout for Parts and Equipments	83
5	RESULTS AND DISCUSSION	87
5.1	Indoor and Outdoor Optical Mark Recognition	89
5.2	Analysis of the Experiments	91
5.3	Sensitivity Analysis	95
5.3.1	Experiments in Relevant Environment	97
5.4	Limitations	98
6	CONCLUSION	102
6.1	Future Work Proposals	104

6.1.1	Large object identification in outdoor environments using multiple cameras	104
6.1.2	Development of new robust optical markers for outdoor applications .	105
6.1.3	Simultaneous optical marker detection and tracking	105
	REFERENCES	109
	APPENDIX A – IDENTIFICATION PICTURES AND RESULTS	118
A.1	Identification Pictures	118

1 Introduction

1.1 Motivation

Construction and assembly (C&A) of large equipments is a very important industrial challenge. Current methods entail human manipulation of extremely heavy parts suspended by cranes. Accessories are welded to these parts to allow ropes and structure locks to be attached during the construction process, which is a procedure that exposes employees to risky situations and which makes the entire assembly process slow and expensive. In addition, scaffoldings must be used to allow inspection and weld repair, if needed, further delaying their availability in refineries.

C&A processes require identification of components in outdoor environments and positioning according to tolerances defined in ASME and API standards in the case of the oil and gas industry. Optical markers are a suitable choice to enable automatic identification because they are simple, inexpensive and robust to harsh conditions, which is not the case, in general, for other methods, such as RFID tags and motion capture systems.

Use of visual identification has been applied in the construction industry for a long time due to its low cost, high capacity of data content and type, high reliability, ease of production and wide availability of image capture devices (OMAR; NEHDI, 2016).

1.1.1 Large Equipments

This work considers large equipments as those whose parts weigh more than 1000 kg, that require field operations such as welding and inspection and that cannot usually be transported to their final location by conventional means such as roads, railroads, regular aircrafts or ships. This definition excludes cars, trucks and equipments which can be entirely built in a factory and includes floating, production, storage and offload ships (FPSOs), heat exchangers, storage tanks, industrial towers and spheres.

In general, Each equipment type has a proper standard to be applied in its design, construction and inspection. Storage tanks, for example, should be built according to

American Petroleum Institute (API) standard 650 (AMERICAN PETROLEUM INSTITUTE, 2013b), and weld requirements follow American Society of Mechanical Engineers (ASME) standard Section IX (AMERICAN SOCIETY OF MECHANICAL ENGINEERS, 2010). Low pressure storage tanks follow API Standard 620 (AMERICAN PETROLEUM INSTITUTE, 2013a) and pressure vessels should be built according to ASME Section VIII (AMERICAN SOCIETY OF MECHANICAL ENGINEERS, 2011). Figure 1.1 provides sample images of such equipments. Oil and gas companies usually have additional internal guidelines on how to design and build pressure vessels (e.g. (BARROS, 2013)).



FIGURE 1.1 – Large equipments for product storage. Left: storage tanks. Middle: low pressure tanks. Right: pressure vessel (LPG sphere). Extracted from (BARROS, 2013)

While ASME and API standards provide best engineering practices for designing large industrial equipments, there are fewer procedure requirements with respect to construction and assembly techniques. It is up to the contractor to provide his own approach to build tanks and vessels from a preliminary project, which usually does not take construction issues into consideration from the beginning. Moreover, current advanced robotic techniques are neither applied during C&A nor considered during preliminary design.

Extraction of oil below the salt layer is one of the most important challenges faced by the Brazilian energy industry. Large volumes of oil are intended to be extracted: Tupi oil reservoirs alone contains 5 to 8 billions of barrels of oil equivalent (combined oil and gas reserves). Located in Santos, the Guará reservoir has 1.1 to 2 billions of barrels of oil equivalent of low density, high quality petroleum associated with gas (PETRÓLEO BRASILEIRO SA, 2013), (PETRÓLEO BRASILEIRO SA, 2016).

This increase in production needs to be accompanied by appropriate capability in terms of transportation and refining which, in turn, requires construction of large industrial equipments such as FPSOs, pipelines, distillation towers, storage tanks and storage spheres.

1.2 Objectives

The industrial challenge of oil and gas companies to maintain competitiveness is how to build large equipments more efficiently, at lower costs and with higher quality. In addition, C&A of large equipments should not expose personnel to hazardous situations

and minimize fieldwork using automation as much as possible in every step that has to be performed in the field. Current large equipment product lifecycle (detailed in Figure 1.2) fails to take into consideration important issues of the C&A process, such as detailed assembly planning, part identification in outdoor environments and the need for systematic monitoring of activities during design stages, ultimately leading to rework and waste.

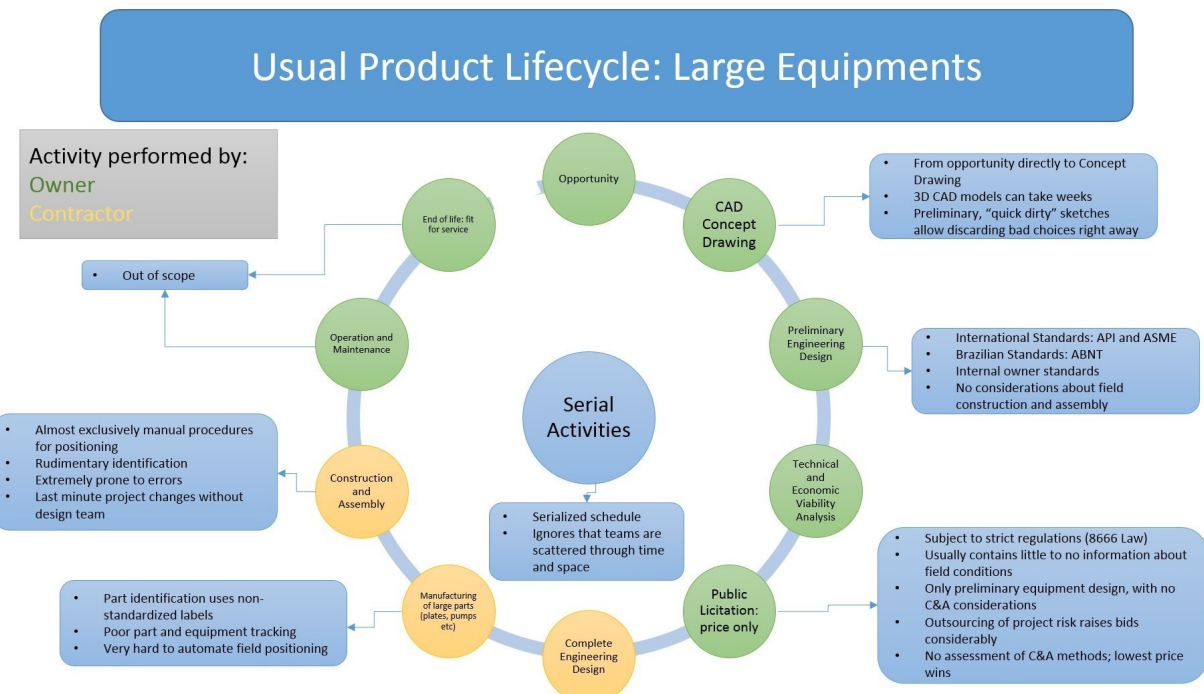


FIGURE 1.2 – Usual product lifecycle for large equipments.

The objective of this work is to address the challenge highlighted in Figure 1.3, related to large volume metrology and automation of the C&A process: recognition and tracking of large objects in outdoor environments. In view of the harsh field conditions, as presented in Chapter 2, the system needs to meet the following requirements:

- Inexpensive and easily replaceable;
- Robust to mechanical impact;
- Easy to implement with currently available hardware;
- Robust with respect to lighting conditions;
- Appropriate algorithm run time - fast enough for field use.

The most used data acquisition solutions for tracking and positioning in construction are (OMAR; NEHDI, 2016):

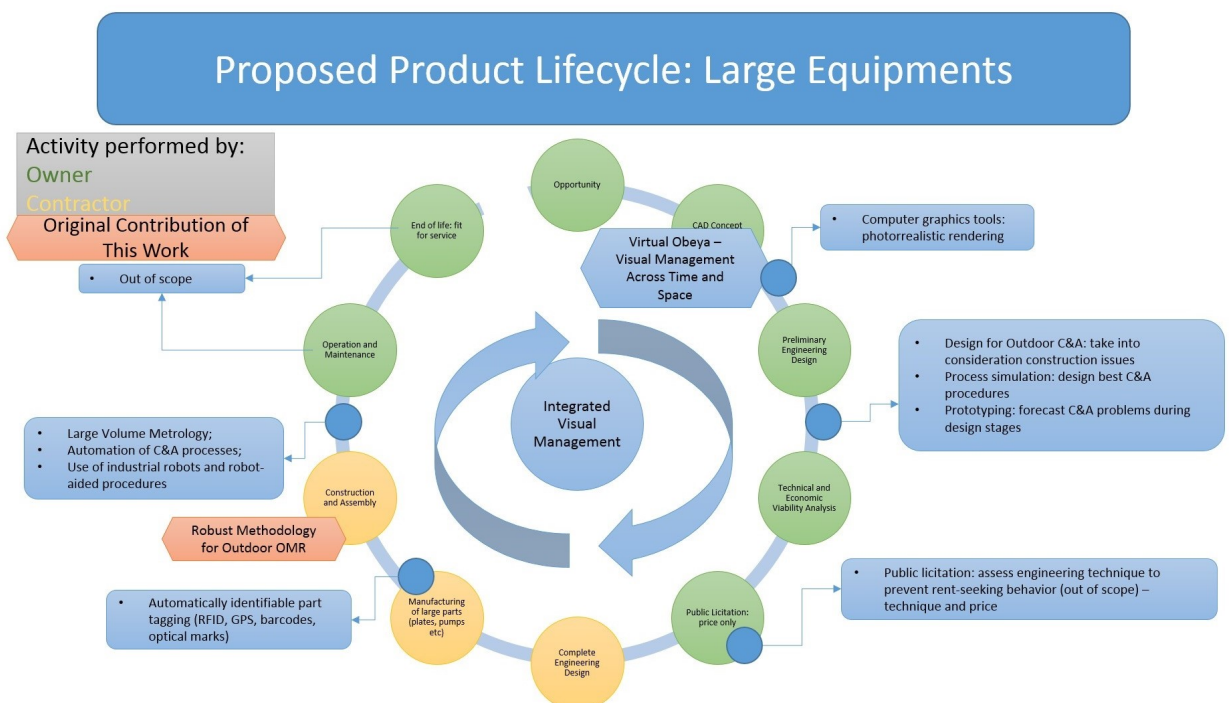


FIGURE 1.3 – Proposed product lifecycle for large equipments. The contribution of this work, a robust methodology for outdoor OMR, improves the C&A process.

- Enhanced IT technologies: multimedia tools (pictures, videos), e-mail services, handheld computing voice-based tools;
- Geospatial technologies: barcoding, ultra-wide band, Indoor global positioning system (iGPS), radio frequency identification (RFID);
- Imaging technologies: 3D laser scanning, motion capture systems, photogrammetry, videogrammetry, and computer vision methods.

At present, laser and photogrammetry constitute the most important tools to perform non-contact metrology of large parts ((MOSQUEIRA *et al.*, 2012), (MURALIKRISHNAN *et al.*, 2016), (SUDATHAM *et al.*, 2016)). Laser radar systems use light time of flight and, due to the limitations of its clock, the uncertainty is around 1 mm. Moreover, it offers no tracking capabilities while iGPS allows tracking but its uncertainty is 1 mm (MUELNER *et al.*, 2012), which is not sufficient for aerospace applications but may be acceptable for thick plate positioning considering that allowable misalignments are 3 mm (BARROS, 2013). Both approaches, however, require expensive equipment and are not designed for outdoor use under harsh conditions.

The iGPS comprises sensors and a transmitter network. Elevation, azimuth and range of each sensing element can be computed from the difference in the rate that sensing elements receive the broadcast signal. However, as the name indicates, iGPS systems are

designed for indoor use. The interference of direct sunlight severely impairs the iGPS identification capabilities in outdoor environments.

Laser tracker systems, based on interferometry, are able to make static range readings by emitting frequency-modulated sawtooth signals whose reflection's frequency shift is compared to that of a control wave. A set of calibrated loop of optical fibers known as Local Oscillators is then adjusted to provide a zero frequency shift and the combination of this information is used to compute the distance to the target. More in-depth description of these systems can be found in (MOSQUEIRA *et al.*, 2012), (MURALIKRISHNAN *et al.*, 2016) and (SUDATHAM *et al.*, 2016). As well as the previous systems, laser ones are not robust for harsh environments and require expensive equipment.

This work aims to provide an inexpensive alternative to large volume identification and tracking via OMR, which will enable the development of site data acquisition tools that compare to the ones currently available according to Table 1.1. The table presents analysis for obtaining dense 3D point clouds, whose setup and cost are high. 3D imaging using stereo cameras has low cost but also lower tracking capabilities. More details about the comparison of technologies for site data acquisition can be found in (OMAR; NEHDI, 2016). In particular, semi-manual processes refer to ones which are mostly manual but have some degree of automation whereas semi-automatic processes are those which are mostly automated but still require some degree of human intervention during processing stages.

Specific objectives of this work to fulfill each requirement are presented in Table 1.2, and achievable with computer vision techniques in combination with heterogeneous computing to speed up computation. It is important to note at this point that the full integration of the developed methodology in a full site data acquisition system is beyond the scope of this work. The information that would be made available is akin to Geospatial technologies, though much more affordable and scalable, hence the improvement in setup/cost, possible automation level, project size and decision support (since many more markers will be available).

TABLE 1.1 – Desired characteristics of acquisition systems using the proposed OMR methodology compared to available technologies for site data acquisition (adapted from (OMAR; NEHDI, 2016))

Criteria	Enhanced IT	Geospatial	3D Imaging	AR	Robust OMR
Setup / cost	Moderate	Moderate	Very high	High	Low
Automation	Semi-manual	Semi-auto	Automated	Automated	Automated
Analysis	Semi-auto	Automated	Automated	Automated	Automated
Applicability	All projects				

Continuation of Table 1.1					
Criteria	Enhanced IT	Geospatial	3D Imaging	AR	Robust OMR
Training	Low	Low	High	Moderate	Low
Pre-processing	Low	Low	Moderate	Low	Low
Readiness	Moderate	Moderate	High	High	Low
Project size	Small/ moderate	Small/ moderate	Moderate/ large	Moderate/ large	Moderate/ large
Computational cost ¹	Low	Low	High	Low	High
Decision support	Moderate	Low	High	High	Moderate

TABLE 1.2 – Approaches for OMR in outdoor environments

Requirement	Specific objectives
Inexpensive and easily replaceable low setup / cost	Markers printed in paper monitored by camera systems which are widely available
Robust to mechanical impact Easy to implement with currently available hardware	Markers printed on paper or directly on equipments Development of computer vision algorithms
Robust with respect to lighting, perspective and occlusion Adequate run time	Development of robust algorithms (requires heavy processing load) Use of heterogeneous computing

1.3 Contribution of this Work

A new optical marker recognition methodology has been developed to address this issue. The proposed methodology identifies contiguous color regions as well as their neighborhood and is able to detect checkerboard and target markers in various outdoor settings. A new parallel flood-filling algorithm has been developed and robust criteria for region grouping and detection of targets and checkerboards are proposed. The regularity analysis task implements a novel square center prediction-match algorithm that

¹Computational cost is understood here as time required to run the entire processing step. The proposed OMR methodology requires heavy computational cost, but since this cost is offloaded to the GPU and runtimes are just a few seconds, its category in this criterion is Low

enables the proposed methodology to automatically identify optical marker features, such as checkerboard sizes.

The flood-filling algorithm requires sampling image pixels multiple times and has been implemented in OpenCL to harness GPU processing power to speed up calculations. Its use can be integrated into a computer vision feedback system using currently available camera systems to provide cheap detection, recognition and positioning systems that can be used in outdoor environments.

Due to the very large physical dimensions and weight of storage tanks, distillation towers and other large equipments it is not feasible to transport them and thus they need to be assembled in place. Large volume metrology, however, is often designed for indoor environments, and indoor GPS systems are designed for this specific purpose, although other applications have been suggested (SCHMITT *et al.*, 2010), (SCHWENDEMANN *et al.*, 2010).

Typical optical marker recognition methods often rely on converting images to grayscale, performing binarization, morphologic operations and blob recognition (RUFLI *et al.*, 2008). Outdoor applications, however, require additional robustness due to numerous environmental issues such as the extremely wide range in lighting conditions.

1.4 Presentation Structure

This work is structured as follows:

- Chapter 2 - Current C&A Methods describes usual design and management methods currently applied in the C&A process for the oil and gas industry;
- Chapter 3 - Theoretical Foundation describes the fundamentals of computer vision applied to optical mark recognition, OpenCL, the heterogeneous computing framework used to accelerate processing of the proposed methodology, and the concept of Extreme Learning Machine (ELM), which can be used to provide initial estimates of optical marker location;
- Chapter 4 - Robust OMR Methodology describes the details of the methodology developed for robust OMR in outdoor environments. The preprocessing steps, parallel flood-filling, region grouping and high-level information algorithms are discussed in depth, as well as preliminary optical marker detection procedure using ELM and suggested optical marker layout in parts and equipments;
- Chapter 5 - Results and Discussion presents the results obtained in tests of the proposed methodology and compares them with existing optical marker detection

systems. The results of indoor and outdoor optical marker recognition experiments are analyzed using ANOVA and experiments in relevant environment are presented;

- Chapter 6 - Conclusion provides an overview of the methodology implementation and results and proposes future work: outdoor OMR with multiple cameras, optical marker design and simultaneous optical marker detection and tracking.

2 Current C&A Methods

This chapter presents tools and methods currently used for C&A of large industrial equipments. Multiple situations found during C&A in outdoor environments, presented in this Chapter, demonstrate that part identification is rudimentary and not suited for automated identification using computers or object manipulation using robots. OMR in outdoor environments is able to provide reference for these tasks.

Research has improved factory stages, such as steel manufacturing. For example, the introduction of high strength steels, the predominant material, allows increased reliability of C&A processes using these materials (POGOZHEV *et al.*, 2013), (GUOHUI *et al.*, 2012), (ZHOU *et al.*, 2001), (BHADESHIA; HONEYCOMBE, 2006).

Field construction, however, still struggles to maintain schedule and deliver C&A according to the project.¹

2.1 Design

Current design standards, such as ASME VIII for pressure vessels (AMERICAN SOCIETY OF MECHANICAL ENGINEERS, 2011) and API 650 for storage tanks (AMERICAN PETROLEUM INSTITUTE, 2013b) contain multiple guidelines for important aspects of the project, such as materials, methods of fabrication, plate thicknesses, tolerances and hydrostatic testing. Since they are general guidelines, these standards neither enforce automation during C&A stages nor provide guidelines for automated outdoor construction. As a result, contracting companies leave all issues concerning the C&A for contractors to solve during execution, effectively postponing important design decisions to later stages of the project.

Conventional feed-forward process uses decision gates, which do not allow projects to go back to an earlier stage if this need is identified. Roadmapping technology and quality

¹It is remarkable that senior consultants from Petrobras whose opinion was sought during the development of this work were unanimous to declare that, aside from stricter health and safety requirements, today's field procedures differ very little if at all from the ones used 30 years ago and improvements have been incremental at best.

gates should be preferred as they allow the project to return to earlier stages if needed and improves competitiveness by allowing organizations to deliver consistent innovative output when required (GIEBEL *et al.*, 2009). Currently, important stakeholders, such as the maintenance team, are involved late in the process.

2.2 Management

2.2.1 Planning

Currently, project planning uses task chain softwares such as Primavera, Tilos and Microsoft Project. These methods are based on text, provide little to no meaningful visual information and do not implement automatic tools to analyze and improve the process. Figure 2.1 presents a chart used for research projects as well as all construction and assembly jobs. Expanding collapsed activities would yield dozens of activities rendering the chart even less comprehensible for professionals unfamiliar to the project.

	B	C	D	E	G	H	I	J	K	L	M
	Identificação	Status IP	Tarefa	Ind. P/ Nome da Tarefa	% Concluído	Inicio	Término	Inicio Real	Término Real	Inicio da Linha	Término da Linha de Base
1	PT-111.01.11967_Robótica e Mecanização de Processos				35%	2/1/2012	30/11/2018	2/1/2012	ND	2/1/2012	30/11/2018
2	1- 4600394630-ITA - Automação de Construção e Montagem Industrial de Grande Porte				27%	26/12/2012	30/11/2018	26/12/2012	ND	26/12/2012	30/11/2018
3	FASE 1 - ESTUDOS				34%	26/12/2012	23/3/2016	26/12/2012	ND	26/12/2012	23/3/2016
4	1.1-Especificação do ambiente laboratorial				44%	7/2/2013	30/4/2014	7/2/2013	ND	7/2/2013	30/4/2014
8	1.2-Simulador 3D de C&M				50%	7/2/2013	12/8/2014	7/2/2013	ND	7/2/2013	12/8/2014
12	1.3-Desenvolvimento de Sistema de Posicionamento				32%	26/12/2012	18/11/2015	26/12/2012	ND	26/12/2012	18/11/2015
17	1.4 -Testes preliminares de soldagem				24%	1/4/2013	27/2/2015	1/4/2013	ND	1/4/2013	27/2/2015
22	23 A Executar NA			1.5-Relatórios Técnicos por Etapa	0%	21/3/2014	27/1/2016	ND	ND	21/3/2014	27/1/2016
27	29 A Executar NA			1.6 - Encerramento	0%	28/1/2016	23/3/2016	ND	ND	28/1/2016	23/3/2016
33	30 A Executar NA			Elaboração Relatório Final Petrobras	0%	28/1/2016	23/3/2016	ND	ND	28/1/2016	23/3/2016
34	31 A Executar NA			Divulgação do Relatório Final através de DIP	0%	23/3/2016	23/3/2016	ND	ND	23/3/2016	23/3/2016
35	32 A Executar NA			FASE 2 - IMPLEMENTAÇÃO	0%	20/3/2014	30/1/2016	ND	ND	20/3/2014	30/1/2016
36	33 A Executar NA			2.1 - Planejamento	0%	20/3/2014	30/4/2014	ND	ND	20/3/2014	30/4/2014
37	35 A Executar NA			2.2 - Contratação	0%	1/5/2014	31/1/2014	ND	ND	1/5/2014	31/1/2014
39	39 A Executar NA			2.3 - Execução	0%	1/1/2015	3/1/2018	ND	ND	1/1/2015	3/1/2018
43	56 A Executar NA			2.4 - Encerramento	0%	4/1/2018	30/11/2018	ND	ND	4/1/2018	30/11/2018
56	53 A Executar NA			2.4.1 - Elaboração Relatório Final Petrobras	0%	4/1/2018	28/2/2018	ND	ND	4/1/2018	28/2/2018
57	54 A Executar NA			2.4.2 - Divulgação do Relatório Final através de DIP	0%	28/2/2018	28/2/2018	ND	ND	28/2/2018	28/2/2018
58	55 A Executar NA			2.4.3 - Visita no ITA e apresentação aos clientes	0%	28/2/2018	30/4/2018	ND	ND	28/2/2018	30/4/2018
59	56 A Executar NA			2.4.4 - Reuniões com os clientes para avaliar os benefícios e próximos passos	0%	2/5/2018	30/8/2018	ND	ND	2/5/2018	30/8/2018
60	57 A Executar NA			2.4.5 - Marco PNG 2018 aprovado com cliente	0%	3/9/2018	30/11/2018	ND	ND	3/9/2018	30/11/2018

FIGURE 2.1 – Typical planning and management chart.

Time location charts are widely used during pipeline project, as shown in Figure 2.2 which is an example of Tilos software (TILOS, 2016).

2.2.2 Part Identification

Currently, part identification during construction of large equipments is extremely poor. In many situations part ID is concealed or written by hand on top of the coating, as shown in Figure 2.3 and 2.4. This procedure is misleading and is the cause of many errors during C&A.

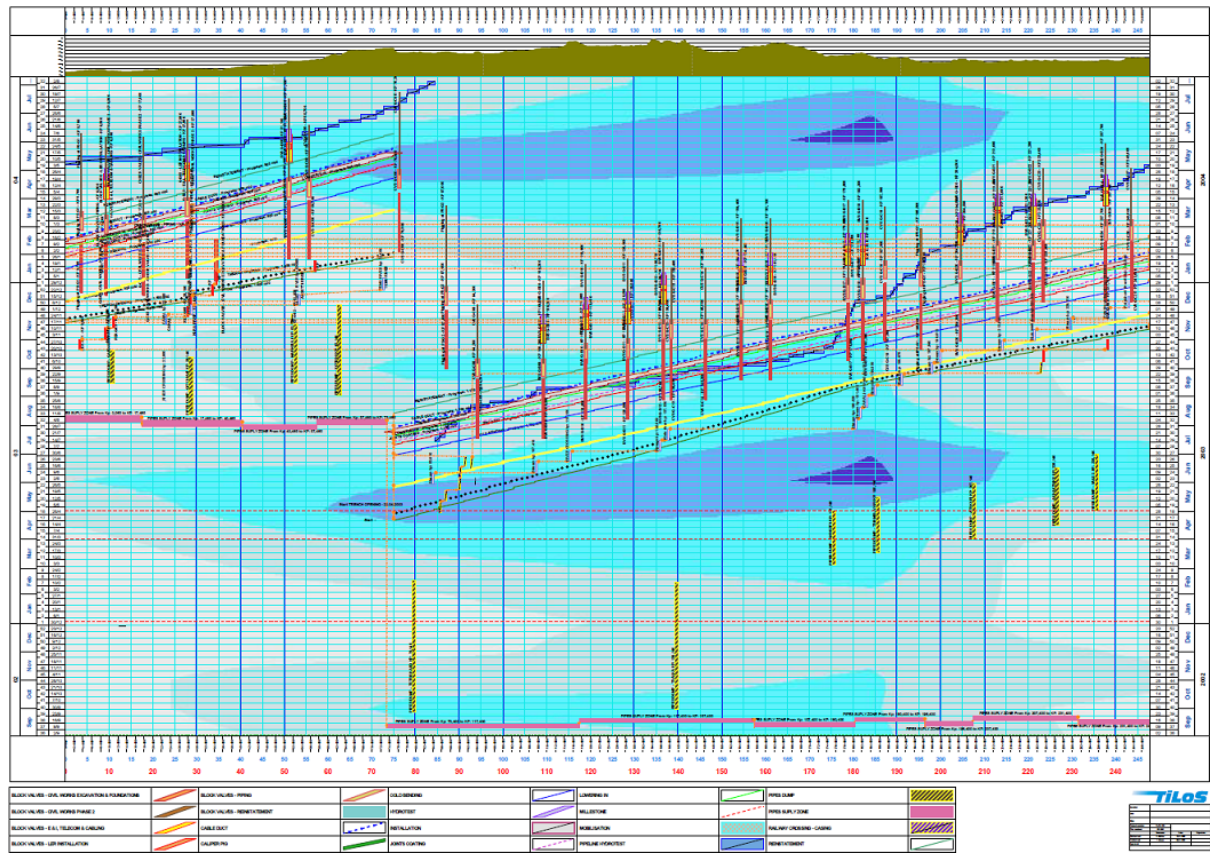


FIGURE 2.2 – Detailed time location chart planning of a pipeline project (appropriate for reading in A0 paper size print). From (TILOS, 2016)

2.3 Construction

All C&A processes require management of inventory and part positioning for joining (mainly welding in the oil and gas industry). Optical markers that can be identified in outdoor environments provide an option for identification and, when coupled with a calibrated camera system, can be used to locate and provide position feedback for robotic manipulation.

2.3.1 Example: Storage Tanks

Storage tanks are ubiquitous in the oil and gas industry. Large tanks, used to store crude oil, may have diameters up to 90 m and heights up to 12 m. Figures 2.5 to 2.11, obtained from Petrobras' Illustrated Technical Guide (PETROBRAS, 2016) and Petrobras' storage tanks manual (BARROS, 2013), illustrate key aspects of the construction process.

It is worth noting that the conventional process for positioning plates involves human labor and the proximity of the workforce to very heavy components. In addition, auxiliary devices must be welded with the sole purpose of aiding plate positioning, further increasing



FIGURE 2.3 – Rudimentary identification on top of concrete coating. The handwritten text is not well suited for automatic identification.

rework which is required to remove them and further inspection of the regions to ensure no crack was induced in the weld region (BARROS, 2013). Large volume metrology and robotic systems have the potential to dramatically improve quality and reduce time and cost of storage tank C&A by reducing this type of rework if the need for auxiliary positioning devices is eliminated.

Figures 2.10 and 2.11 illustrate the final steps during storage tank construction as required by API Standard 650 (AMERICAN PETROLEUM INSTITUTE, 2013b).

2.3.2 Example: LPG Container Spheres

Liquefied petroleum gas (LPG) container spheres are another type of static equipment present in refineries and distribution stations. Their construction must also follow ASME standards (AMERICAN SOCIETY OF MECHANICAL ENGINEERS, 2011) (AMERICAN SOCIETY OF MECHANICAL ENGINEERS, 2010). Figures 2.12 to 2.19 (extracted from (PETRO-BRAS, 2016)) illustrate conventional construction process for this type of equipment. Note that, since spheres are more complex than storage tanks, more auxiliary devices are used



FIGURE 2.4 – Stored valves. No evident part identification.

during C&A process.

Large equipments that have more complicated C&A processes, such as spheres, LNG ships and FPSO units, benefit even more from precise large volume metrology and robotic actuation. Human manipulation of more complex part geometries may lead to positioning errors, especially when matching surface normal vectors of adjacent parts.

2.3.3 Example: Pipelines

Pipelines are large industrial equipments used for hydrocarbon transportation in the energy industry. They are the preferred way to supply hydrocarbons over land, in Brazil, according to Transpetro corporate information (TRANSPETRO, 2016).

Pipelines traverse large distances across countries and their construction involves many administrative, legal and engineering aspects. Construction of this type of equipment is peculiar because of typical long lengths (above 50 km) and that all work must be performed within a narrow Right of Way (RoW - typically 20 m wide). Figures 2.20 to 2.28, taken in a field visit to Petrobras' Gasoduto Cacimbas Catu pipeline job, summarize C&A steps of pipeline construction. These pictures provide an overview of pipeline C&A steps.



FIGURE 2.5 – General overview of storage tank construction stages. From (PETROBRAS, 2016)

It is important to notice throughout the pictures the absence of intelligent systems or robotic equipments in the field. A more comprehensive description of pipeline C&A phases is available in (MCALLISTER, 2014). Pipes for pipelines are designed according to API Spec 5L standard (AMERICAN PETROLEUM INSTITUTE, 2012), while design and construction follow ASME B31.4 and B31.8 (AMERICAN SOCIETY OF MECHANICAL ENGINEERS, 2006) (AMERICAN SOCIETY OF MECHANICAL ENGINEERS, 2012) and, specifically in Brazil, ABNT standards (ASSOCIAÇÃO BRASILEIRA DE NORMAS TÉCNICAS, 2009), (ASSOCIAÇÃO BRASILEIRA DE NORMAS TÉCNICAS, 2011).



FIGURE 2.6 – Conventional positioning of plates. From (PETROBRAS, 2016)

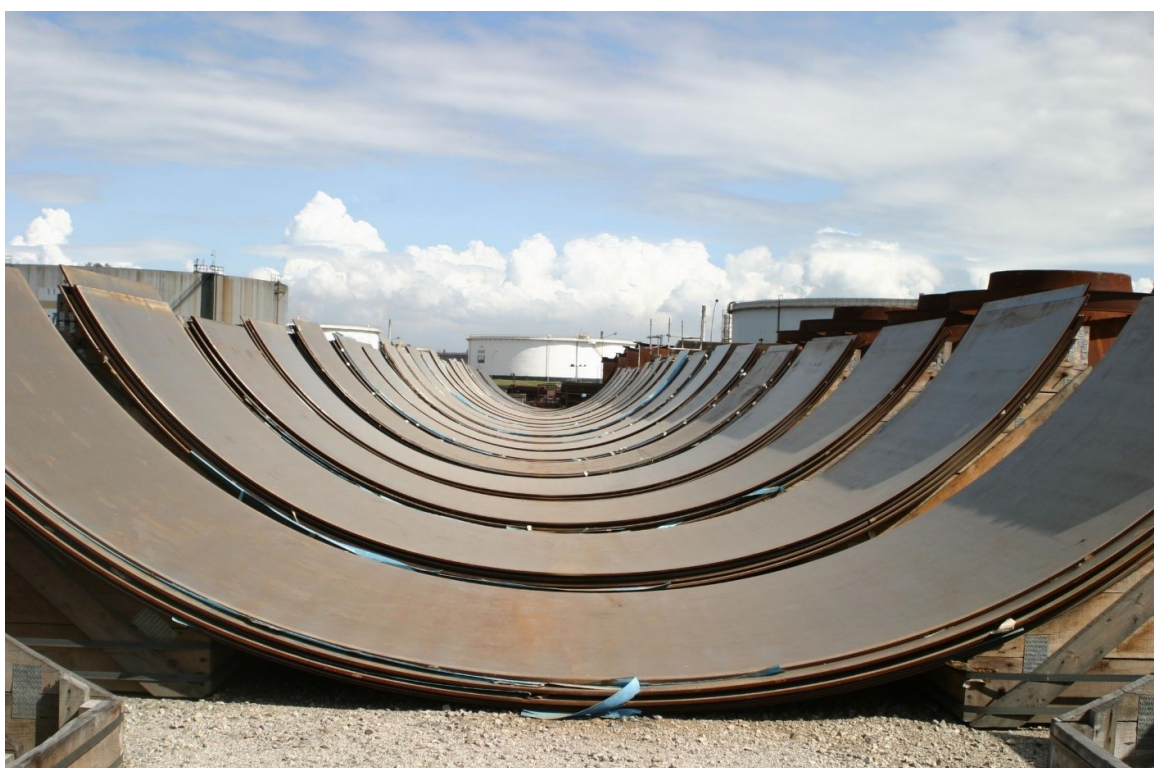


FIGURE 2.7 – Bent plates used to construct storage tanks. From (PETROBRAS, 2016)



FIGURE 2.8 – Auxiliary devices used to aid positioning. From (BARROS, 2013)



FIGURE 2.9 – Scaffoldings built during storage tank construction. From (PETROBRAS, 2016)



FIGURE 2.10 – Storage tank hydrostatic testing. From (PETROBRAS, 2016)



FIGURE 2.11 – Storage tank painting. From (PETROBRAS, 2016)



FIGURE 2.12 – LPG sphere supporting structure. From (PETROBRAS, 2016)



FIGURE 2.13 – LPG sphere scaffolding setup. From (PETROBRAS, 2016)



FIGURE 2.14 – Positioning LPG sphere plates. Accessories must be welded to the plate to allow crane grasp. From (PETROBRAS, 2016)



FIGURE 2.15 – Auxiliary devices used to aid positioning. From (PETROBRAS, 2016)



FIGURE 2.16 – NDT testing in welded regions (penetrant liquid testing). From (PETROBRAS, 2016)



FIGURE 2.17 – LPG sphere after removal of auxiliary devices. Each region must be inspected using penetrant testing. From (PETROBRAS, 2016)



FIGURE 2.18 – Painting LPG spheres. From (PETROBRAS, 2016)

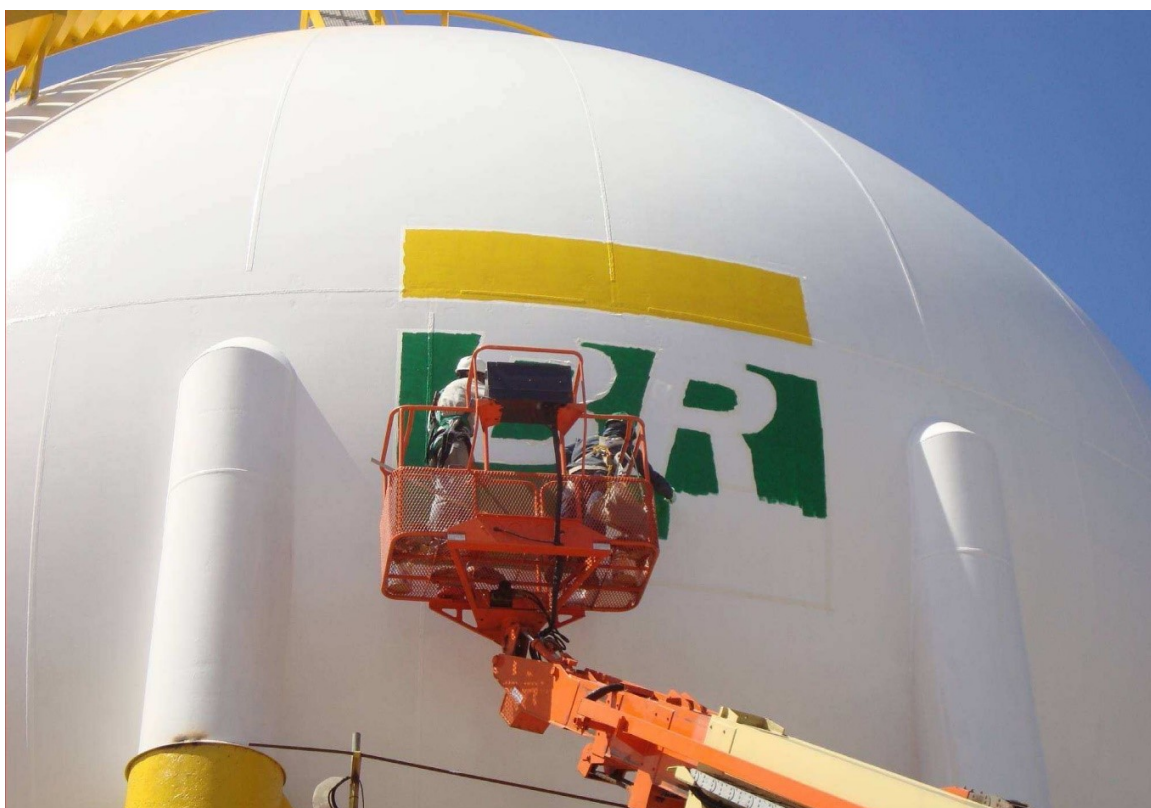


FIGURE 2.19 – Final painting for identification in LPG spheres. From (PETROBRAS, 2016)

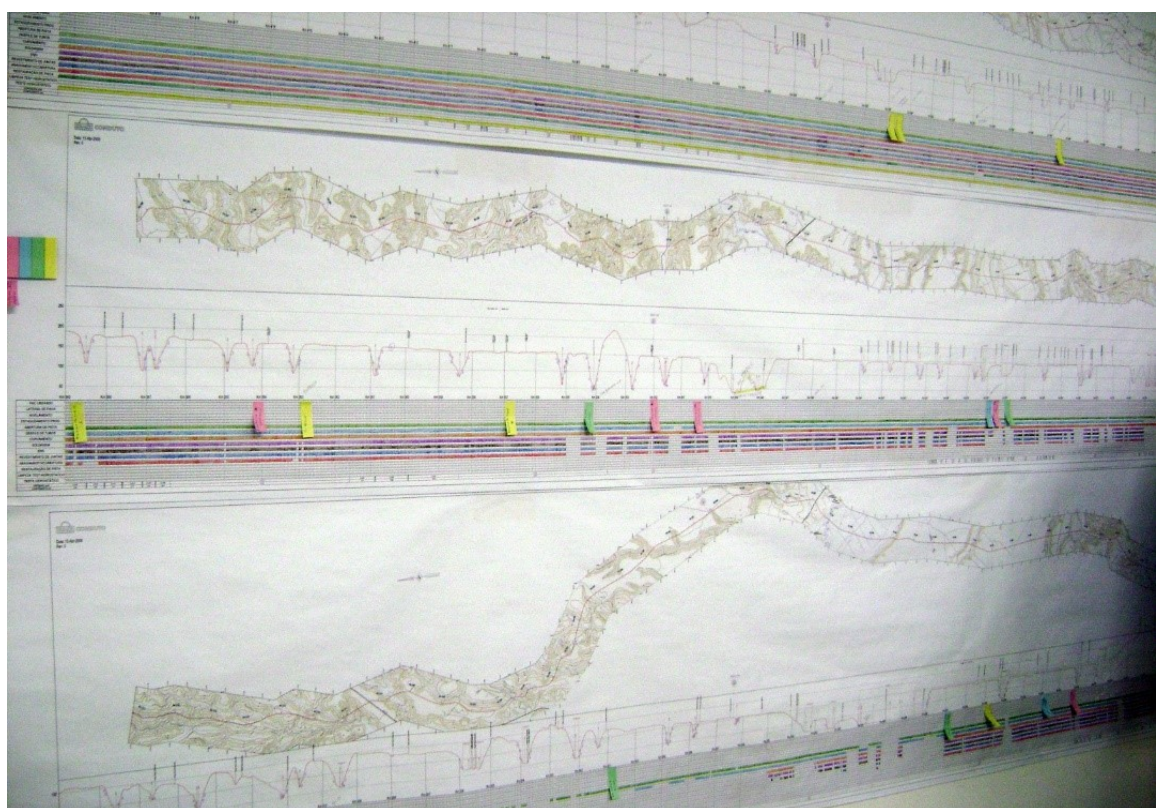


FIGURE 2.20 – Pipeline time location chart for C&A management.



FIGURE 2.21 – Pipes laid on the right of way.



FIGURE 2.22 – Pipe being positioned prior to welding.



FIGURE 2.23 – Pipe welding in the field.



FIGURE 2.24 – Ultrasound inspection of welded joint.



FIGURE 2.25 – Welded pipeline column.



FIGURE 2.26 – Thermo contractile coating in welded region.



FIGURE 2.27 – Pipeline being positioned inside trench.



FIGURE 2.28 – Pipeline being buried after being positioned inside trench.

3 Theoretical Foundation

This Chapter introduces important concepts used throughout the development of this work and previous studies related to robust OMR under variable lighting conditions. The concept of heterogeneous computing and the OpenCL language enable exposing the parallelism and explicit memory control in the implementation of key algorithms. Important edge detection methods are discussed and a fast OpenCL formula for the Sobel method is presented. Extreme learning machines are introduced as a fast training method to compute bounding boxes of optical markers. Finally, previous work on robust calibration patterns and OpenCV calibration checkerboard are discussed and their results are qualitatively compared to what is obtained using the proposed methodology.

3.1 Heterogeneous Computing

Spurred by the very profitable gaming market, current GPUs have extremely efficient hardware to compute graphics specific tasks. Their architecture provides thousands of Single Instruction Multiple Data (SIMD) processors whose instructions are specialized for interpolation, texture sampling and, more recently, dynamic parallelism (NVIDIA, 2012b). Moreover, very fast global memory and local caches are present in modern GPU architectures, as shown in Figure 3.1.

Computer graphics are an invaluable tool for process simulation, and multiple techniques have been developed to address specific situations.

Generally speaking, rendering involves analyzing 3D vertex information, materials, textures and light properties and producing 2D images from this information. This task can be accomplished in several ways: Traditional implementations, used in real time games, use a combination of rasterization and either shadow maps or shadow volumes to simulate lighting. Other approaches delve into physical properties of light and generate much better images at the cost of increased processing requirements (PHARR; HUMPHREYS, 2010).

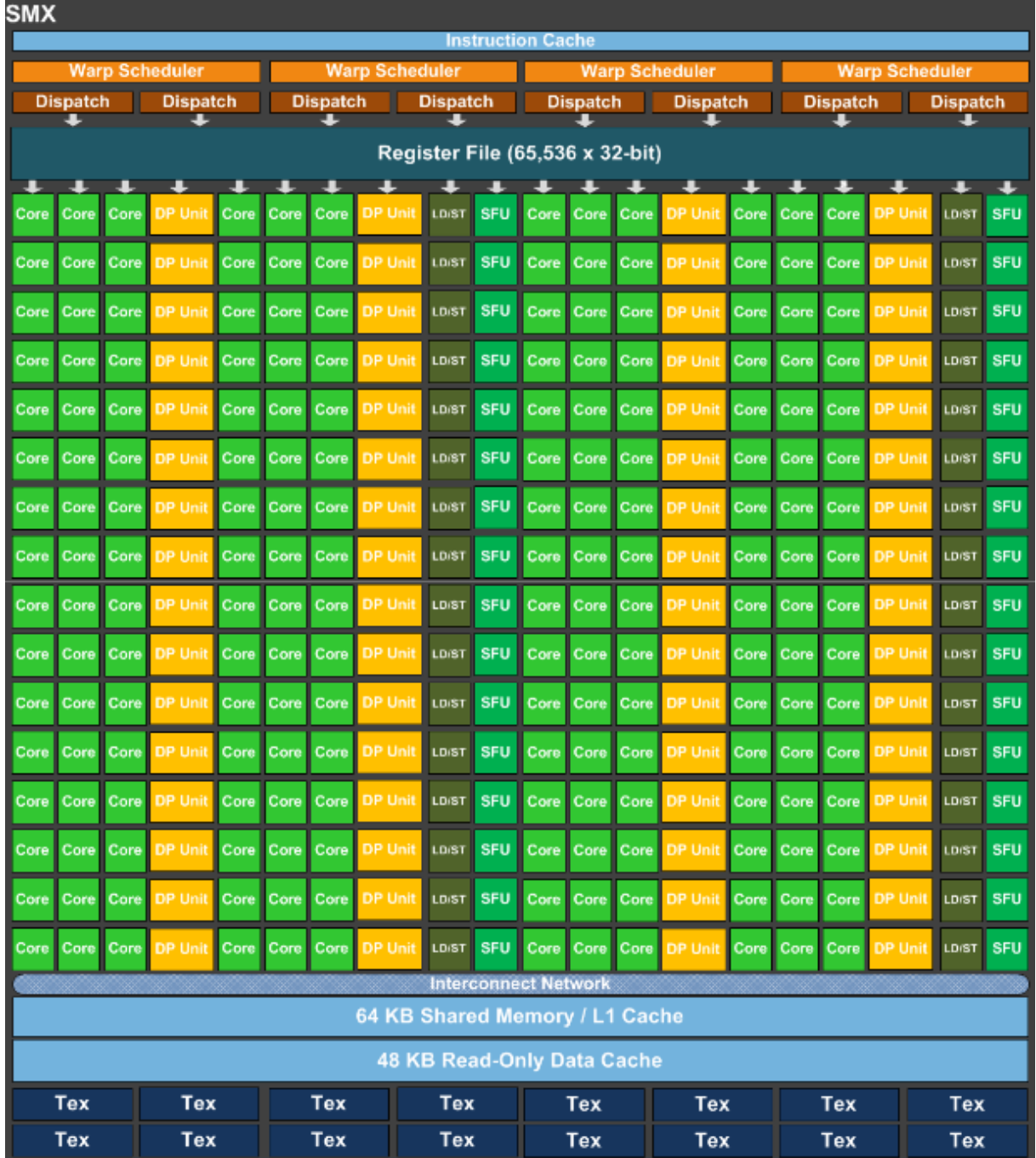


FIGURE 3.1 – NVidia’s Kepler architecture. From (NVIDIA, 2012b)

3.1.1 Motivation

Parallel hardware such as GPUs, FPGAs and multicore CPUs have become ubiquitous in all companies, laboratories and for personal use. To exploit full capabilities of this architecture, programmers need to explicitly expose parallelization of the code. There are multiple benefits of adopting the parallel paradigm, as summarized in Table 3.1.

In particular, spurred by games, GPU development has been extremely fast and their theoretical peak performance has been increasing steadily when compared to CPUs as

shown by (BADGUJAR, 2013) in Figure 3.2.

TABLE 3.1 – Benefits of adopting the parallel paradigm

Parallel feature	Description
High availability of multicore devices	Practically, all devices such as computers, smartphones and tablets have GPUs and multicore CPUs. Most of the processing power remains idle if the user only needs text editors, spreadsheets and office programs in general
Dramatic performance increase	It is possible to accelerate a wide variety of algorithms by large factors by parallelizing inner loops of computations.
Relative ease of use	Even a non-optimized, copy-paste C code from an innermost for-loop will probably yield acceleration to a given application. In addition, there are free, open source codes that exploit parallel capabilities of the hardware
Strong industry support	Multiple companies have started to adopt and encourage use of parallel programming techniques
Raising interest in parallel processing	Manufacturers' interest in parallel processing is raising as this technology will enable smaller devices to have better performance and battery life
Open possibilities	Few programs use GPU acceleration effectively at the moment. Scientific softwares like MATLAB and AnSys have maturity with GPGPU and math algorithms like FFT and BLAS (linear algebra) is not high. Even Photoshop, Vegas and Camtasia, which are softwares designed to manipulate images, do not use all GPUs have to offer

3.1.2 Platform Model

The platform model for heterogeneous computing consists of a host processor that issues execution commands to processing devices. In this model the host is composed of a single CPU thread while devices may be multicore CPUs, GPUs or FPGAs.

Since the number of parallel workitems is greater than the number of processors, the GPU schedules processing in execution warps. These warps are used to hide latency in memory fetch operations, match workitems with processors and synchronize execution (KHRONOS GROUP, 2013).

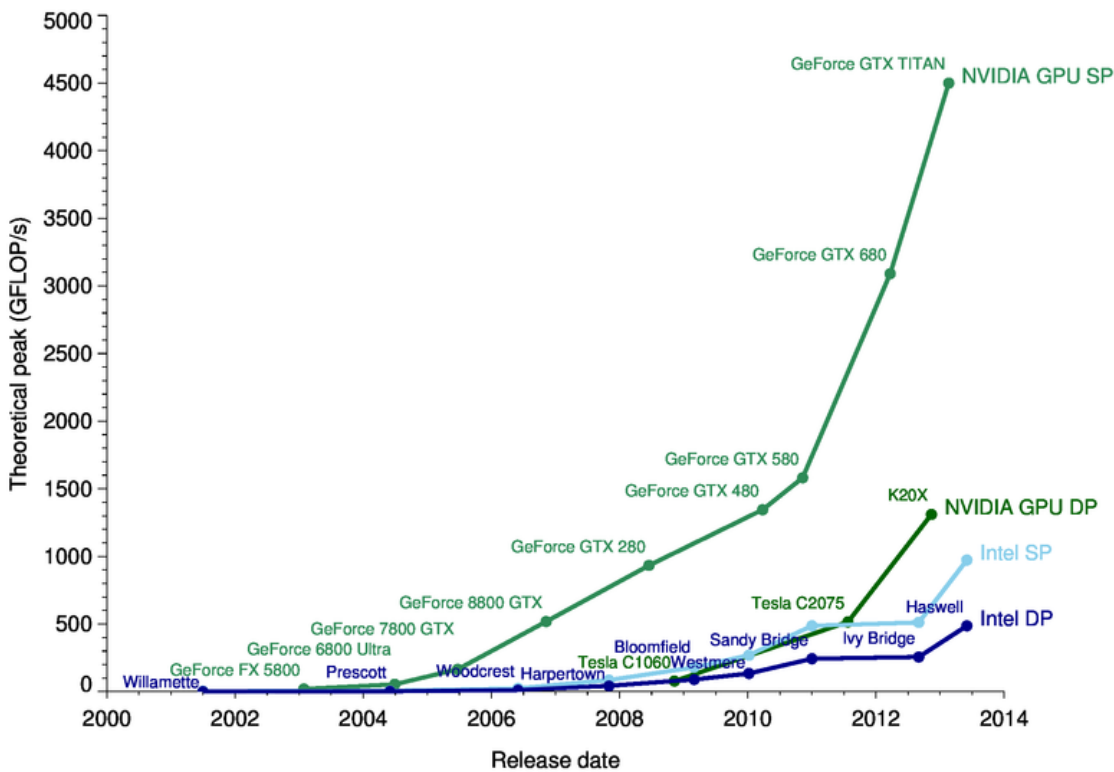


FIGURE 3.2 – CPU vs. GPU theoretical peak performance. From (BADGUJAR, 2013)

Figure 3.3 illustrates the heterogeneous computing model currently used to exploit parallelism in multicore devices. Written in a standard programming language, the host code makes calls to the OpenCL API, which issues instruction sets, execution commands and data read/write requests to the Devices. Notice that OpenCL enabled CPUs, which are usually employed as hosts, can also be the target of parallel OpenCL C99 code.

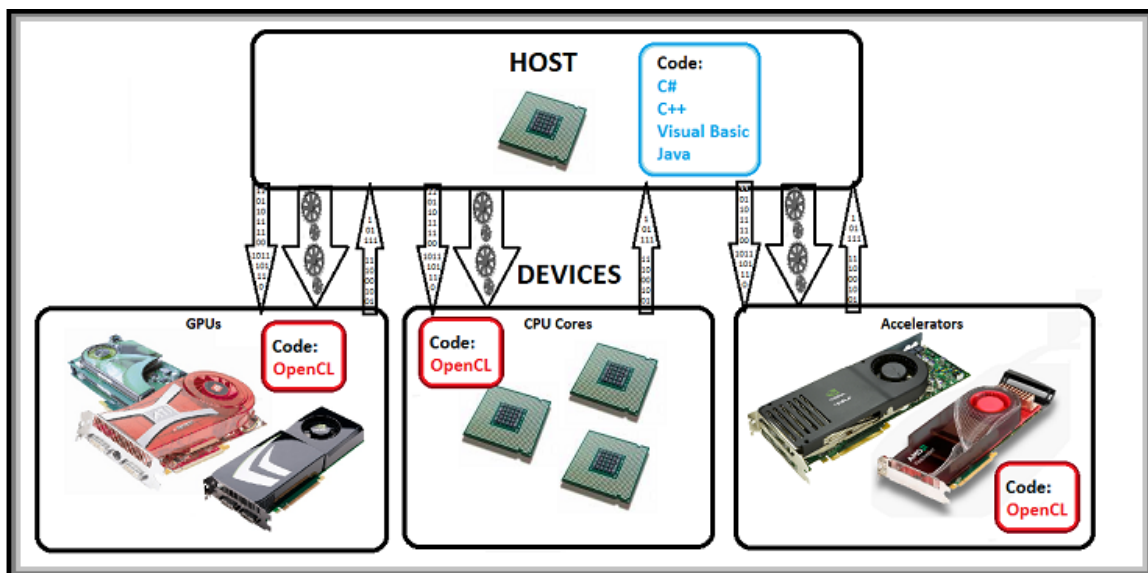


FIGURE 3.3 – Heterogeneous computing model.

Currently, the design trend is to have GPUs whose architectures are designed for heterogeneous computing, like NVidia Fermi and Kepler and AMD Stream Processor optimizations. Table 3.2 shows configurations of current high-end consumer GPUs, as informed by manufacturers (ADVANCED MICRO DEVICES, 2016) (NVIDIA, 2012a). Prices (obtained from (AMAZON.COM, 2016)) are shown to demonstrate that computing power has become available for a relatively affordable price.

TABLE 3.2 – Typical modern GPU parameters relevant to heterogeneous computing

Feature	GeForce GTX 780 Ti	AMD Radeon R9 290
Number of processors	2880	2560
Maximum clock speed (MHz)	928	947
Maximum memory bandwidth (GB/s)	336	320
Global memory (GB)	3, GDDR5	4, GDDR5
Price (USD)	243.01	289.99

Khronos Group’s Open Computing Language (OpenCL) is a framework for writing programs that execute across heterogeneous platforms, including central processing units (CPUs), graphics processing units (GPUs), digital signal processors (DSPs), field-programmable gate arrays (FPGAs) and other hardware accelerators. OpenCL allows explicit control over memory allocation and explicit parallelization control. The standard is supported by all major CPU and GPU manufacturers. OpenCL uses a subset of the C99 language as its parallel instruction set, augmented with specific functions (KHRONOS GROUP, 2013).

At its current stage, unlike NVidia’s CUDA, OpenCL provides no support to the C++ templating tool, whose offload can be automated to a satisfactory extent (CHEN *et al.*, 2012).

OpenCL provides the programmer with the unique opportunity to explicitly control data allocation in Device memory, as shown in Figure 3.3. Memory speed and size varies across vendors and, as a general rule, the more memory available of a given type, the slower its access, as summarized in Table 3.3.

TABLE 3.3 – OpenCL memory types

Memory	Speed	Size	Visibility	Requires sync
Private	Fastest	Small	Workitem only	No
Local	Fastest	Small	Workgroup only	Yes
Constant	Fast	At least 64 kb	Global	No
Global	Slow	Big	Global	No

“Slow” memory speed refers to Graphics DDR synchronous dynamic random-access memory (SDRAM) 5 - GDDR5, ranging from 100 to 640 Gb/s in modern hardware (ADVANCED MICRO DEVICES, 2016). “Fast” memories are caches, whose speed is implementation dependent but typically at least one order of magnitude faster. “Big” memory size means global memory size, from 2 Gb to 4 Gb. “Small” size means workitems receive a portion of the L2 cache memory (around 2 Mb in size - implementation specific).

Private memory is a workitem’s exclusive access memory (no sharing). Local memory is a special type shared by workitems in the same workgroup and requires explicit barriers to ensure proper execution order, thus making its use more complicated. Constant memory is allocated in the constant cache, whose access is almost as fast as private memory access and has fast access in any order. Global memory, which holds the bulk of the data, uses prefetching instructions and benefits from coalesced access, which is not always possible in every algorithm but should be used whenever possible.

Coalesced memory access or memory coalescing refers to combining multiple memory accesses into a single transaction, which significantly speeds up data retrieval from global memory because the device coalesces global memory loads and retrieves data requested by workitems of a workgroup into as few transactions as possible to minimize DRAM bandwidth (NVIDIA, 2013). Successive byte sequences can be accessed by a warp in a single transaction. Some conditions, however, may result in uncoalesced load, i.e., memory access becomes serialized (CORNELL, 2016):

- Memory is not sequential;
- Memory access is sparse;
- Misaligned memory access.

In this work, computationally intensive algorithms were implemented using OpenCL because the proposed algorithms rely intensely on sampling and writing textures and GPUs have specific hardware for this purpose. OpenCL exposes the functionality of GPU texture samplers which are faster than conventional CPU image sampling from RAM memory: typical BUS settings running at 1313 MHz clock rate allow 20 Gb/s versus typical 300 Gb/s in GPUs.

3.1.3 CUDA vs. OpenCL

Currently, NVidia’s CUDA and Khronos Group’s OpenCL specification are the standard programming environments for parallel programming. CUDA is a more mature technology, albeit restricted to NVidia hardware, while a wider variety of devices support

OpenCL. This portability is such a desirable feature that research has been developed to create and assess a CUDA-to-OpenCL translator (GARDNER *et al.*, 2013). Table 3.4 presents a comparison of CUDA and OpenCL features.

TABLE 3.4 – CUDA vs. OpenCL comparison chart. Desired property in **bold**

OpenCL	CUDA
Open standard	Proprietary
Code compilation at runtime	No runtime compilation
Any vendor may become compliant	Brand-specific
Source code reusable across platforms	No source code reusage across platforms
No vendor specific optimizations	Allows vendor-specific optimizations
Manual fine-tuning	Compilers fine-tune the code

3.1.4 Capabilities and Limitations

Like all technologies, parallel processing and OpenCL have strengths and weaknesses. The main strength of parallel processing (and thus OpenCL) is the ability to use all the processing power of CPUs and GPUs simultaneously to speed up computation. Its main disadvantage is that not all algorithms are designed for parallel processing and re-coding algorithms to run in parallel is not straightforward and often a tedious task. NVidia presents guidelines that should be followed in order to obtain best performance from parallel processing (NVIDIA, 2009) and we present our comments to NVidia's guidelines in 3.5. These comments come from the author's experience with OpenCL programming, thoroughly described in (CMSOFT, 2014).

TABLE 3.5 – Parallel programming best practices. Comments on NVidia's recommendations

NVidia recommendation	Relevance	Comments
To get the maximum benefit from OpenCL, focus first on finding ways to parallelize sequential code.	Crucial	Creating efficient parallel code is extremely important. This usually involves explicit vectorization of the code
Use the effective bandwidth of your computation as a metric when measuring performance and optimization benefits.	Low	Effective computation bandwidth define how scalable the code is. However, run times are also important

Continuation of Table 3.5		
NVidia recommendation	Relevance	Comments
Minimize data transfer between the host and the device, even if it means running some kernels on device that do not show performance gains when compared with running them on the host CPU	Very important	Data transfer consumes energy and time. Generate data directly inside the computing Device whenever possible
Ensure global memory accesses are coalesced whenever possible.	Medium	Coalesced access means, roughly speaking, to access OpenCL memory in worker order. This is only possible in very specific cases.
Minimize the use of global memory. Prefer shared memory access where possible.	Important	Not only shared memory, local memory as well. If feasible, the first operation of each kernel should be the copy of needed resources to local memory
Avoid different execution paths within the same warp.	Important	Has to do with the quality of the parallel code and its capability to exploit the SIMD or MIMD structure of each specific device
Use the -cl-mad-enable build option.	Medium	This allows the compiler to optimize instructions of the type $a \cdot b + c$. Precision is often enough for image processing and resampling tasks

3.2 Computer Vision

3.2.1 Edge Detection

Multiple algorithms exist for edge detection, from classical mask operators that output quantitative values for border intensity (Sobel, Roberts) to zero-crossing, Gaussian and Laplacian of Gaussian (LoG) techniques. Some studies show that, under noisy conditions, the Canny is the most accurate edge detection algorithm, followed by LoG, Sobel, Prewitt and Roberts (MAINI; AGGARWAL, 2009), (LAKHANI *et al.*, 2016). Others, however, show that adaptations in the Sobel filter yield the same performance when compared to other state-of-art methods (Canny, Sobel and Laplacian operator) (BISWAS; GHOSHAL, 2016) or

even better results (RAZALI *et al.*, 2014).

Sobel operator is the choice in this work because:

- Algorithm performance and parallelization are requirements to increase performance of the proposed methodology. Sobel edge detection is more suited to parallelization than Canny and was the choice for implementation in FPGA (SANDUJA; PATIAL, 2012);
- Main advantages of Sobel and LoG are: localization and better detection, especially in noisy conditions (MAINI; AGGARWAL, 2009). The proposed flood-filling algorithm, described in Section 4.2.3, is robust to the presence of noise and border location. Border continuity is the main requirement of the algorithm, and setting a conservative threshold after Sobel computation satisfies this requirement under tested settings;
- High accuracy Canny operators, which can detect border location precisely, rely on iterative procedures (not ideal for parallelization) that build upon Sobel edges, thus reducing performance (KIM; LEE, 2015);
- Sobel operator is not worse than Prewitt and Roberts' operators in practice (MAINI; AGGARWAL, 2009), (LAKHANI *et al.*, 2016).

The Sobel operator uses a pair of 3×3 convolution masks: one estimates the gradient in the X-direction and the other estimates the gradient in the Y-direction (rows), as shown in Equation 3.1. Usually, the final Sobel edge intensity square root operation is approximated as $G = |G_x| + |G_y|$. Using OpenCL and native GPU instructions (as discussed in Section 3.1) this approximation is no longer necessary because native functions are implemented in hardware and G can be computed using Equation 3.2, without loss of performance (KHRONOS GROUP, 2013).

$$G_x = \begin{bmatrix} -1 & 0 & 1 \\ -2 & 0 & 2 \\ -1 & 0 & 1 \end{bmatrix}, G_y = \begin{bmatrix} -1 & -2 & -1 \\ 0 & 0 & 0 \\ 1 & 2 & 1 \end{bmatrix} \quad (3.1)$$

$$G = \text{native_sqrt}(\text{mad}(G_x, G_x, G_y * G_y)) = \sqrt{G_x \cdot G_x + G_y \cdot G_y}. \quad (3.2)$$

3.2.2 Optical Mark Recognition

Optical mark recognition is a field of computer vision dedicated to creating specific markers that can be easily and uniquely identified on an image. Optical character recog-

nition (OCR), a very related problem, tackles the problem of how to find and identify characters in images.

OCR approaches are widely used in a broad range of applications, and they have been well established for a long time (HALL, 1968), (LEIMER, 1962). Modern applications include license plate recognition to scanned document information retrieval (RAMANATHAN *et al.*, 2009), (QADRI; ASIF, 2009). OCR utilizes image processing, feature extraction and machine learning techniques, and the vast number of works in the literature reflects its relevance; nonetheless, robustness in object identification and processing speed are paramount and OMR is better suited in large equipment part location in outdoor environments than other approaches.

Work by Manduchi (MANDUCHI, 2012) demonstrated how to use color information to allow cell phones to be used as navigation devices for blind people, while Barresi and Allasia (BARRESI; ALLASIA, 2013) studied a method to use OMR to aid unmanned aerial vehicle landing. Such environments are way more controlled than outdoor settings in which refineries, FPSOs and pressure vessels are built (as one can infer from the various C&A pictures throughout this work) and specific robustness for highly variable lighting conditions is called for.

Recently, performance considerations have been addressed as multicore CPUs and GPUs have become standard personal computer hardware (AL-MARAKEBY, 2013).

3.3 Extreme Learning Machine

The Extreme Learning Machine (ELM), originally derived from single hidden layer feedforward networks, has a rather simple structure and has been successfully applied to image recognition tasks (HUANG *et al.*, 2004). In this work, it was applied to demonstrate how to perform preliminary identification of optical marker bounding boxes. Given a training set

$$\mathbf{T} = \{(\mathbf{x}_i, \mathbf{t}_i) | \mathbf{x}_i \in \mathbb{R}^{nFeat}, \mathbf{t}_i \in \mathbb{R}^{nOut}, i = 1, 2, \dots, nSamples\}, \quad (3.3)$$

where $nFeat$ is the number of features per sample, $nOut$ is the number of possible categories and $nSamples$ is the total number of training samples, the ELM output o_i for i -th input x_i is given by:

$$G(\mathbf{x}_{i,1 \times nFeat} \cdot \mathbf{W0}_{nFeat \times nHidden}) \cdot \mathbf{W1}_{nHidden \times nOut} = \mathbf{o}_{i,1 \times nOut}, \quad (3.4)$$

where $nHidden$ is the number of neurons in the hidden layer, $\mathbf{W0}$ are connection

weights from input to the hidden layer, $\mathbf{W1}$ are connection weights from hidden layer to the output and G is a hidden node nonlinear transfer function. In matrix form, the $nSamples$ outputs can be computed by:

$$G(\mathbf{X}_{nSamples \times nFeat} \cdot \mathbf{W0}_{nFeat \times nHidden}) \cdot \mathbf{W1}_{nHidden \times nOut} = \mathbf{O}_{nSamples \times nOut}. \quad (3.5)$$

The ELM training consists in generating random input to hidden node weights $\mathbf{W0}$ and solving for $\mathbf{W1}$:

$$\mathbf{H}_{nSamples \times nHidden} = G(\mathbf{X}_{nSamples \times nFeat} \cdot \mathbf{W0}_{nFeat \times nHidden}), \quad (3.6)$$

$$\mathbf{H} \cdot \mathbf{W1} = \mathbf{O} \Rightarrow \mathbf{W1} = \mathbf{H}^\dagger \mathbf{O}, \quad (3.7)$$

where \mathbf{H}^\dagger is the Moore-Penrose generalized pseudoinverse of \mathbf{H} . As proposed by (HUANG *et al.*, 2012), adding regularization improves stability of the method, as shown in Equation 3.8:

$$\mathbf{W1} = \begin{cases} \mathbf{H}^T (\lambda^{-1} \mathbf{I} + \mathbf{H} \mathbf{H}^T)^{-1} \mathbf{O}, & nSamples \leq nHidden \\ (\lambda^{-1} \mathbf{I} + \mathbf{H}^T \mathbf{H})^{-1} \mathbf{H}^T \mathbf{O}, & nSamples > nHidden. \end{cases} \quad (3.8)$$

3.4 Related Work

Detection of patterns in outdoor settings is a challenging task that has deserved research attention in multiple fields, from face recognition to calibration patterns located under irregular lighting conditions ((WANG *et al.*, 2004), (KANG; LEE, 2010), (KANG; JEONG, 2008)). Currently, there are no guidelines for designing markers that can be tracked reliably (KHAN *et al.*, 2015), and field implementation of augmented reality currently presents as main challenges, among others, the ability to function in harsh environments, robust image registration for outdoor uncontrolled conditions, filtering ambient noise and interferences (OMAR; NEHDI, 2016).

Detection of concentric regions is another robust approach proposed for camera calibration in outdoor environments (JIANG; QUAN, 2005) as are 2D markers (LIU *et al.*, 2008). However, little attention has been given to the problem of locating optical markers (not just for camera calibration) in outdoor settings, where lighting may vary not only in intensity but also color and global histogram distribution. Principles of machine vision techniques have been proposed by (ASLUZEK, 2010), who claims that accuracy of

object detection is enhanced when optical markers are used; however, no implementation is provided.

Edge detection is a preprocessing step used to segregate color regions. Pre-filtering yields better results in edge detection, which may or may not help depending on the quality and noise to signal ratio of the camera. Advanced denoising techniques have been presented in the literature (e.g. (FABIJANSKA; SANKOWSKI, 2011), (UTAMININGRUM *et al.*, 2013) and (AYSAL; BARNER, 2007)) and are used to improve edge detection accuracy.

For field applications, performance is an important consideration because the identification algorithm has to provide information to operators during construction and assembly processes. A possible strategy in embedded systems is the use of FPGAs when custom hardware is made for the application (SÁNCHEZ-FERREIRA *et al.*, 2016). Another approach used to accelerate computation is to take advantage of high parallelism and low cost of graphic processing units (GPUs) (CARRION *et al.*, 2015), (FRANCO *et al.*, 2015). In this work, GPU implementation was chosen to allow implementation of the robust optical mark recognition at a very low cost, without using custom hardware. Once optical markers are recognized, multiple efficient image tracking algorithms can be used to follow and predict their location ((LUCAS; KANADE, 1981), (ZHANG *et al.*, 2016), (WU *et al.*, 2016)), including applications in welding (XU *et al.*, 2015).

Flood-filling algorithms analyzed require a seed point and propagate regions from there. Many search strategies and methods have been proposed to optimize the process (DUO-LE; MING, 2011). Flood-filling algorithms without edges are used to detect regions of interest in outdoor images (HSIEH *et al.*, 2011). The method, however, requires blurring images to a level that would not be acceptable for optical marker recognition. A pattern of dots was proposed to increase the robustness of pattern identification (KANG; JEONG, 2008). The method entails binarization of the image using Otsu method followed by identification of neighboring dots, as shown in Figure 3.4 and Figure 3.5.

In (KANG; JEONG, 2008) it is shown that Otsu's method, as any binarization, faces problems trying to split regions from a grayscale image under uneven lighting settings. The ellipses inserted into Figure 3.5 mark regions from where noise significantly reduces quality of dot identification. Moreover, color cameras are widely available and there is no reason not to take advantage of the extra information provided by RGB pixel components. For the purpose of comparison, the result of the algorithm developed in this work is shown in Figure 3.6 where blue color denotes background color and adjacent regions of contiguous color are clustered together in a group. This result is superior in the sense that no white dots are lost in the binarization processes. Further details of the proposed algorithm are provided in the following sections.

It is also worth noting that Kang et al (KANG; JEONG, 2008) images sizes were 640x480

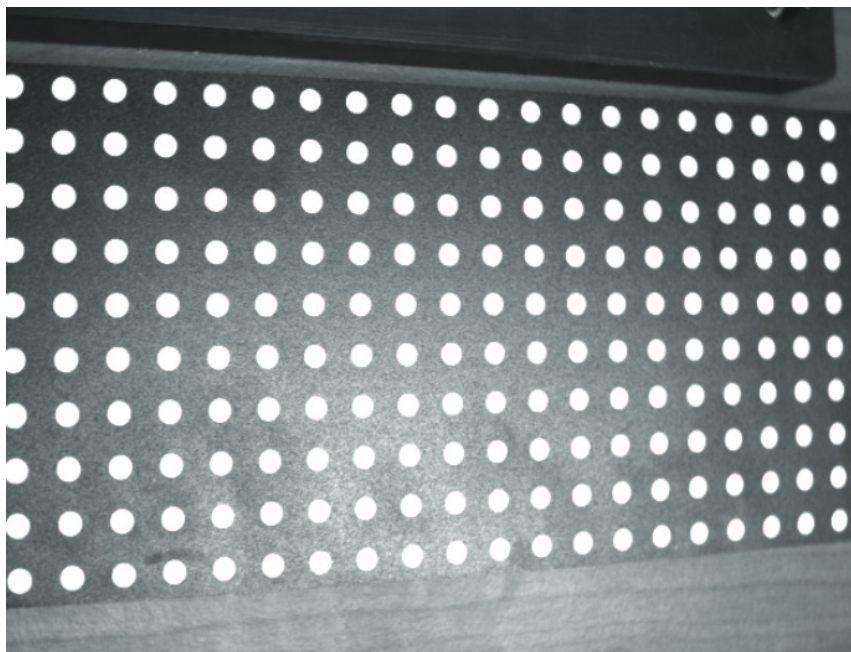


FIGURE 3.4 – Robust calibration pattern proposed by (KANG; JEONG, 2008).

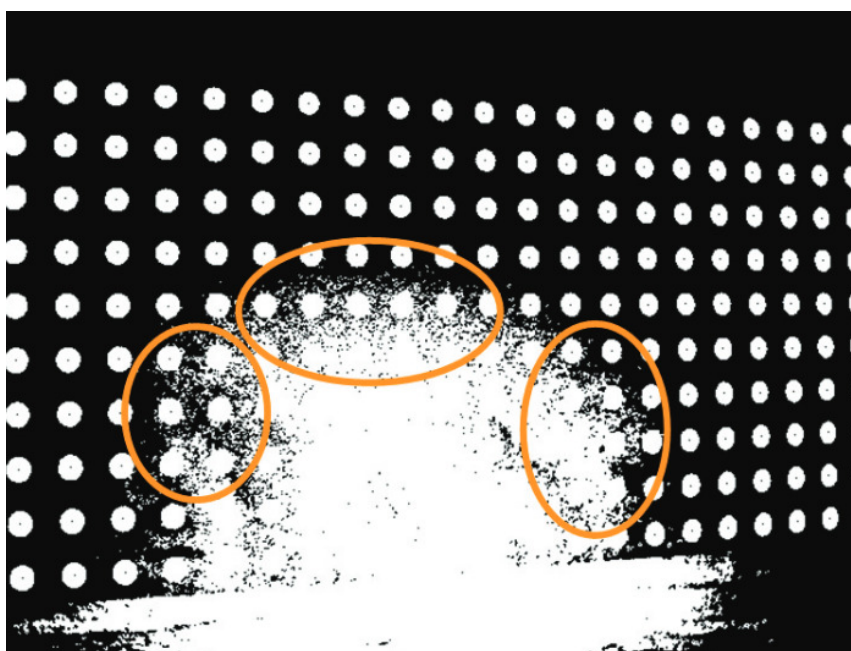


FIGURE 3.5 – Otsu binarization of source image, as obtained by (KANG; JEONG, 2008).

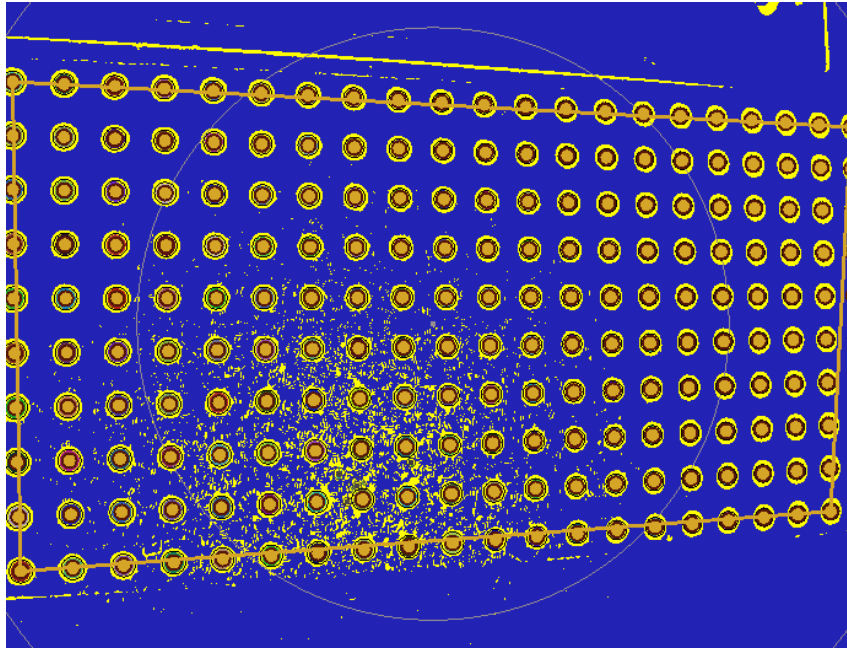


FIGURE 3.6 – Calibration pattern by (KANG; JEONG, 2008) processed using the proposed methodology.

and their processing time was 1s using a Pentium IV processor. In this work, the exact same image, using modern hardware and GPU computing with a Radeon 7970 GPU, was processed in 0.13 s and better results were obtained. Since no pre-filtering was applied in the original work, this comparison also skipped the pre-filtering step.

OpenCV algorithm for checkerboard detection relies on binarization of input image followed by morphologic procedures (erosion) and quadrant linking heuristics, which have been proposed by (RUFLI *et al.*, 2008). This procedure has been designed for indoor camera calibration. Thus, for the purposes of outdoor identification of large parts, a more robust alternative is required. For comparison purposes, the typical image (shown in Figure 3.7) from (RUFLI *et al.*, 2008) has been processed using the proposed methodology, demonstrating that no features are lost: as in the original work, all checkerboard squares are detected. The proposed flood-filling algorithm, which will be described in Chapter 4, does not rely on morphologic procedures and allows robust outdoor detection.

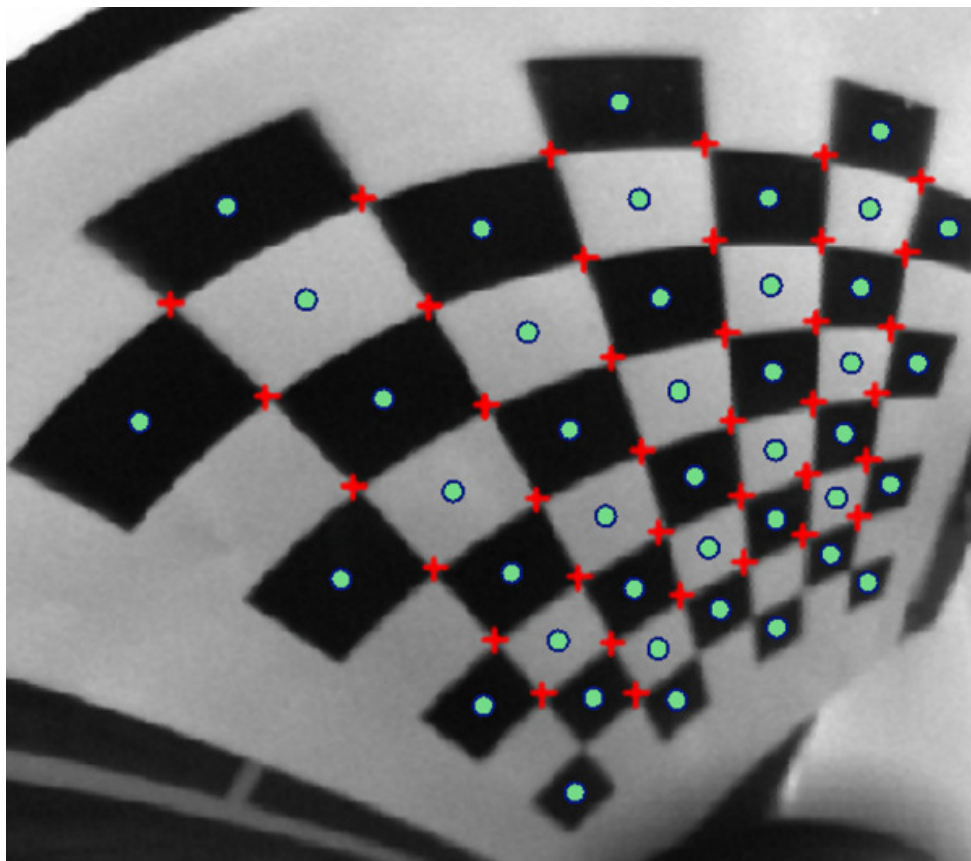


FIGURE 3.7 – Comparison of proposed algorithm to OpenCV using the same input image from (RUFLI *et al.*, 2008). Red crosses: OpenCV output. Green circles: output of proposed algorithm.

4 Methodology for OMR in Outdoor Environments

4.1 Structure

In this work, a robust methodology has been developed for OMR in outdoor environments. Figure 4.1 summarizes the methods, tasks and algorithms of the proposed methodology. The rightmost column provides illustrations of information retrieved during the recognition process.

The main requirement posed is robustness, in order to find markers in a wide range of lighting conditions. To allow visualization of results, the following graphical elements are created in processed images:

- A yellow circle is used to mark concentric region centers along with an ID (identification) code;
- A circle of the same color is drawn at the center of neighboring contiguous color regions;
- If requested, all pixels belonging to the same color regions are painted using the same randomly generated color. Pixels which belong to edges are marked in yellow.

The first color identified in the image is forced to be blue when identification of contiguous color regions is requested (usually identifies the background). It is worth noting that edge detection and region filling are crucial time-consuming steps for which parallel implementation using OpenCL has been developed.

The methodology goes through the following steps:

- **Identification of contiguous color regions:** image borders are computed using a Sobel filter. Parallel region filling is performed (Section 4.2) to extract contiguous color regions using pixel-to-region association;

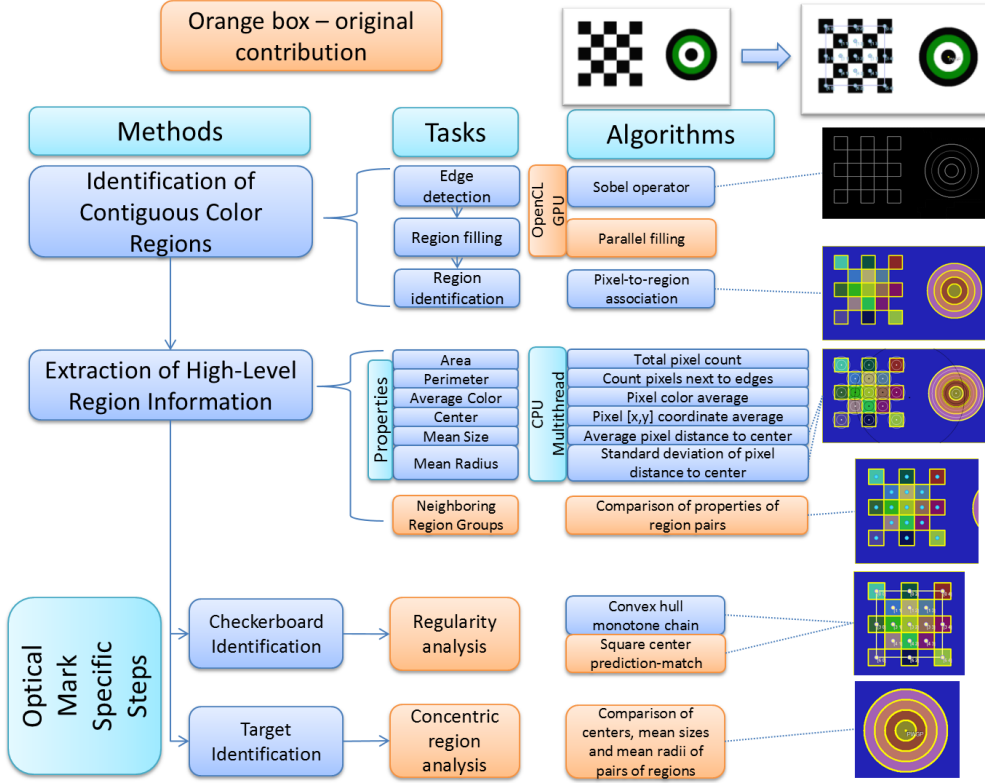


FIGURE 4.1 – Robust Outdoor OMR Structure. Original contributions of this work are highlighted in orange.

- **Extraction of high-level region information:** after extracting pixels of each color region in the previous step, properties such as area and perimeter of each region are estimated (Table 4.1);
- **Checkerboard identification:** Adjacent regions are grouped together and their characteristics are analyzed to predict outer position (using the convex hull algorithm) and inner squares position (testing multiple checkerboard sizes). Details of this procedure are presented in Section 4.4.1;
- **Target identification:** Region properties are used to detect which color regions are circular (disk-shaped). Then, circular regions whose center coincides are grouped into a target, as described in Section 4.3.

4.2 Identification of Contiguous Color Regions

4.2.1 Image Filtering

An important preprocessing step used to reduce image noise is image filtering. Prior to the edge detection task, three filtering approaches were considered: no filter, Gaussian

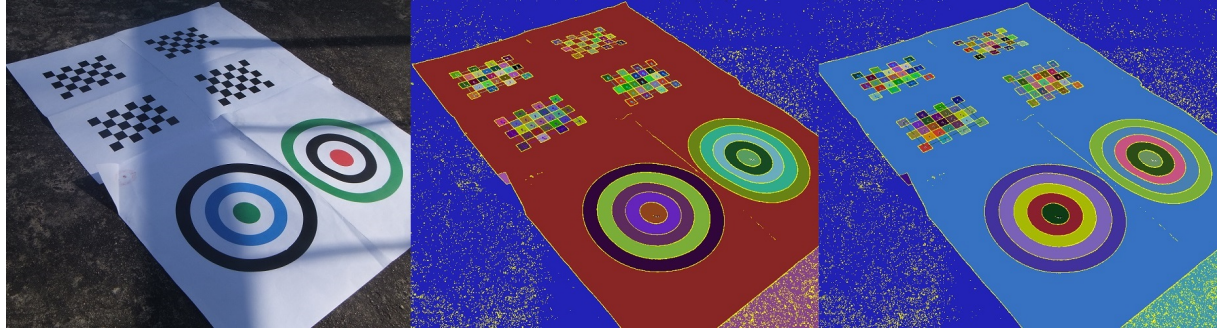


FIGURE 4.2 – Performance comparison of Gaussian and median filters show very small difference in tested settings. Identified borders in yellow. Left: original image. Center: Gaussian filter result. Right: Median filter result.

filter and median filter. Median filtering often preserves edges with a good degree of accuracy, which makes this method the usual choice in biomedical imaging (VERMA *et al.*, 2015). The increased accuracy, however, comes at the cost of increased processing times.

In the case of GPU implementation, median filtering leads to data-dependent execution paths that increases execution time by an order of magnitude when compared to Gaussian filtering and tests conducted show that, in the proposed methodology, gains are negligible.

Using a NVidia Quadro FX 5800 hardware to compute filter times using the picture shown in Figure 4.2, Gaussian filter takes 0.057 s and median filter takes 0.75 s (average values over 10 tests). No improvement can be observed and tests conducted show that the image filtering algorithm influence on the final result is negligible compared with other factors (as described in Section 5.2).

4.2.2 Edge Detection

Robust edge detection is a crucial preprocessing step for the proposed flood filling algorithm in order to correctly segregate contiguous color regions. Multiple border detection algorithms have been considered.

The Canny edge detector is the optimal edge detection method, working on three main principles: low error rate, well localization of edge points and one response to a single edge. Nonmaximum suppression and double thresholding are used to select the edge points. However, the hysteresis used to segment the gradient image are usually set experimentally and automatic methods need to precompute the gradient histogram produced by the Sobel operator (CANNY, 1986) (BISWAS; SIL, 2012).

The Sobel method (DUDA; HART, 1973) has appropriate accuracy regarding border location and continuity for multiple applications (BAGLODI, 2009). In addition, it requires a single pass over the image and its GPU implementation is both robust in the sense

that it is possible to consider RGB components and fast because texture samplers will retrieve RGB components practically as fast as they would retrieve a single value, because memory is accessed in strides. The edge detection algorithm implemented in this work computes Sobel edge values as the maximum of absolute differences of each RGB component. In summary, the Sobel edge detection algorithm was chosen in this work because of its proper accuracy (especially regarding border continuity) and high performance when implemented in parallel using OpenCL and in practice, for the experiments conducted, the threshold values set for the Sobel edge detector were sufficient to robustly identify the markers.

Threshold levels are chosen to guarantee continuity of the edges while still allowing for fast parallel computation of the edges. Continuous edges are a requirement of the parallel flood filling algorithm shown in Section 4.2.3.

4.2.3 Region Filling

In this work, a new parallel flood-filling algorithm is developed to simultaneously identify all contiguous regions without any seed points. The outline of this algorithm is as described in Algorithm 1:

Algorithm 1: Parallel flood-filling

Input: Edge map of the image

Output: Unique number assigned to each contiguous color region

Find regions in the image that have the same color;

Receive edge map and create color region map ;

Initialize the region map by assigning each pixel a unique color number ;

while *region map changed OR MAXITER ≥ 15* **do**

Sweep region map from left to right, from right to left, from top to bottom and from bottom to top in parallel;

if *current pixel is not located on any edge and its index is greater than previous pixel* **then**

└ assign current pixel the same index than previous pixel;

MAXITER++;

Figures 4.3 to 4.8 illustrate the proposed algorithm using an image created for this purpose. The two regions of the image are identified when the algorithm terminates.

The number of parallel workitems is equal to the image height when sweeping lines and to image width when sweeping columns, yielding over 1000 workitems in each case when processing a full-HD (1920x1080 pixels) image, which is appropriate for latency hiding purposes. Sweeping in both directions (left-right, right-left, top down and bottom up) is required because edge index switch only happens when current pixel color index is greater

than previous pixel color index.

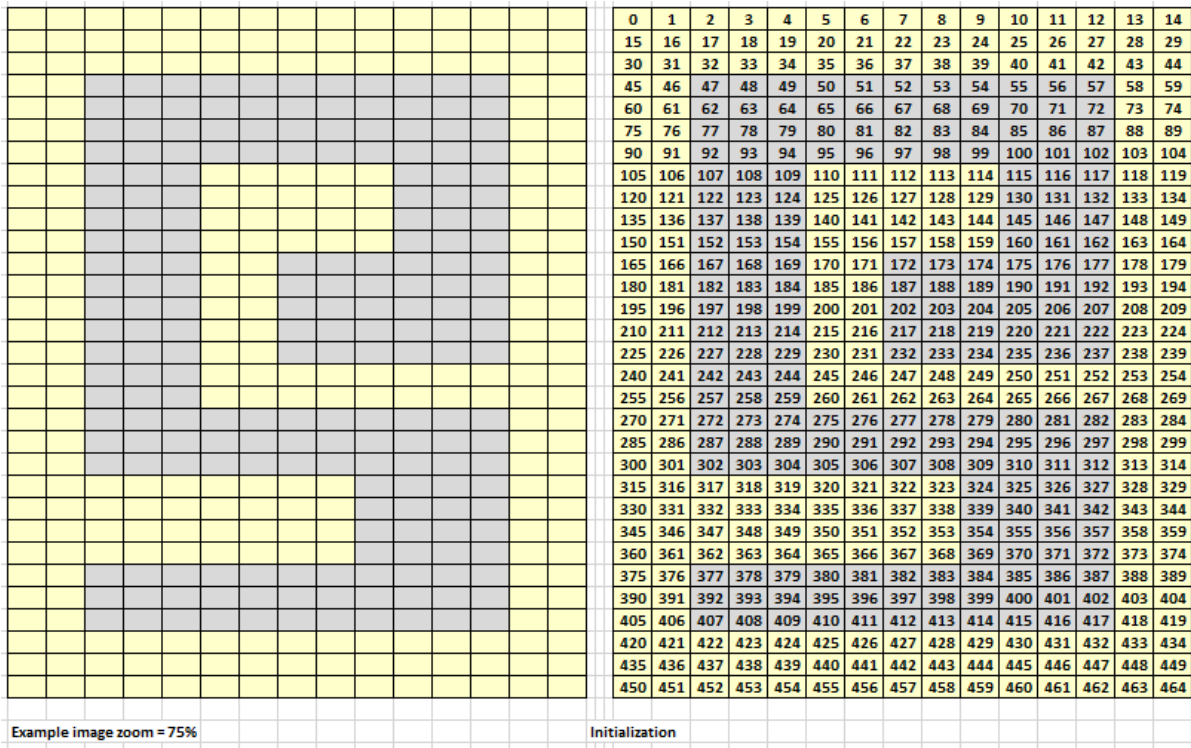


FIGURE 4.3 – Example image in gray and unique color map initialization.

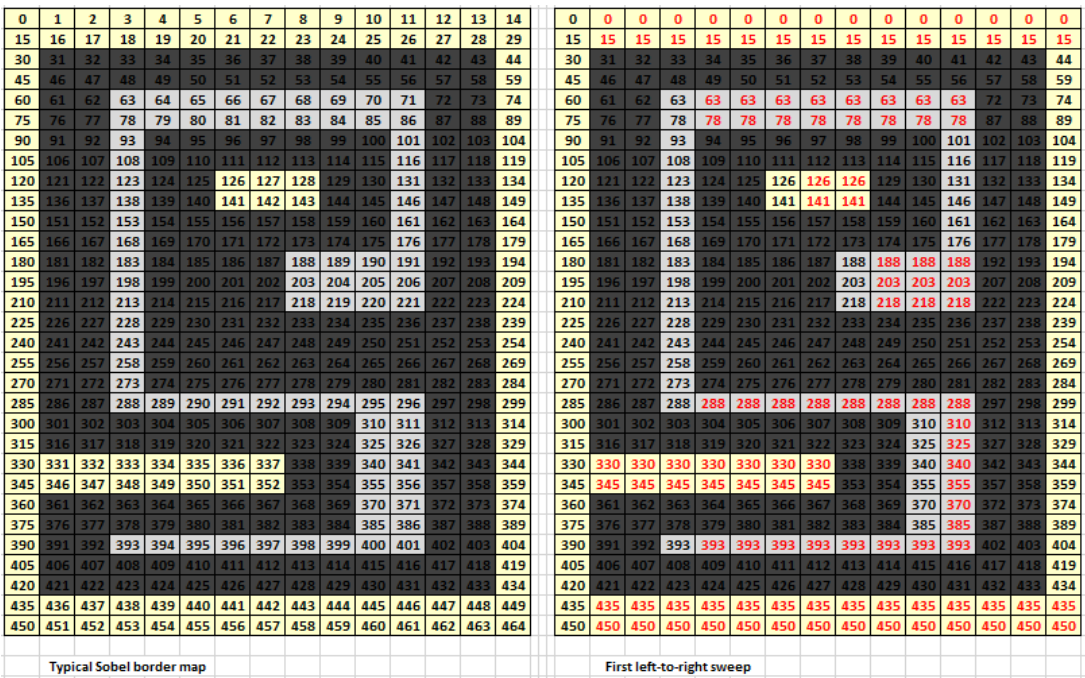


FIGURE 4.4 – Border map and first left-to-right sweep.

FIGURE 4.5 – First right-to-left and top-to-bottom sweeps.

0	0	0	0	0	0	0	0	0	0	0	0	0	0	0
0	0	0	0	0	0	0	0	0	0	0	0	0	0	0
0	31	32	33	34	35	36	37	38	39	40	41	42	43	0
0	46	47	48	49	50	51	52	53	54	55	56	57	58	0
0	61	62	63	63	63	63	63	63	63	63	72	73	0	0
0	76	77	63	63	63	63	63	63	63	63	87	88	0	0
0	91	92	63	94	95	96	97	98	99	100	63	102	103	0
0	106	107	63	109	110	111	112	113	114	115	63	117	118	0
0	121	122	63	124	125	126	126	126	129	130	63	132	133	0
0	136	137	63	139	140	126	126	126	144	145	63	147	148	0
0	151	152	63	154	155	156	157	158	159	160	63	162	163	0
0	166	167	63	169	170	171	172	173	174	175	63	177	178	0
0	181	182	63	184	185	186	187	188	188	188	63	192	193	0
0	196	197	63	199	200	201	202	188	188	188	63	207	208	0
0	211	212	63	214	215	216	217	188	188	188	63	222	223	0
0	226	227	63	229	230	231	232	233	234	235	236	237	238	0
0	241	242	63	244	245	246	247	248	249	250	251	252	253	0
0	256	257	63	259	260	261	262	263	264	265	266	267	268	0
0	271	272	63	274	275	276	277	278	279	280	281	282	283	0
0	286	287	63	288	288	288	288	288	288	288	297	298	0	0
0	301	302	303	304	305	306	307	308	309	288	288	312	313	0
0	316	317	318	319	320	321	322	323	324	288	288	327	328	0
0	330	330	330	330	330	330	330	338	339	288	288	342	343	0
0	330	330	330	330	330	330	330	353	354	288	288	357	358	0
0	361	362	363	364	365	366	367	368	369	288	288	372	373	0
0	376	377	378	379	380	381	382	383	384	288	288	387	388	0
0	391	392	393	393	393	393	393	393	393	288	288	402	403	0
0	406	407	408	409	410	411	412	413	414	415	416	417	418	0
0	421	422	423	424	425	426	427	428	429	430	431	432	433	0
0	435	435	435	435	435	435	435	435	435	435	435	435	435	0
0	435	435	435	435	435	435	435	435	435	435	435	435	435	0

First bottom-to-top sweep (does nothing)

Second left-to-right sweep

FIGURE 4.6 – First bottom-to-top and second left-to-right sweep.

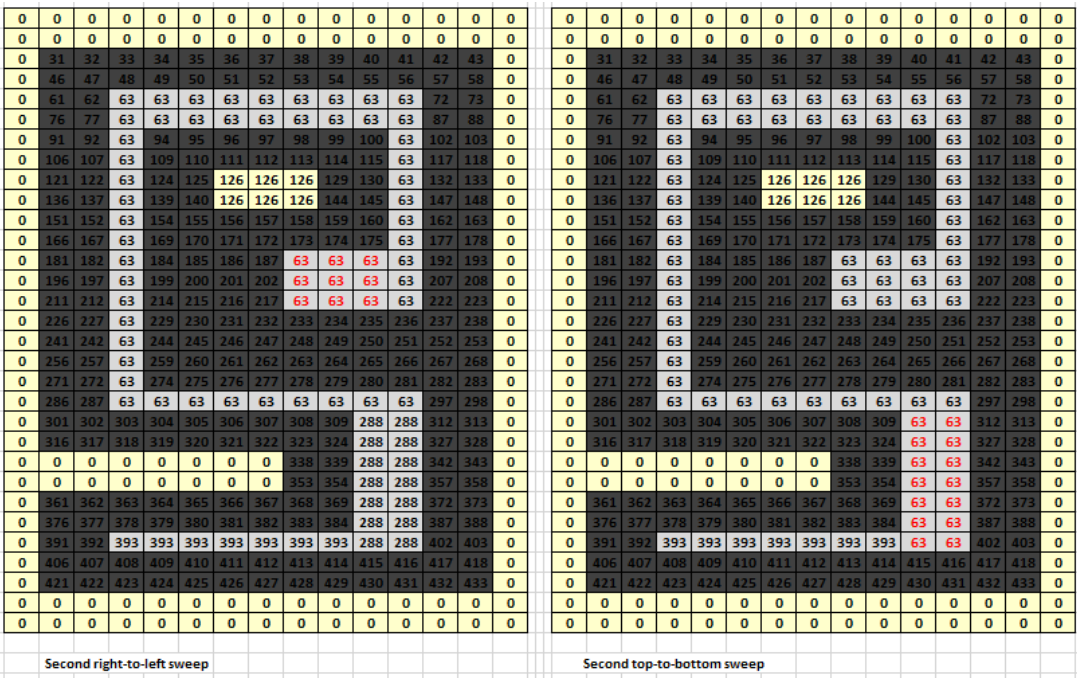


FIGURE 4.7 – Second right-to-left and top-to-bottom sweeps.

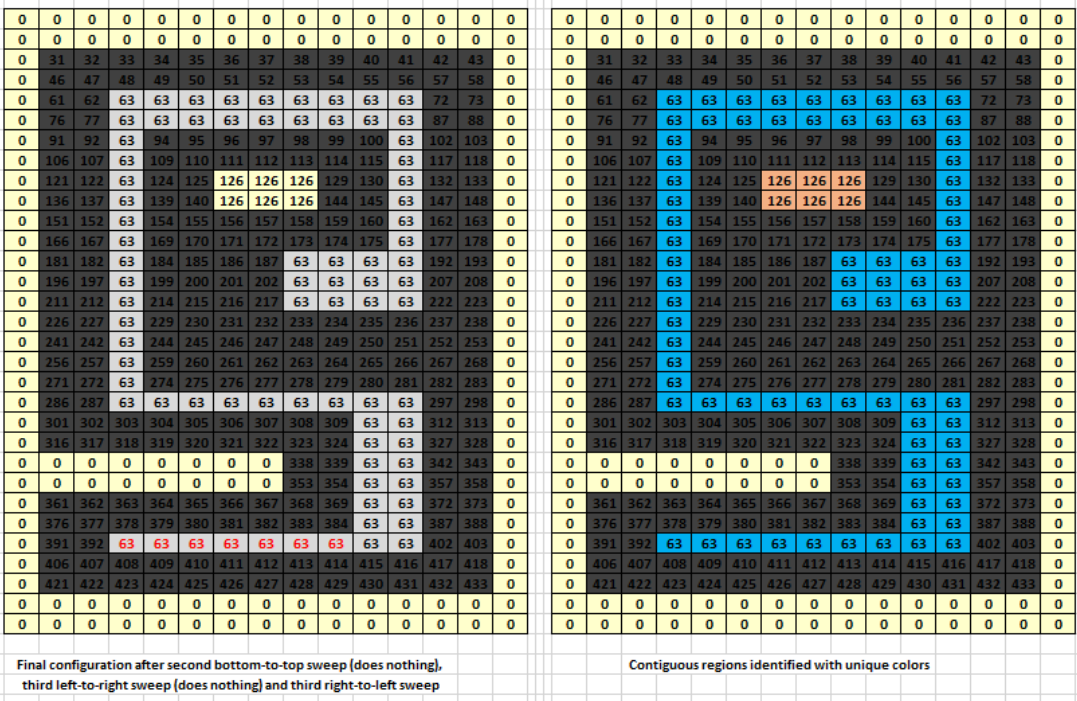


FIGURE 4.8 – Final configuration and visual identification of contiguous regions.

When the flood-filling procedure is complete, colors are remapped to unique sequential indexes and a list of the pixels that belong to these regions is created. In the example shown in Figure 4.8, the remapping algorithm maps unique region 0 to index 0 and 63 to index 1. Properties and higher level information is then extracted for each region.

4.2.4 Region Identification

After computing color regions, region properties are computed for each of these regions. Table 4.1 shows the region properties computed for each region.

TABLE 4.1 – Region data properties computed in the proposed method

Region Property	Computation Method
Area	Number of pixels in region
Perimeter	Number of pixels next to edges
Average color	Color average of pixels which in region
Center	Average coordinate ([x,y]) of pixels in region
Mean size	Average pixel distance to region center
Mean radius	Standard deviation of pixel distance to center

4.3 Extraction of High Level Region Information

4.3.1 Circular and Concentric Regions

Concentric regions are composed of multiple annuluses of the same color as shown in Figure 4.9. Each annulus has its own mean distance to center r and width w . Approximating the region using an ellipsis would be more accurate when images of concentric regions are obtained under perspective. However, results show that the proposed identification criteria retain robustness in these cases. Region data properties shown in Table 4.1 can be used to approximate annulus properties (Table 4.2).

TABLE 4.2 – Approximation of annulus properties using computed region data

Annulus property	Exact computation in terms of r and w	Approximation using region data properties
Mean distance to center	r	Mean size
Width	w	Mean radius
Area	$\pi \left[\left(r + \frac{w}{2} \right)^2 + \left(r - \frac{w}{2} \right)^2 \right] = 2\pi rw$	Region area
Perimeter	$2\pi \left[r + \frac{w}{2} + r - \frac{w}{2} \right] = 4\pi r$	Region perimeter

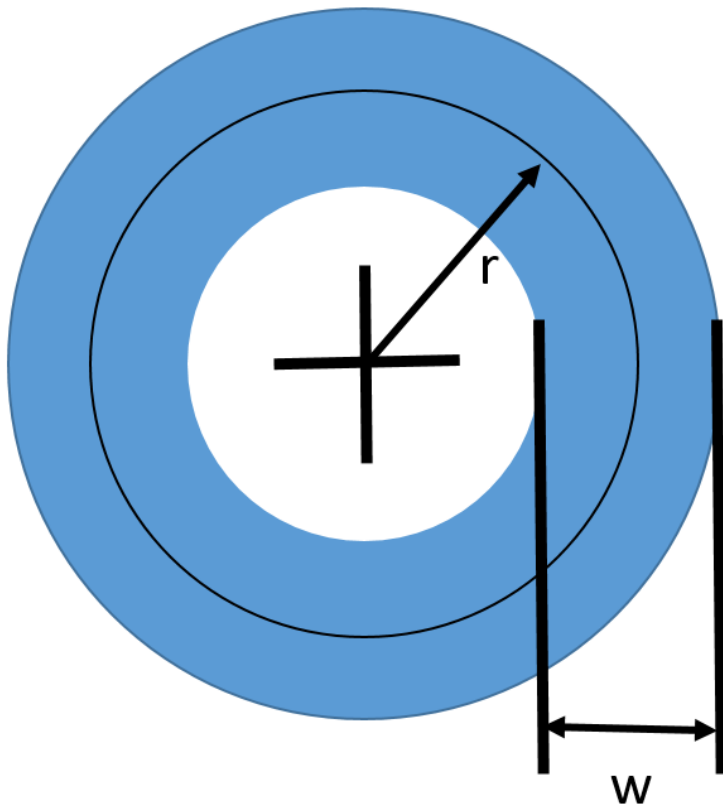


FIGURE 4.9 – Contiguous color region in the shape of an annulus with mean distance to center r and width w .

4.3.2 Neighboring Regions

Contiguous color regions (superpixels, homogeneous regions - (CHOI; OH, 2016)) segmentation in a picture provide valuable information about object structure and are useful in a vast number of applications, such as image classification, segmentation, object recognition and learning frameworks (LU *et al.*, 2013), (TASLI *et al.*, 2015), (ZHANG; VERMA, 2015).

In order to identify optical markers, criteria are proposed in this work to identify and to assign groups to neighboring regions. Region properties (Table 4.1) allow deciding which regions are adjacent to each other (Table 4.3). Post processing adjacency information then leads to the creation of groups of neighboring regions, which are marked with a circle of a common random color in this implementation, for debugging and visualization purposes, as shown in Figure 4.10. The constants used were calibrated experimentally using test images taking into consideration that similar regions should be grouped together even in the presence of perspective distortions, while still rejecting regions whose characteristics are too different.

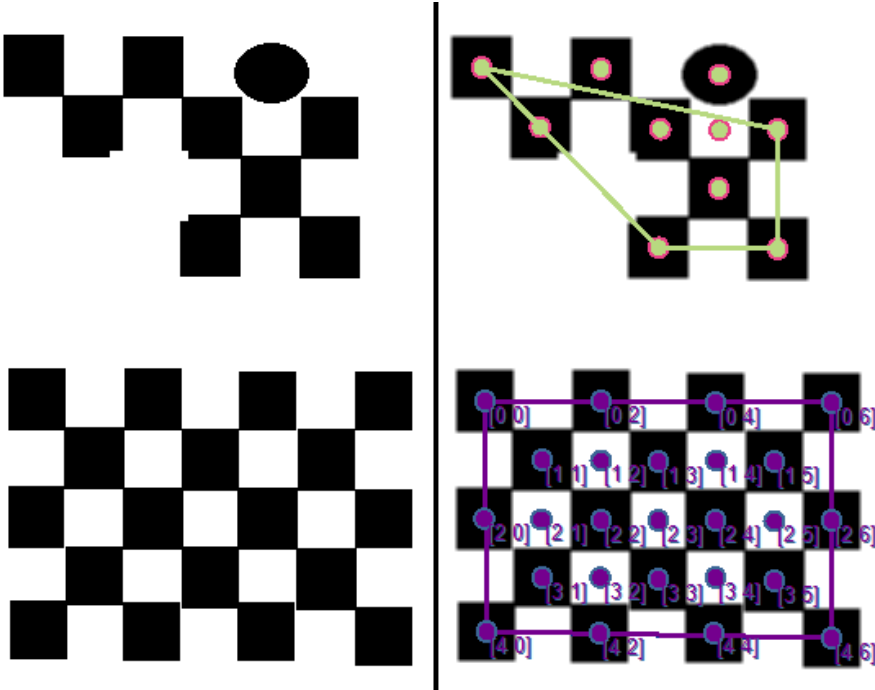


FIGURE 4.10 – Visualization of neighboring regions. Regularity analysis proposed in this work allows recognizing the bottom image as a checkerboard.

TABLE 4.3 – Criteria for robust identification of adjacent regions

Subjective criterion	Relevant properties	Mathematical models
Adjacent regions must be close to each other	Region centers, mean sizes and mean radii	$Dist(Center_1, Center_2) < 14 + 2MeanSize_1 + 9.8MeanRadius_1$ $Dist(Center_1, Center_2) < 14 + 2MeanSize_2 + 9.8MeanRadius_2$ Note: The constant 14 has been added to compensate for pixels assigned to edges instead of color regions
Adjacent regions should be separated (no overlap)	Region centers, mean sizes and mean radii	$\frac{\max(MeanSize_1, MeanSize_2)}{Dist(Center_1, Center_2)} < 1$
Geometric properties of adjacent regions should be similar	Region areas and perimeters	$\frac{\max(Area_1, Area_2)}{\min(Area_1, Area_2)} < 1.7$ $\frac{\max(Perimeter_1, Perimeter_2)}{\min(Perimeter_1, Perimeter_2)} < 1.7$

It is worth noting that, as discussed in Section 4.4.1, checkerboards are particular cases of neighboring regions which have specific regularity properties. New algorithms

can build up on this concept to identify other neighboring region patterns and create new custom optical markers.

4.4 Recognition of Specific Optical Marks

4.4.1 Checkerboards

Checkerboard identification can be accomplished by counting the number of contiguous color regions in the group as well as checking the regularity of internal places.

A post-processing step applied to the group of neighboring region locates the corners of the checkerboard and fits a rectangle to the point cloud as detailed in Algorithm 2:

Algorithm 2: Identification of checkerboard corners

Input: Location of the centers of each region in a group

Output: Indexes of the four regions which are the corners of the checkerboard

Compute the convex hull of contiguous color region centers grouped to the same region (details in Section 4.4.1.2);

Initialize the region map by assigning each pixel a unique color number;

for *each vertex in the convex hull* **do**

\lfloor Compute the angle between the lines formed by $v_n \rightarrow v_{n-1}$ and $v_n \rightarrow v_{n+1}$;

Sort vertexes by their angle;

Keep the first four vertexes and discard regions whose opposing angles are too different.

Number of squares in checkerboards should not be smaller than 5x7 because the tests showed that cluttered scenes are less likely to generate false positives (see Appendix A). Random patterns on the ground generate false checkerboard positives, as shown in Figure 4.11. This scenario is unusual in real applications because optical marks will be stuck onto equipment parts and modules, which have homogeneous colors (no cluttered background). Moreover, applying blur filter proved effective to prevent this problem and it is unlikely that such an identification would remain consistent across multiple images such as in a video stream. The maximum number of checkerboard squares is 21x21, which is appropriate for field construction and assembly applications.

4.4.1.1 Planar Checkerboard Structure

Planar checkerboards can be used to identify equipment parts whose curvature is low to the point that an optical mark stuck to its surface would not suffer considerable deformations. In our implementation, we require the edges of the checkerboard to be composed of black squares, as shown in Figure 4.12.



FIGURE 4.11 – Checkerboard false positives.

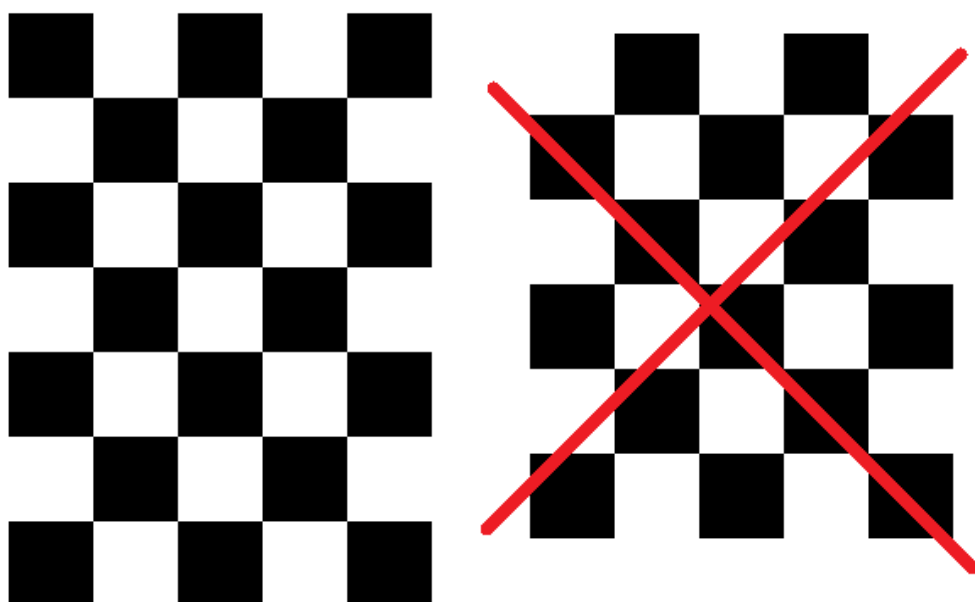


FIGURE 4.12 – Checkerboard structure. Left: valid checkerboard. Right: invalid checkerboard.

The proposed methodology can be applied in the development of systems with multiple calibrated cameras that would allow extraction of normal vector information from the checkerboard markers ensuring that part orientation as well as positioning is correct.

4.4.1.2 Regularity Analysis

Once checkerboard dimensions are known, it is possible to estimate where the centers of its internal regions should be located. Checkerboard regularity analysis is performed in groups of contiguous color regions according to Algorithm 3:

Algorithm 3: Assignment of the centers of the internal regions of a checkerboard

Input: Location of the centers of each region in a group

Output: 2D indexes of each group region corresponding to positions in a $N \times M$ checkerboard

Apply the convex hull algorithm using the 2D center of the contiguous region to find border squares;

Compute and store predicted square locations using the four outer black squares as a reference;

if region group being analyzed has enough regions **then**

└ assign regions to their closest checkerboard position;

Reject checkerboard if more than one region is assigned to the same position.

Detailed analysis of the regularity analysis algorithm is provided in this section.

The convex hull is computed using Andrew's algorithm (ANDREW, 1979), and a rectangle is fit to the computed region centers as shown in the top right region of Figure 4.10. The best square that fits the data is then computed using Algorithm 4:

Algorithm 4: Best square that fits a set of 2D points

Input: List of 2D coordinates of points

Output: Four points in the list that best approximate the set with a rectangle

Given a 2D point P_k , compute its associated angle θ_k from line segments $\overline{P_{k-1}P_k}$ and $\overline{P_kP_{k+1}}$;

Sort points in descending order according to their associated angle;

Return $N = 4$ points with smallest angle values - border points B_0 to B_4 .

At this point, the algorithm checks if the region group (containing N_R regions) being analyzed is a candidate for a checkerboard of size $N \times M$. A total of $(N - 2)(M - 2) + N + M - 2$ squares is expected.

The group is rejected as not having enough regions if $N_R < (N - 2)(M - 2) \cdot p_{Checker} + N + M - 2$. It is also rejected as having too many regions if $N_R > (N - 2)(M - 2) + N + M - 2$. The parameter $p_{Checker}$ defines the percentage of inner squares that must be identified. It has been manually tuned to 0.4 in this work. This value allows checkerboard recognition

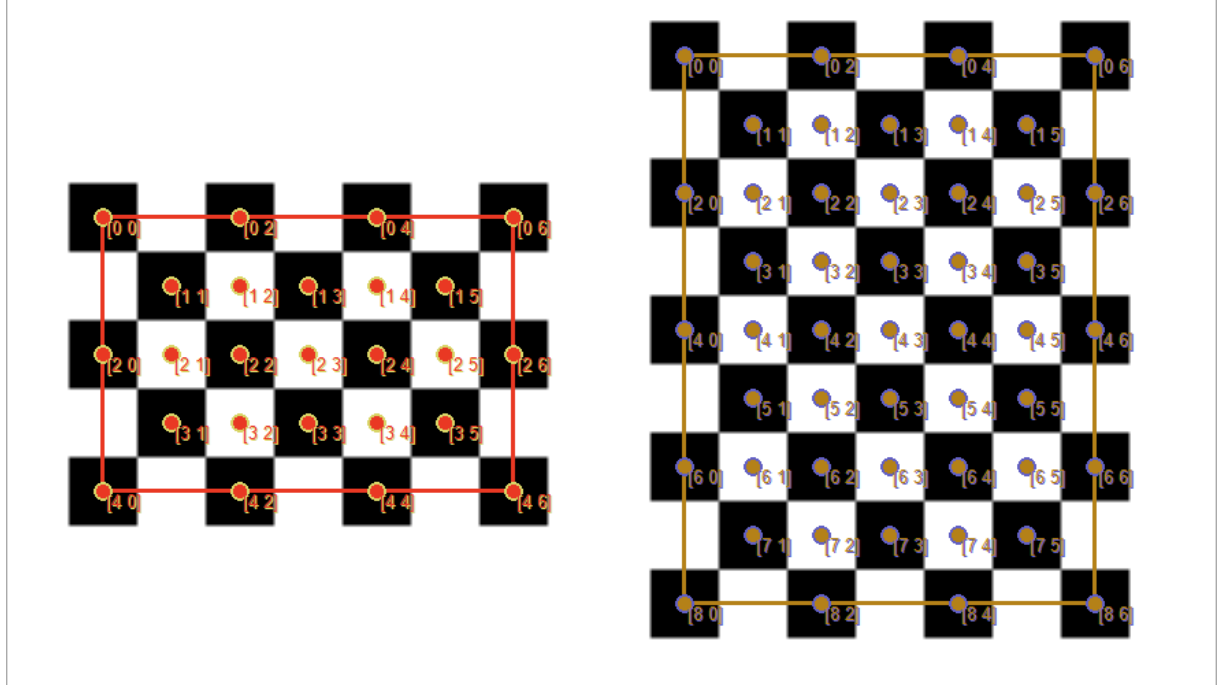


FIGURE 4.13 – Assignment of checkerboard positions to each color region. Number of squares is identified automatically.

while still being robust to occlusion, provided that border squares are visible.

If the group region is accepted, the **square center prediction-match** is used to associate color regions to checkerboard square centers. Equation 4.1 allows predicting the position of the (i, j) th square, $C_{i,j}$ ($MidPt$ is defined in Equation 4.2).

$$C_{i,j} = MidPt(MidPt(\mathbf{B}_0, \mathbf{B}_3, \frac{i}{N-1}), MidPt(\mathbf{B}_1, \mathbf{B}_2, \frac{i}{N-1}), \frac{j}{M-1}), \quad (4.1)$$

$$MidPt(\mathbf{A}, \mathbf{B}, \alpha) = \mathbf{A} + \alpha \cdot (\mathbf{B} - \mathbf{A}). \quad (4.2)$$

The center property of each region in the group is then used to assign the region to its nearest predicted center. If multiple regions are assigned to the same center, the group is considered to be an invalid $N \times M$ checkerboard and it is rejected. If all conditions are met, the group is a valid $N \times M$ checkerboard and to each of its regions an index (i, j) is assigned according to the nearest predicted center $C_{i,j}$.

Regularity analysis allows for automatic identification of checkerboard dimensions by successively checking different sizes, as shown in Figure 4.13 (synthesized) and Figure 4.14 (picture taken with commercial camera, automatic settings).

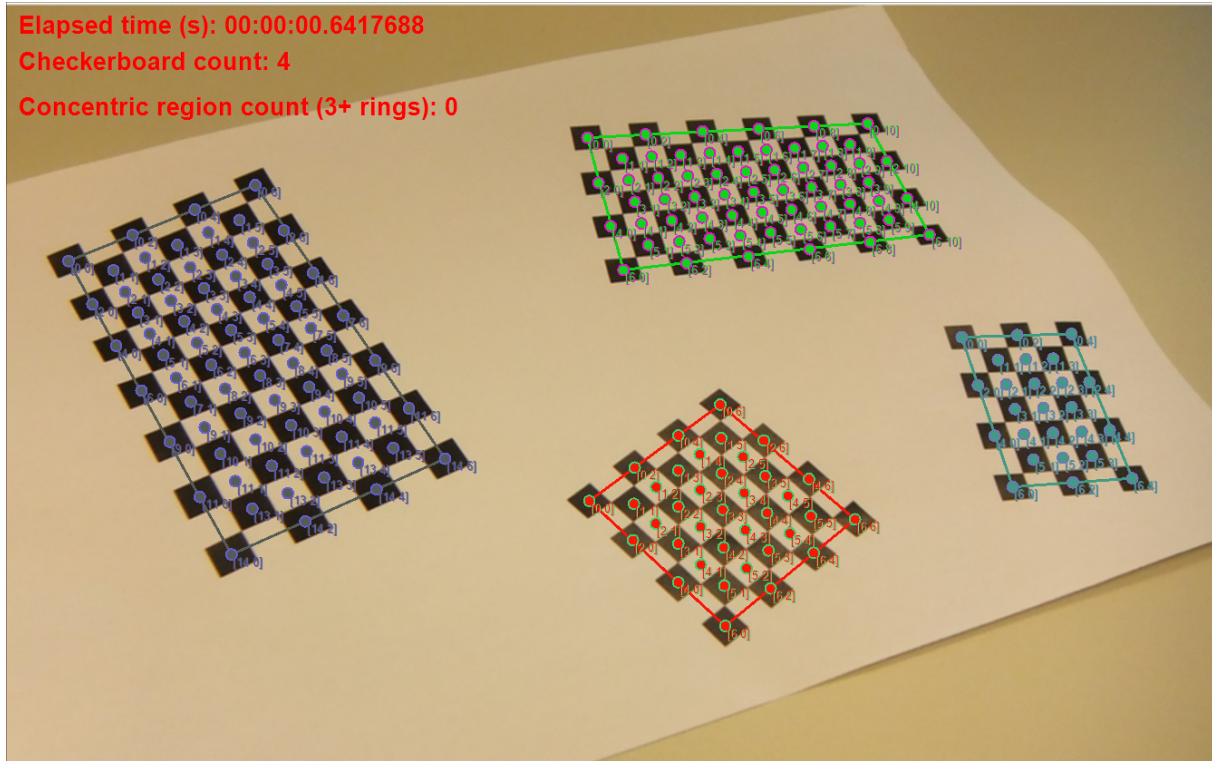


FIGURE 4.14 – Automatic identification of checkerboard sizes inside image. Number of squares: 15x7, 7x11, 7x7 and 7x5.

4.4.1.3 Robustness to Occlusion

Regularity analysis can compensate for partial occlusion in checkerboard squares. Neighboring region groups may be partially occluded or its internal regions may not have been identified properly due to the lighting conditions. In these cases, comparing actual identified region centers to expected square positions enable checkerboard recognition even when many squares are missing, as long as the four corner squares are visible. Note that regularity analysis will accept checkerboards even when not all predicted positions in the checkerboard are occupied by a color region. Figure 4.15 shows examples of occlusion patterns under which checkerboard identification would still succeed.

4.4.2 Targets

Robust identification of targets (groups of concentric regions) can be achieved by analyzing each contiguous color region data properties as summarized in Table 4.4, where mathematical models uses the region data properties. Values used in the implementation of the criteria were obtained by trial and error during tests performed in the development of the algorithm. The proposed criteria allow the system to cluster concentric regions whose width is approximately equal. All adjacent concentric annuluses are then grouped together in a concentric region.

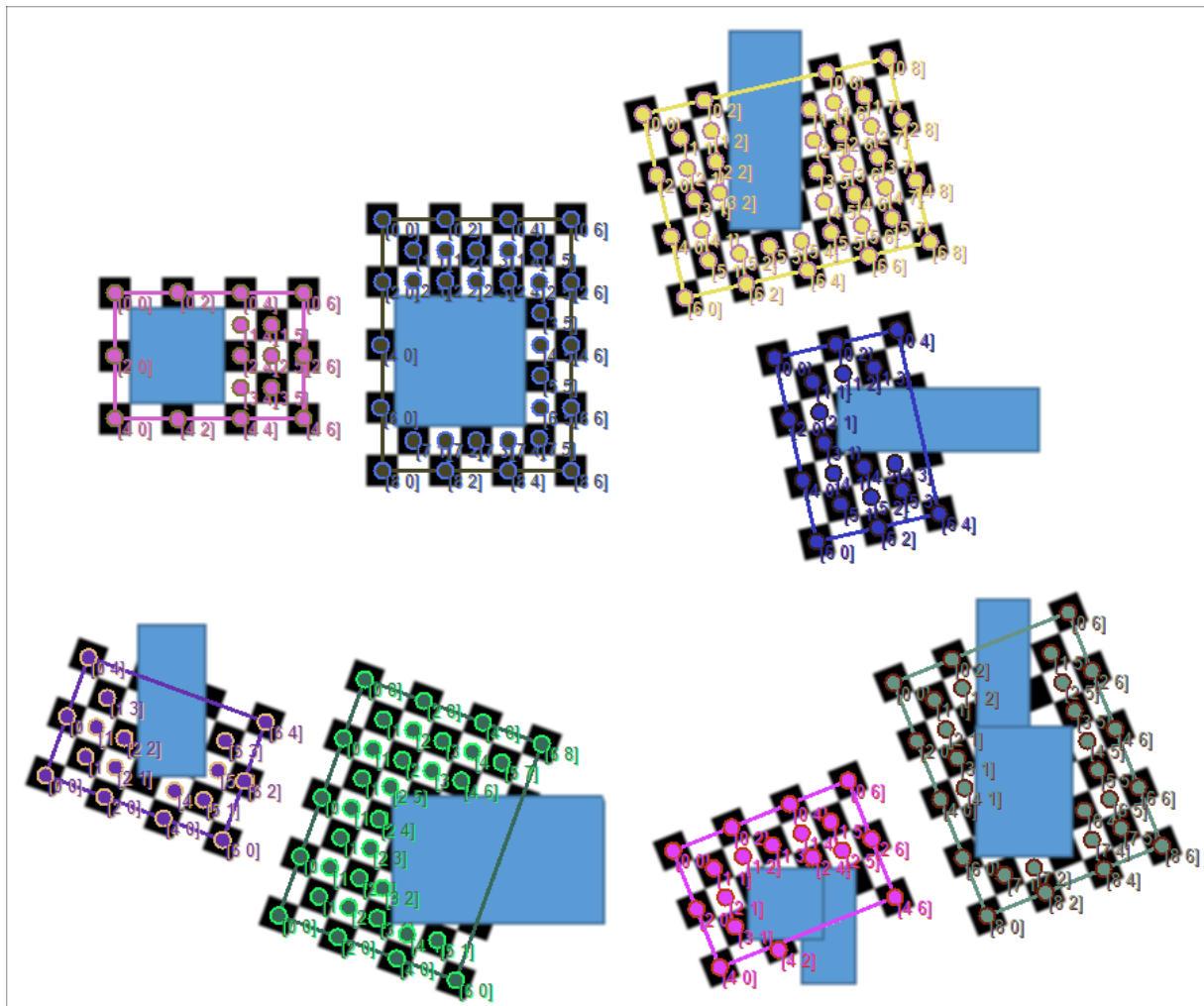


FIGURE 4.15 – Robust checkerboard identification under occlusion. Dimensions are identified automatically. Corner squares must be visible for proper identification.

TABLE 4.4 – Criteria for robust identification of targets

Subjective criterion	Relevant properties	Mathematical models
Contiguous color region must look like a circular ring	In a circular ring there is a constant ratio: $\frac{\text{Perimeter} \cdot \text{Width}}{\text{Area}} = 2$	$\frac{\text{Perimeter} \cdot \text{MeanRadius}}{\text{Area}} < 3$
In a circular ring, typically $r > w$	Circular ring properties: r and w	$\frac{\text{MeanSize}}{\text{MeanRadius}} > 0.5$
Adjacent centers of rings which compose concentric regions must be close	Distance between region centers and their widths (reference of scale)	$\frac{\text{Distance}(\text{Center1}, \text{Center2})}{\min(\text{MeanRadius}_1, \text{MeanRadius}_2)} < 1.3$
Widths of adjacent rings should be approximately equal	Width w of the regions	$\frac{ \text{MeanRadius}_1 - \text{MeanRadius}_2 }{\min(\text{MeanRadius}_1, \text{MeanRadius}_2)} < 1.5$

After identifying contiguous color regions, it is possible to extract and store region data, such as which pixels belong to each region (list of [x,y] coordinates) and from there compute parameters presented in Table 4.1. Combinations of these parameters allow the identification of targets (concentric regions - annuluses of the same color whose center is close, as shown in Figure 4.16) and neighboring regions (adjacent color regions without overlap whose properties are approximately equal). Targets are identified by a string related to their color sequence, according to the following key:

- W: white;
- P: black;
- R: red;
- G: green;
- B: blue;
- ?: unknown color (not identified as W, P, R, G or B).

For example, a sequence RWP?G means that the color of the inner region is red, followed by white, black, unidentified color and green. Figures 4.17 and 4.18 demonstrate results of the proposed algorithm.

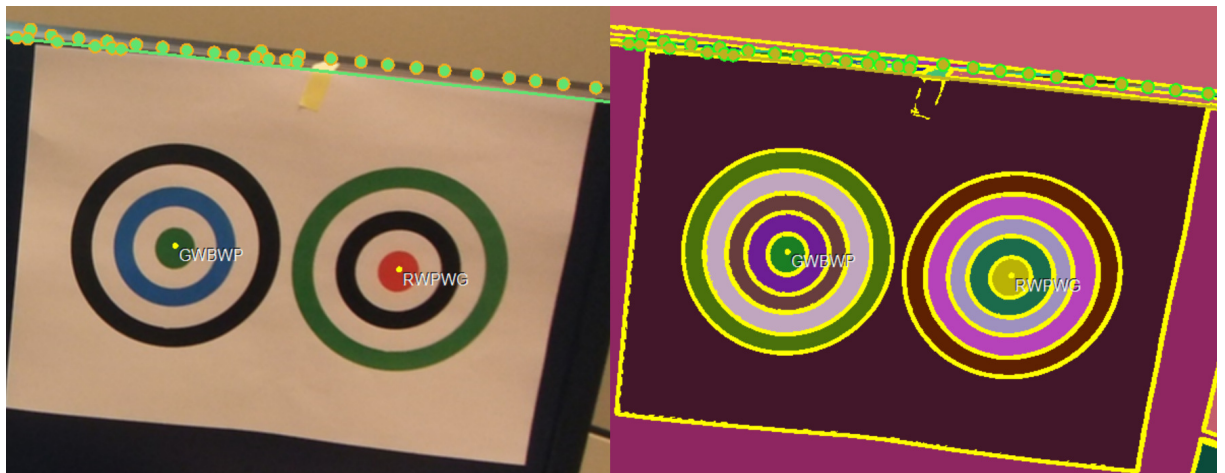


FIGURE 4.16 – Identified targets with proper label. Left: cropped picture Right: identified contiguous color regions. GWBWP and RWPWG are target color label strings, denoting the sequence of colors from the inside out.



FIGURE 4.17 – Picture from (JIANG; QUAN, 2005) processed by our methodology. The middle circle was edited to remove its marks.

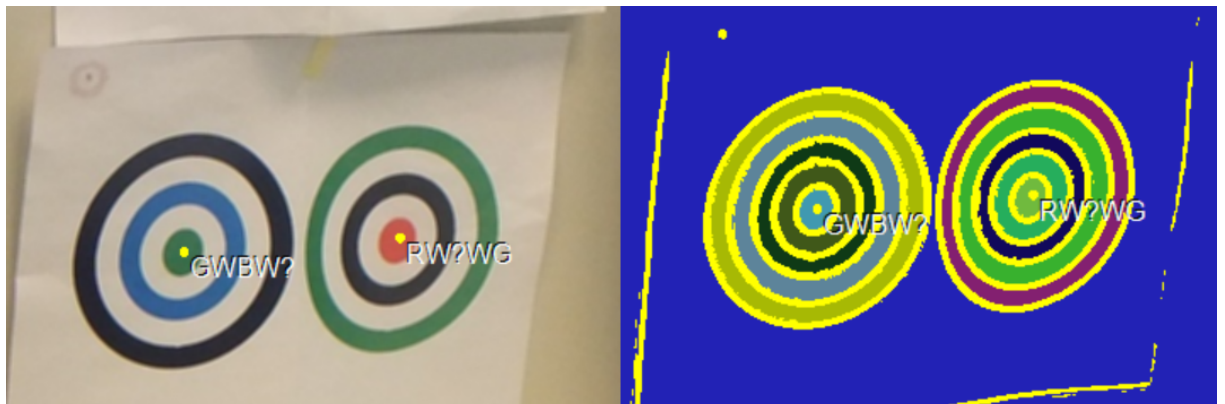


FIGURE 4.18 – Partially identified targets. Chromatic variations impair proper color classification. Left: cropped picture Right: identified contiguous color regions.

TABLE 4.5 – Algorithm runtime for processing full HD (1920x1080) images. Times in seconds. Average values - 10 runs.

Algorithm step and execution hardware	Core i5-3317U 1.7GHz + Intel HD 4000 GPU	Xeon X5650 2.66 GHz + Tesla C1060	Core i7 3820 3.6GHz + Radeon 7970
Median filter (GPU)	0.45	0.18	0.1
Contiguous color detection (GPU)	0.29	0.14	0.1
Pixel list per color region (CPU+GPU)	0.19	0.14	0.15
Region data information (parallel CPU)	0.41	0.26	0.22
Total time	1.34	0.72	0.57

4.5 Considerations About Running Time

All algorithms were implemented using Microsoft Visual C# 2010 and OpenCL to offload workload to the GPU. Table 4.5 shows computing times for a full HD (1920x1080) picture and describes which hardware is used for each step when extracting region data information that is used for concentric region and neighborhood computation. These figures were obtained using hardware that was available for this research. Note that GPU computation of Sobel borders takes negligible time in comparison to the other steps. In addition, although computation of median filter yields the best results, a simpler blur filter takes negligible time and still produces acceptable results. Note that, while there are very fast optical marker recognition algorithms that run even in smartphones, these are not designed to be robust under different lighting settings or occlusion.

The proposed parallel filling algorithm for contiguous color detection is designed to run in parallel and fits nicely the SIMD (Single Instruction, Multiple Data) structure of GPUs since all workitems perform approximately the same amount of computation per kernel launch.

Segregation of region pixels and computation of region data properties, on the other hand, are better suited to the MIMD (Multiple Instruction, Multiple Data) structure of the GPU considering that the number of pixels per region may vary considerably.

Runtime of the proposed algorithm was compared to that presented in (DUO-LE; MING, 2011). Their reported runtime to identify a 100 pixel radius circle, a 100x100 square and a random pattern (their three test cases) they created was 38017 ms, although that is probably a typo and their real result should read 380 ms. To fully exploit GPU parallelism, a joint image with multiple circles, squares and pattern was created. Its dimensions are 1200x1000 pixels, whose region filling is presented in Figure 4.19. Note that the proposed

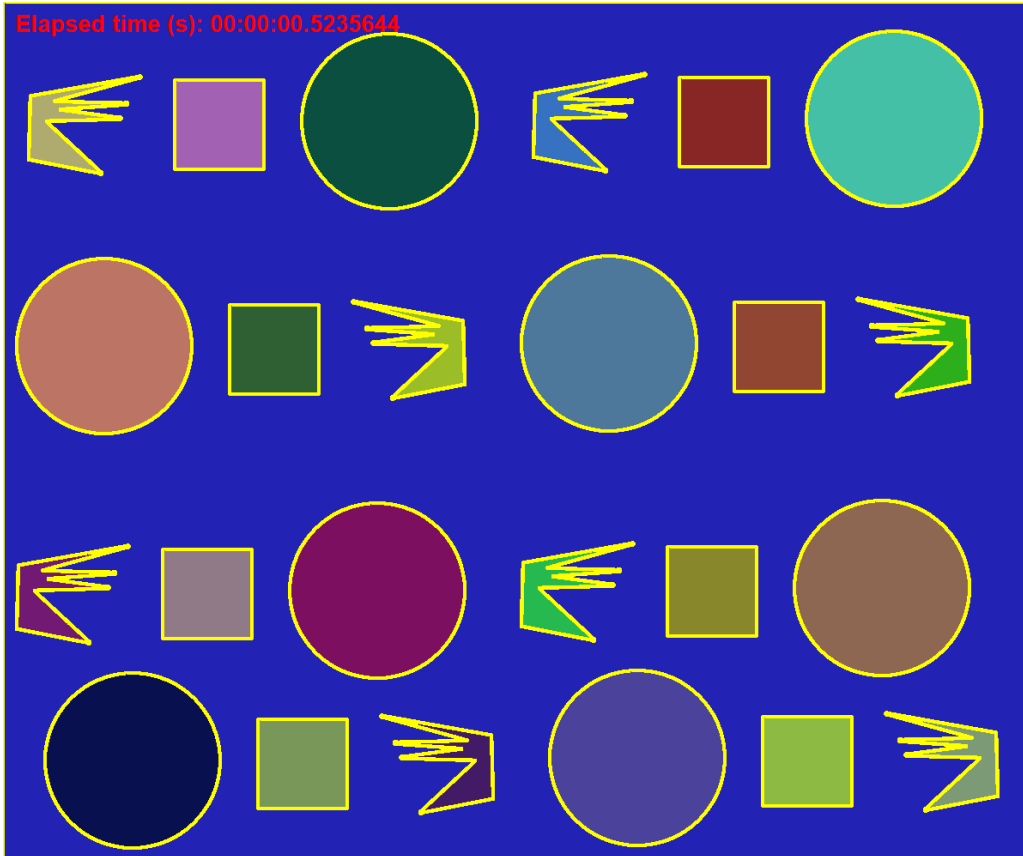


FIGURE 4.19 – Region filling image for runtime comparison purposes.

methodology requires no seed points and runs in 523 ms using the Intel HD 4000, 482 ms in the Tesla C1060 and 282 ms in the Radeon 7970, which is $380/(282/24) = 32$ times faster despite the extra time spent filling background pixels which alone would probably take way longer than filling the patterns since it has as many pixels as the other regions combined.

4.5.1 Preliminary Optical Marker Detection

In real applications, machine learning techniques can be used to allow detection of optical markers that appear small in the image and guide the camera automation system to zoom in to image locations where optical markers are likely to be found, by providing bounding boxes. In order to obtain a preliminary bounding box of the optical marker, a single hidden layer feed-forward neural network was trained to recognize optical markers. Color Haar features are extracted from the pictures using an OpenCL implementation of image integrals (VIOLA; JONES, 2001), as shown in Figures 4.20 and 4.21. This method has the advantage of that it does not require edge information, but precise optical marker location still requires the refinements implemented in the proposed methodology to be able perform OMR robustly.

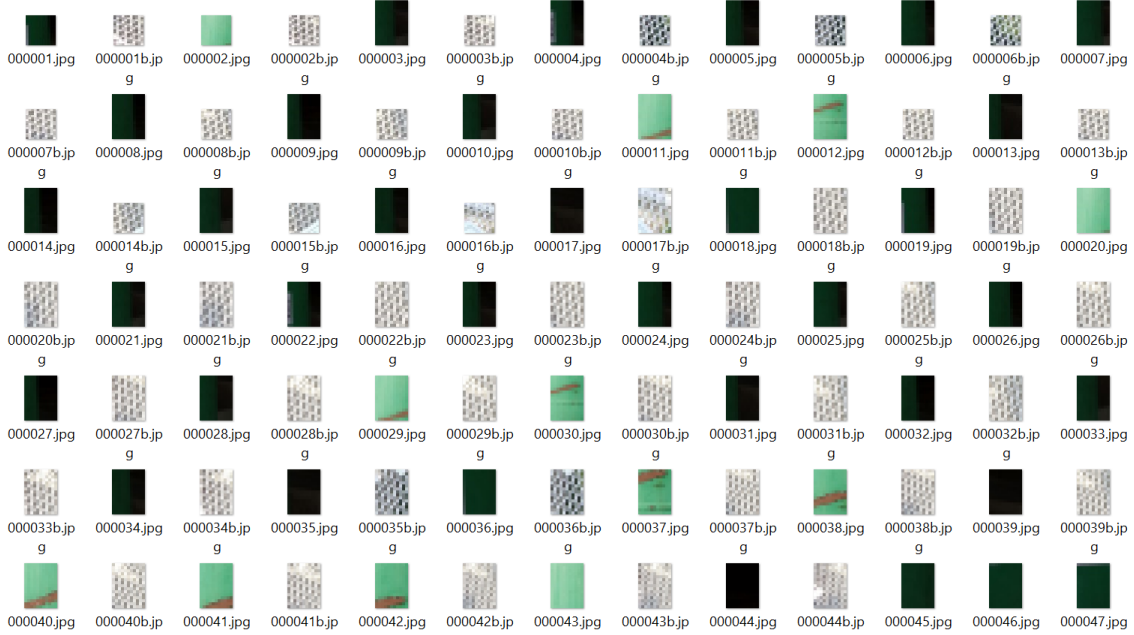


FIGURE 4.20 – Extracted images containing samples of the environment.

The industrial area of Petrobras’ Research Center (CENPES) was used to obtain a database of markers and environment consisted of 564 training images and 112 test images (obtained in a different environment). In each iteration, the training images were randomly split into a direct training set of 518 images and the remaining 46 were used as validation set.

Considering that optical markers are *designed* to be easily identified, a very high accuracy is expected. In fact, using a neural network with a single hidden layer yields 99.5% accuracy in the test set. The classifier’s precision is 100% and recall is 90% which indicates that, taking into consideration the higher performance of neural networks in visual tasks, this approach is valid for initial bounding box extraction prior to refinement using the proposed methodology to obtain more precise optical marker position and orientation.

4.6 Identification Layout for Parts and Equipments

A layout for identification of metal plates was used for validation in a joint research project conducted by Petrobras and ITA. In these tests, fixation of the optical markers was tested and successfully demonstrated that an optical system can be used to control robots for part positioning and identification. The robust OMR methodology was not fully developed at the time of the tests and the scope of the project only included indoor testing. Nonetheless, proper feedback using computer vision techniques was sufficient for position control, as shown in Figures 4.22 and 4.23, and future research can incorporate the methodology presented in this work for position feedback.

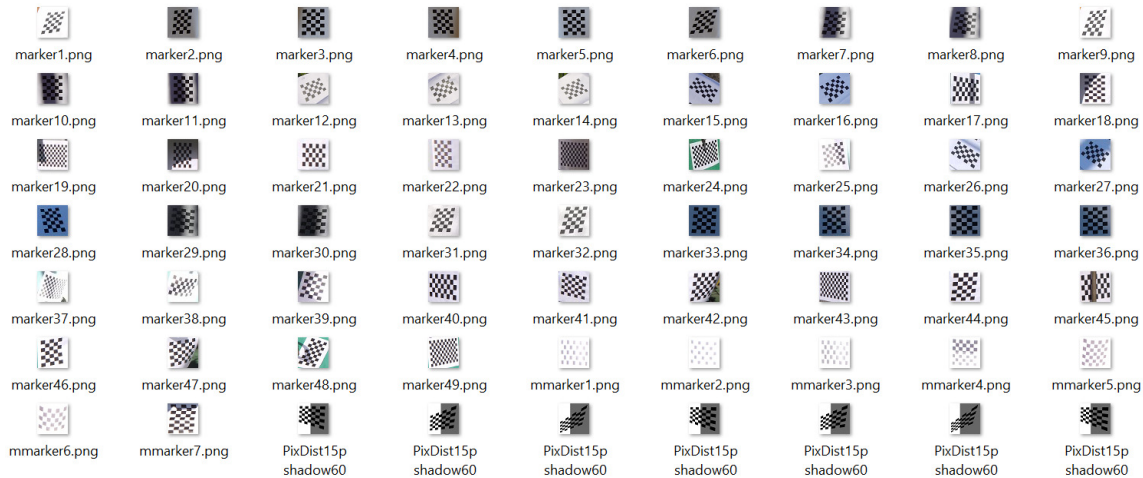


FIGURE 4.21 – Extracted images containing samples of optical markers (checkerboards) in the presence of non-uniform lighting and perspective.

The combination of robust optical markers for part recognition and Quick Response (QR) codes has also been considered as a possibility for field identification of parts (Figure 4.24).

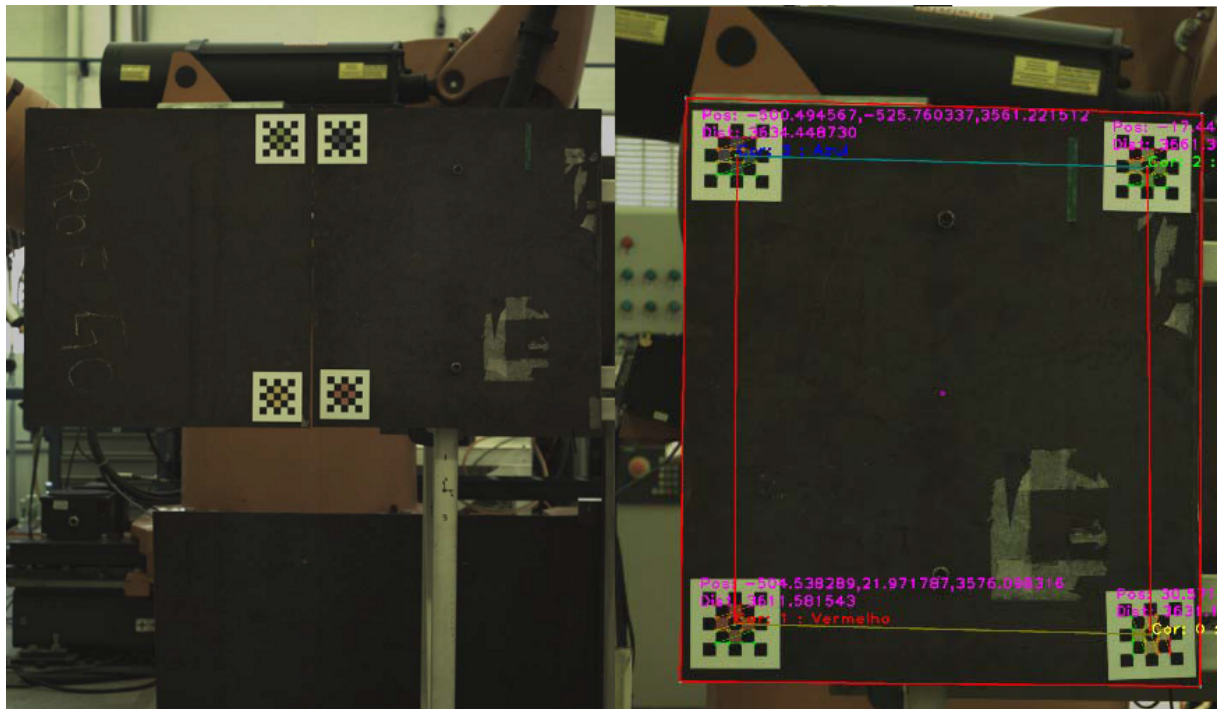


FIGURE 4.22 – Left: Plates aligned using robotic systems, aided by optical markers. Right: visual identification feedback in the identification system. From CCM-LAM digital database.

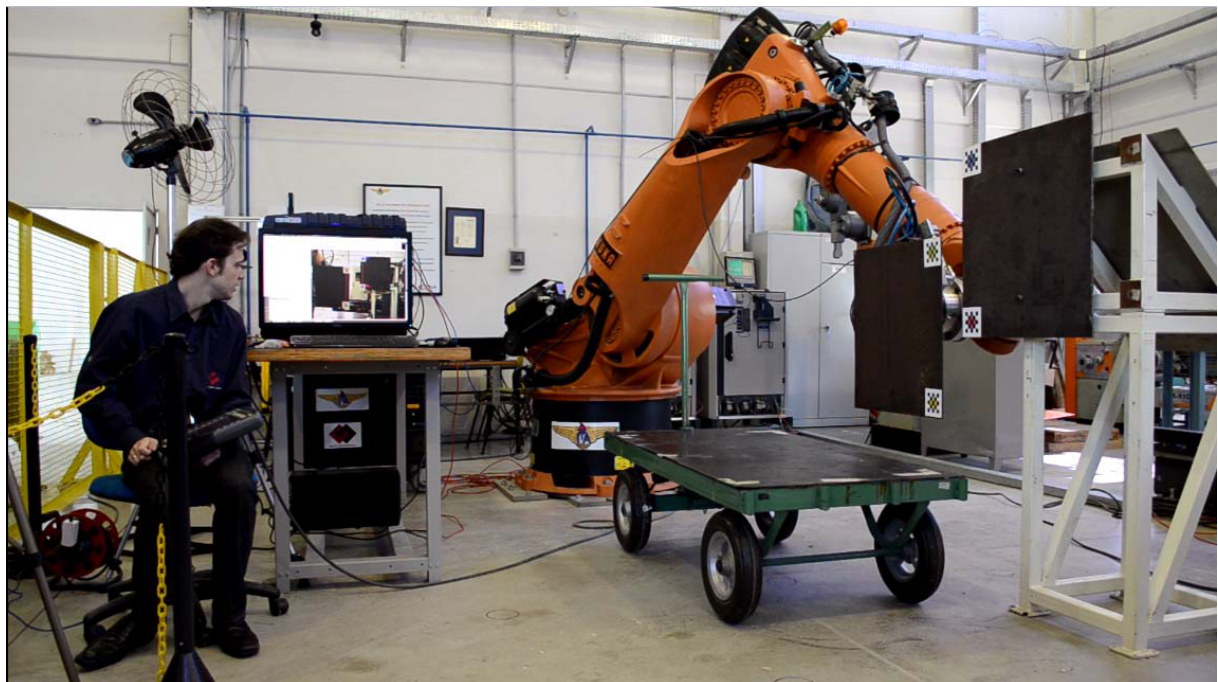


FIGURE 4.23 – Automatic positioning of plates with robots using optical marker feedback. From CCM-LAM digital database.

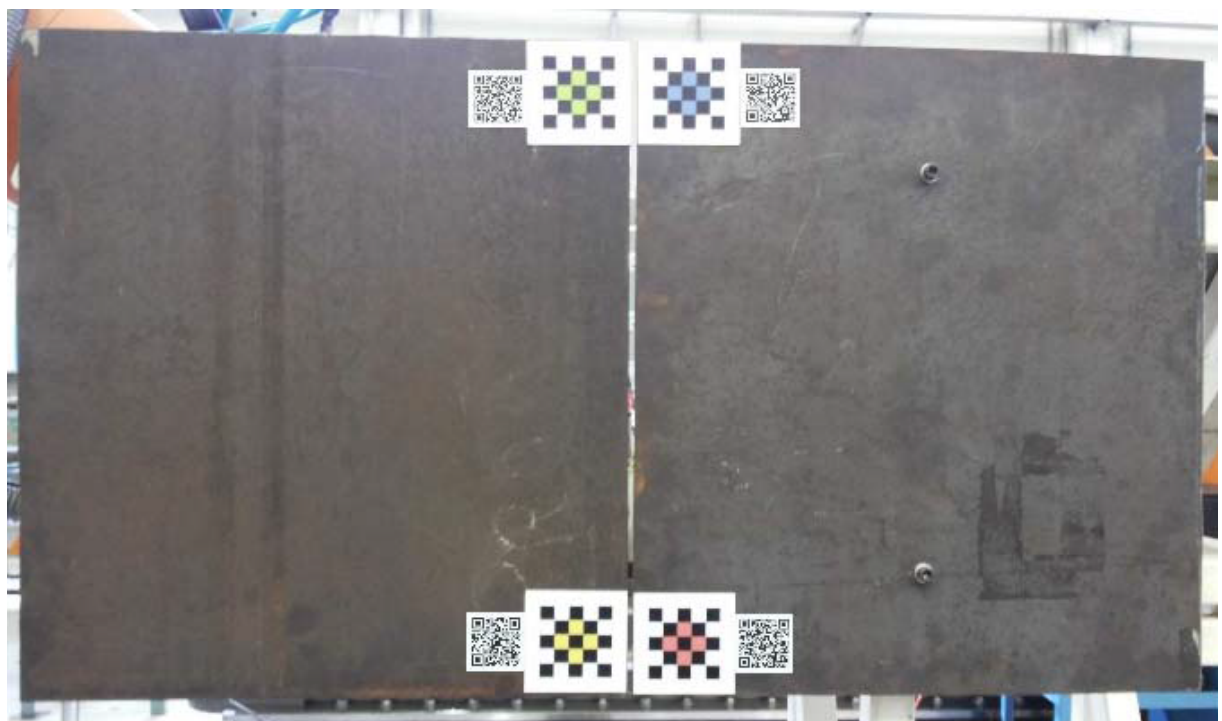


FIGURE 4.24 – Combination of optical markers for recognition and QR codes for information retrieval. From CCM-LAM digital database.

5 Results and Discussion

In order to identify parts and modules, checkerboards can be designed to use different inner square count layouts or color patterns for unique identification, but this uniqueness is still difficult to guarantee. Targets are specially promising considering that their center is essentially invariant to the camera pose. Using the proposed methodology, all information is simultaneously available basically for free (i.e. requiring negligible extra computation) once contiguous regions and their properties are computed. Combinations of targets and checkerboards can be used (Figure 5.3) to compute rough position estimates with identification and checkerboards for local normal vector estimate and position fine-tuning using well-established algorithms such as the one proposed by (ZHANG, 2000). Color codes may be used to add information and uniquely identify checkerboards.

Even though there is no algorithm or quantitative measure guide for the Augmented Reality Toolkit (ARToolKit) (KHAN *et al.*, 2015), and that its algorithm is not designed for outdoor applications, the proposed methodology was qualitatively compared to AR-ToolKit with regards to robustness. Figures 5.1 and 5.2 demonstrate that very slight occlusion or variation in lighting is enough to disrupt ARToolKit's identification capabilities, whereas the proposed OMR methodology still gives correct results.

The proposed methodology presents robust checkerboard identification capabilities, as demonstrated in Figure 5.4.



FIGURE 5.1 – ARToolKit OMR. Left: identified optical marker (rectangle with text “Hiro”). Center: slight occlusion prevents marker identification. Right: slight variation in lighting prevents marker identification.

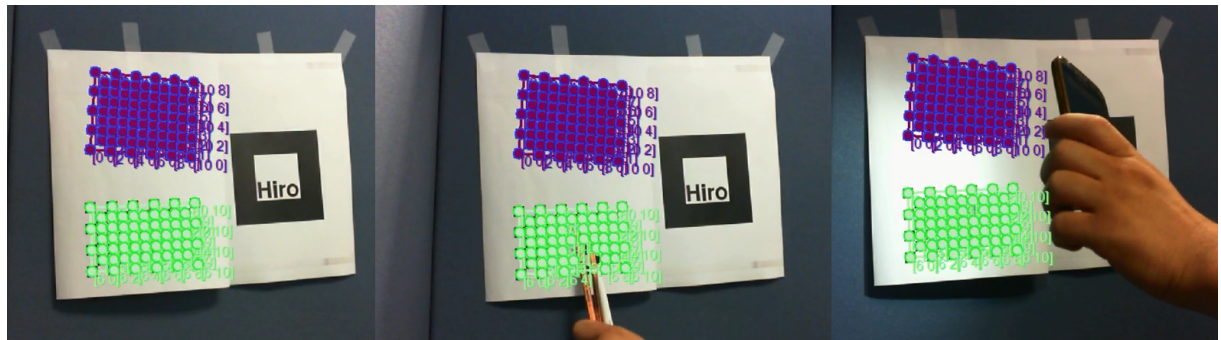


FIGURE 5.2 – Proposed robust OMR methodology. Left: identified optical markers (checkerboards). Center: robustness to occlusion. Right: robustness to variation in lighting.

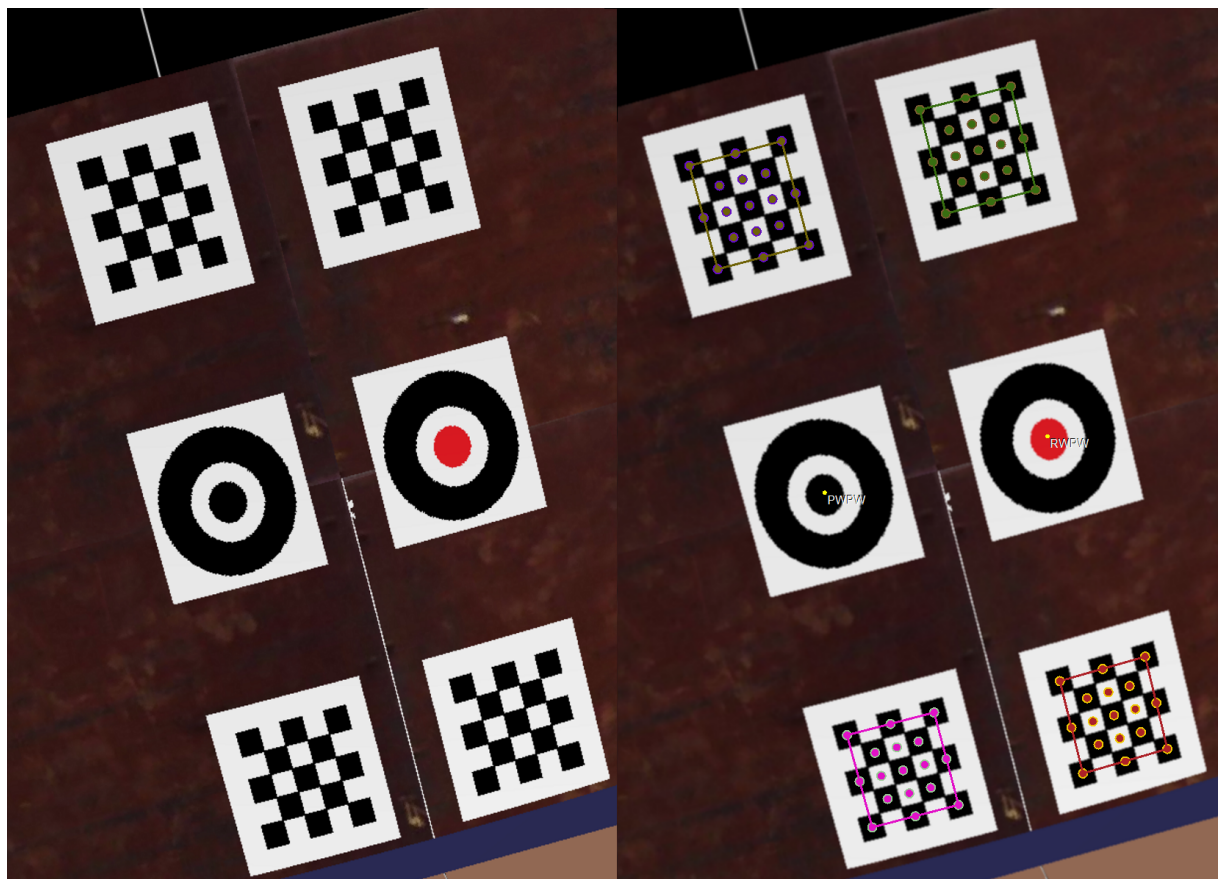


FIGURE 5.3 – OMR in storage tank plates. Left: detail of simulated camera input. Right: desired recognition software output.

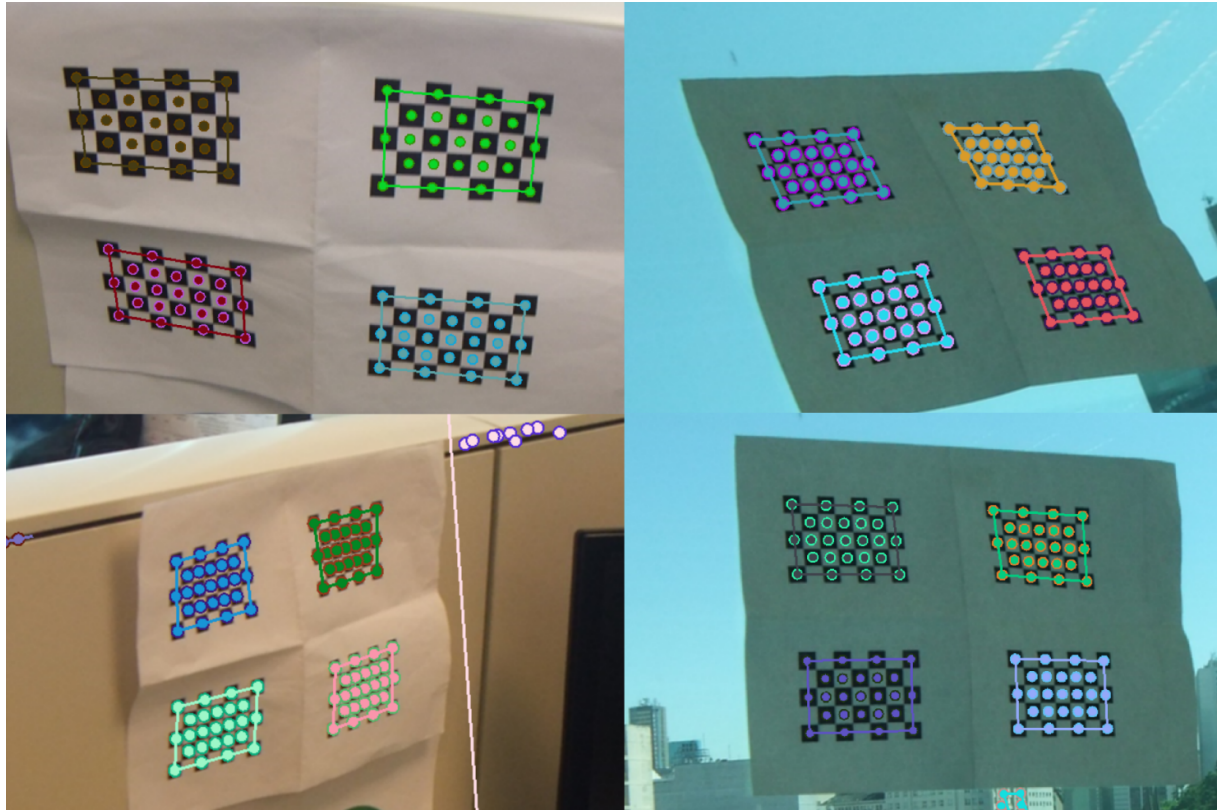


FIGURE 5.4 – Simultaneous multiple checkerboard identification under highly variable lighting and orientation settings.

5.1 Indoor and Outdoor Optical Mark Recognition

An experiment has been designed to check the robustness of the proposed methodology. A total of 90 images containing four checkerboard patterns and two targets containing five concentric regions (see Figure 5.5) were photographed using different cameras and settings (see details in Table 5.1), generating a total of 360 checkerboard samples and 180 target samples. The markers were printed using regular ink and A4 paper to simulate scenarios where markers are not specifically manufactured for the application.

In the tests performed, pre-filtering with a simple homogeneous Gaussian filter was enough to reduce noise while still maintaining edges identifiable at a negligible computational cost due to use of GPU acceleration via OpenCL. Median filtering provides the best noise removal while still preserving borders and allows detection of patterns from greater distances; simple Gaussian filter, however, still provided good results without the large computational burden of median filter. In addition, camera resolution and distance to optical markers can be controlled in an outdoor industrial environment, eliminating the need to identify very small regions.

Four lighting conditions were used as a means to simulate possible field conditions (Table 5.2). Worst case scenarios are hard shadows and sunlight reflection on ink (Sec-

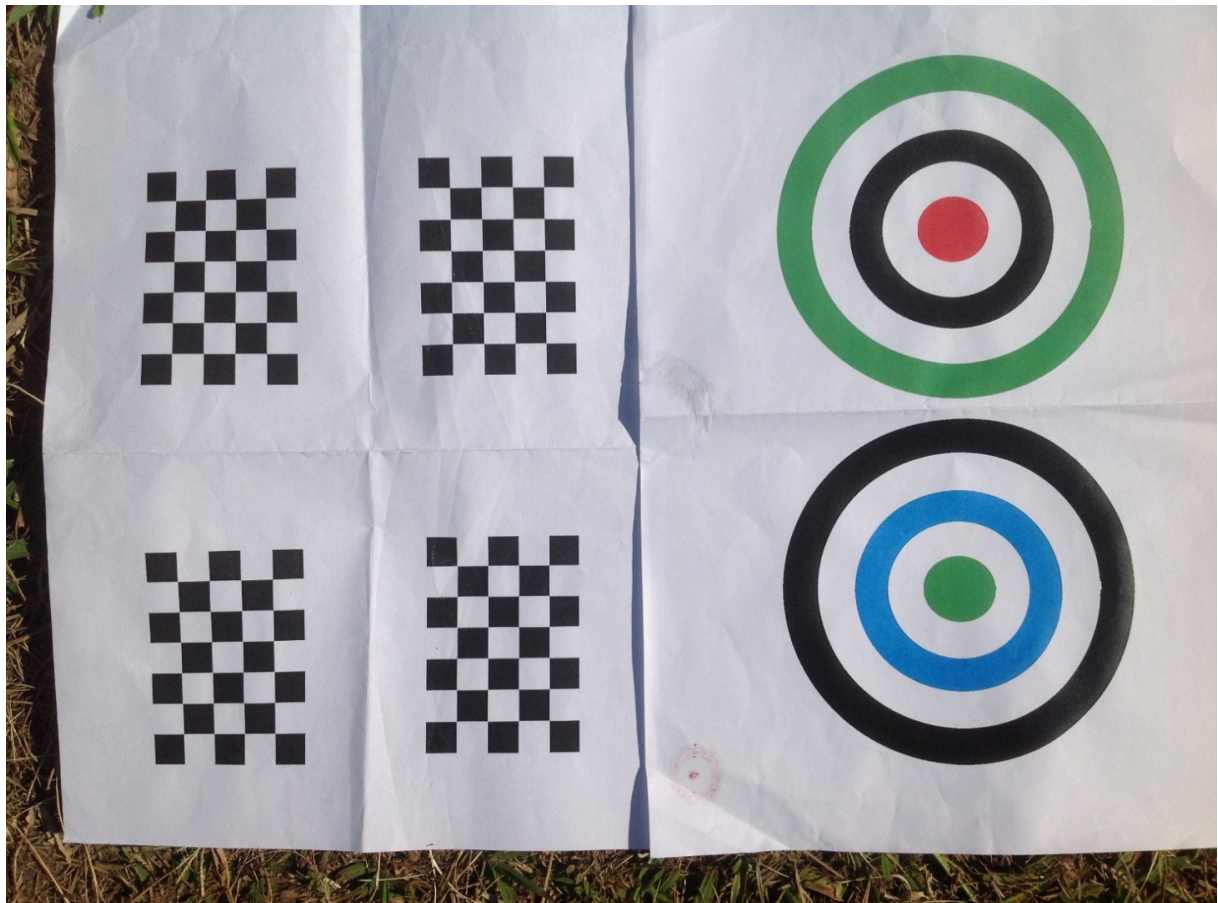


FIGURE 5.5 – Checkerboard and target patterns used to test robustness of proposed methodology.

TABLE 5.1 – Relevant parameters for outdoor optical mark recognition

Controlled variable	Possible values
Camera brand	Apple iPad 3 camera / Fuji W1 3D / Sony Cybershot DSC-WX7
Algorithm filter	None / Gaussian / Median
Environment	Indoor / Outdoor
Perspective	Frontal / Side / Skewed
Lighting	Direct light / Uniform shadow / Soft shadow / hard shadow

TABLE 5.2 – Field lighting conditions

Condition	Lighting condition on marker	Possible scenarios
Direct light	Direct daylight	Sunlight hitting marker directly
Uniform shadow	Only ambient light	Marker facing direction opposite to sun or cloudy environment
Soft shadow	Smooth transition light / shadow	Shadow from cloud/part partially cast on marker
Hard shadow	Harsh transition light / shadow	Shadow cast from cranes and robots on top of marker

TABLE 5.3 – Performance criteria for the proposed identification algorithm

Criterion	Desired value per picture
True 5x7 checkerboards	4
False checkerboards	0
Targets with five concentric regions	2
Correctly identified concentric region in targets (proper color ID)	10
False target with three or more concentric regions	0

tion 5.4) and these should be addressed using low pixel noise cameras and less reflective ink. The Fuji W1 camera uses two CCD sensors while the DSC-WX7 and the iPad 3 use a CMOS sensor. Color images were obtained in RGB format (1 byte per color). Proper color identification depends on the color filter array used to acquire the image and thus color recognition requires calibration.

Figures 5.6, 5.7 and 5.8 show sample images used to test the methodology and the respective results. When using the system for part identification, one is interested in optical mark recognition as well as its unique identification. As proposed in Section 4.3, the combination of targets and checkerboards allows better identification and geometric parameter estimation. Considering these factors, the performance of the algorithms used to perform OMR has been measured with criteria shown in Table 5.3.

5.2 Analysis of the Experiments

Table 5.4 summarizes identification performance of the proposed OMR methodology. The test cases, obtained from 90 pictures with 4 checkerboards and 2 targets each, were used as input to the Analysis of Variance (ANOVA) to detect which parameters have influence in OMR. Pictures and further analyses are shown in Appendix A. It is worth mentioning that OMR is not intended as a metrology system and that computing these parameters would require specific system calibration.

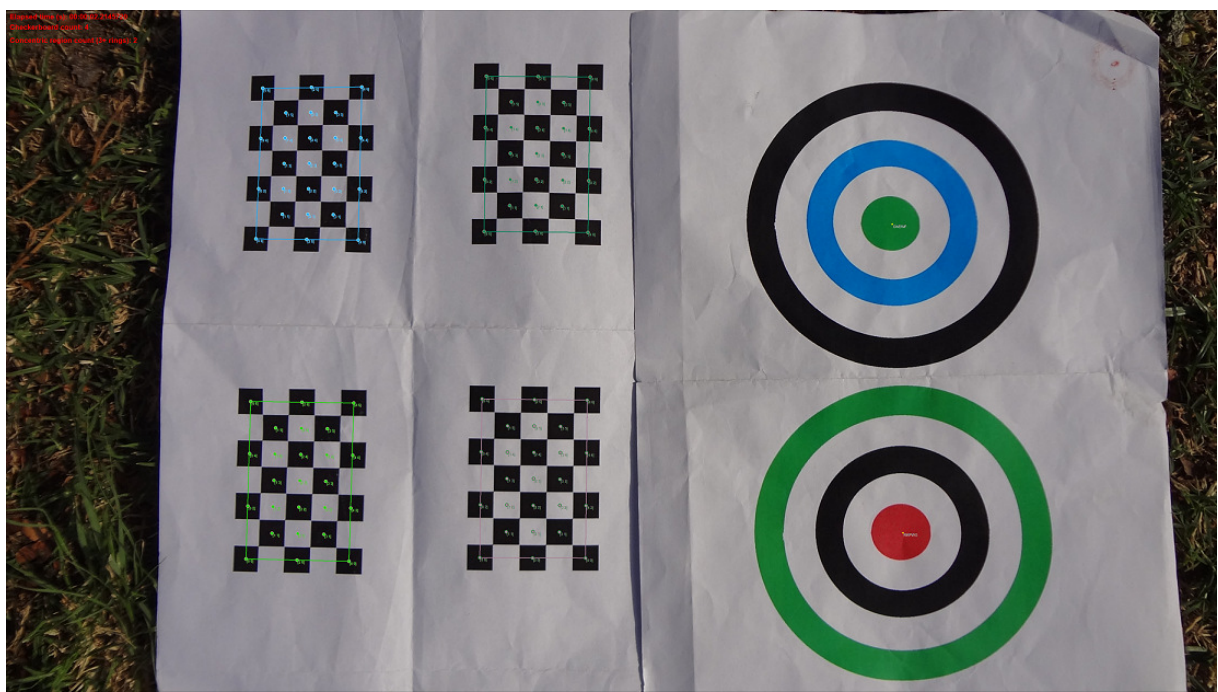


FIGURE 5.6 – Sample test image: Sony Cybershot DSC-WX7 camera, outdoor environment, frontal pose, uniform shadow.

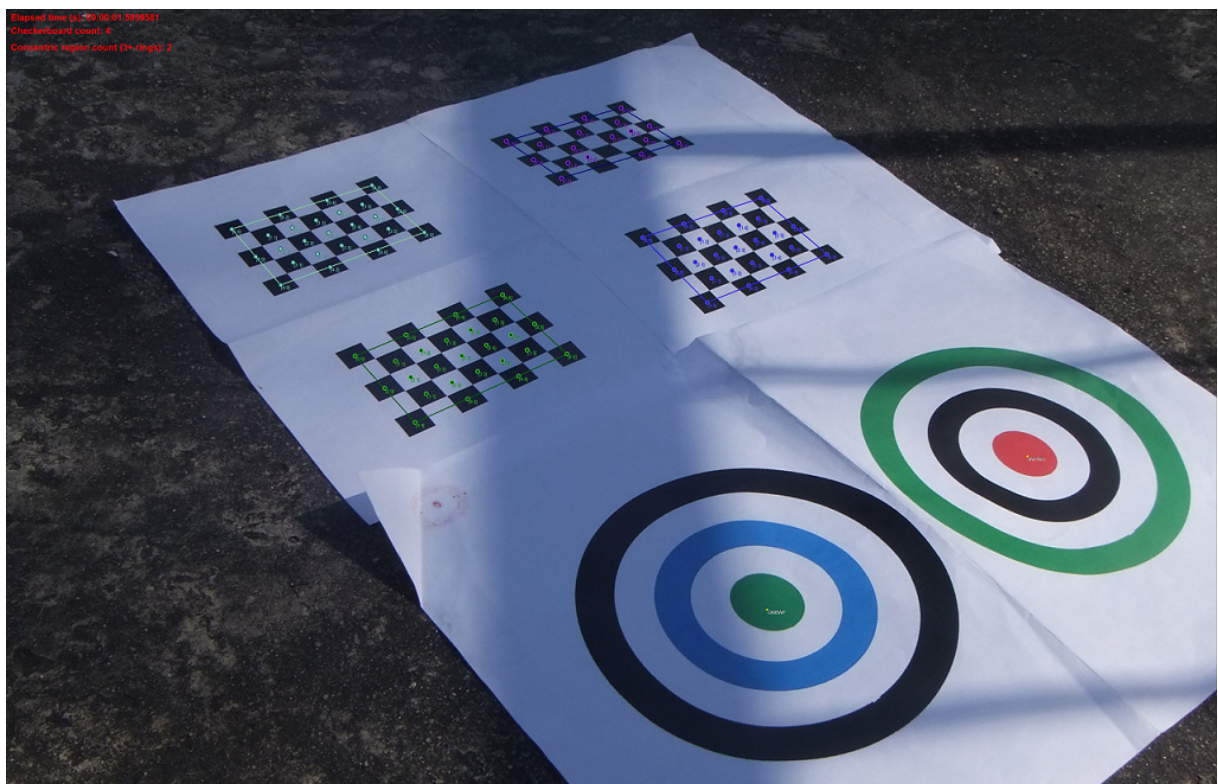


FIGURE 5.7 – Sample test image: Fuji W1 camera, outdoor environment, skewed pose, hard shadow.

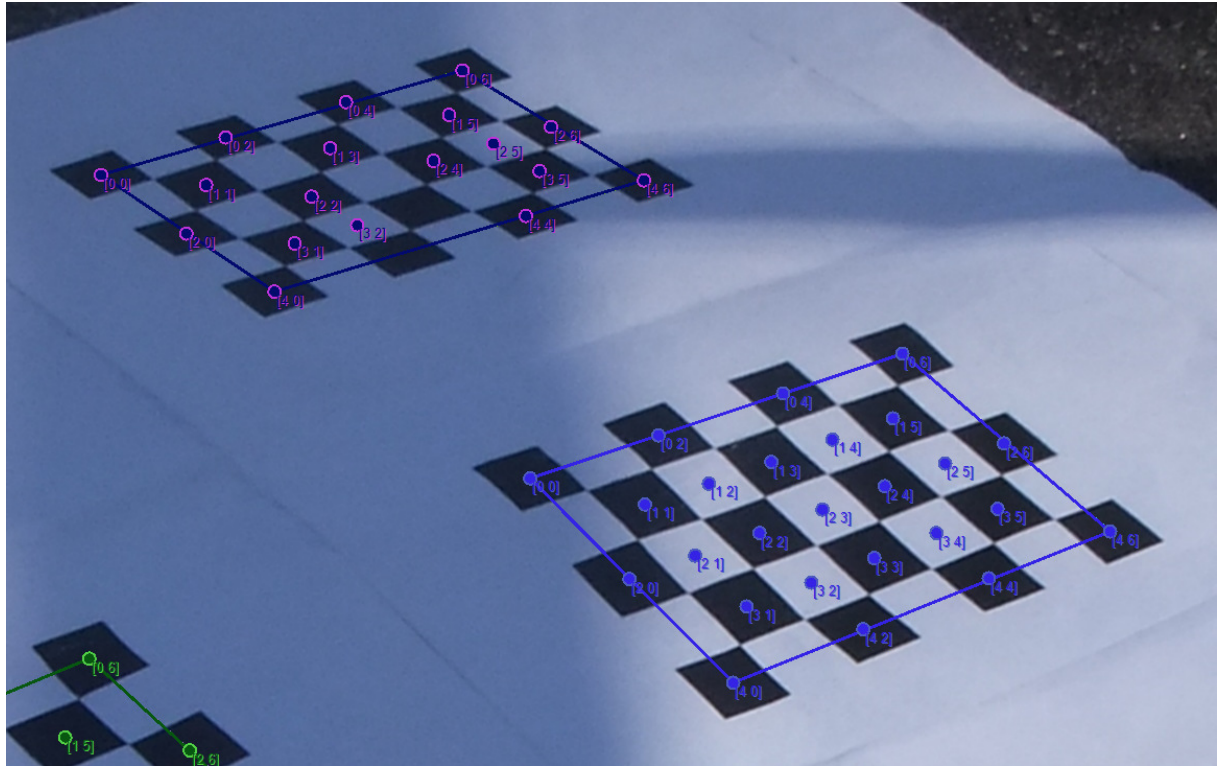


FIGURE 5.8 – Identification detail: Fuji W1 camera, outdoor environment, skewed perspective, hard shadow.

Hard shadows are not common field conditions; these could be corrected controlling camera exposure and applying high dynamic range corrections. These settings were included along with using no special ink, paper or camera adjustment to test algorithm robustness under worst-case scenarios. For all these reasons, performance figures excluding hard shadows are the ones expected as worst case in the field.

Images obtained were analyzed to verify which of the parameters from Table 5.1 are important for checkerboard and target identification using performance criteria presented in Table 5.3. One image was obtained for each possible combination of parameters and analysis of variance tests allowed proper assessment of algorithm robustness. Analysis

TABLE 5.4 – Summary of identification performance of proposed algorithm. Results were computed using 90 images and criteria shown in Table 5.3

Parameter	Global results (average)	Results excluding hard shadows
Checkerboard precision	98.2%	98.5%
Checkerboard recall	94.5%	98.8%
Checkerboard F-Score	95.5%	98.5%
Target precision	92.0%	98.0%
Target recall	89.8%	97.2%
Target F-Score	90.3%	97.2%
Target color accuracy	79.5%	83.5%

of variance (ANOVA) (MONTGOMERY, 2006) was then applied to verify the influence of each parameter on algorithm precision, recall and F-score. Checkerboard F-Score results are as follows:

	Df	Sum Sq	Mean Sq	F value	Pr(>F)							
environment	1	0.6277	0.6277	90.83	<2e-16 ***							
lighting	3	0.7366	0.2455	35.52	<2e-16 ***							
camBrand	2	0.0105	0.0053	0.76	0.469							
filters	2	0.0216	0.0108	1.56	0.212							
perspective	2	0.0048	0.0024	0.35	0.705							
Residuals	259	1.7900	0.0069									
<hr/>												
Signif. codes:	0	'***'	0.001	'**'	0.01	'*'	0.05	'.'	0.1	'	'	1

If hard shadow conditions are removed, the new analysis yields:

	Df	Sum Sq	Mean Sq	F value	Pr(>F)							
environment	1	0.0014	0.001414	0.607	0.4369							
lighting	2	0.0115	0.005765	2.475	0.0867 .							
camBrand	2	0.0070	0.003517	1.510	0.2234							
filters	2	0.0114	0.005685	2.440	0.0896 .							
perspective	2	0.0033	0.001672	0.718	0.4892							
Residuals	206	0.4799	0.002329									
<hr/>												
Signif. codes:	0	'***'	0.001	'**'	0.01	'*'	0.05	'.'	0.1	'	'	1

This analysis shows that it is important to prevent or correct hard shadows should they happen in the field, which is unexpected. The most important influence are filter type which can be chosen to be the one that performs best (Gaussian filter).

Concentric region F-Score:

	Df	Sum Sq	Mean Sq	F value	Pr(>F)							
environment	1	1.341	1.3411	29.272	1.43e-07 ***							
lighting	3	4.321	1.4404	31.440	< 2e-16 ***							
camBrand	2	0.542	0.2711	5.918	0.00307 **							
filters	2	0.001	0.0003	0.007	0.99320							
perspective	2	0.583	0.2914	6.360	0.00201 **							
Residuals	259	11.866	0.0458									
<hr/>												
Signif. codes:	0	'***'	0.001	'**'	0.01	'*'	0.05	'.'	0.1	'	'	1

Concentric region F-Score below (no hard shadow)

```
Df Sum Sq Mean Sq F value Pr(>F)
environment    1 0.0015 0.00154   0.116 0.7335
lighting       2 0.0559 0.02794   2.104 0.1245
camBrand       2 0.1133 0.05663   4.265 0.0153 *
filters        2 0.0002 0.00008   0.006 0.9938
perspective    2 0.0929 0.04644   3.498 0.0321 *
Residuals     206 2.7348 0.01328
---
Signif. codes:  0 '***' 0.001 '**' 0.01 '*' 0.05 '.' 0.1 ' ' 1
```

In the case of targets, camera brand has an important influence. This is due to better optical systems leading to well defined edges and low noise inside color region. While accurate target center prediction may be impaired when the image is not frontal, its identification was possible. When color identification is important, it is better to use custom-made algorithms for each application and lighting conditions instead of the absolute criteria used in the implementation described herein.

5.3 Sensitivity Analysis

Further investigation was conducted to numerically analyze the robustness of the methodology varying perspective and shadow intensity.

To analyze influence of perspective, multiple pictures of a 7×7 checkerboard were simulated under various camera poses. The image projection was computed using Euler rotation angles (YING; KIM, 2002). Coordinates (0,0), (1,0), (0,1), (1,1) were assigned to the checkerboard edges.

The influence of shadows was analyzed by synthesizing dark areas in a homogeneous picture. Specifically, three parameters were created: initial shadow coordinate s_{x0} , final shadow coordinate s_{xf} and shadow intensity s_{intens} .

Let $xRel = \frac{x}{W}$ be the X relative coordinate of pixel $P_{x,y}$ in an image of width W . Each pixel RGB color is modified according to Equations 5.1 to 5.2.

$$s_{weight} = \begin{cases} 0 & xRel < s_{x0} \\ s_{intens} & xRel > s_{xf} \\ \frac{xRel - s_{x0}}{s_{xf} - s_{x0}} s_{intens} & s_{x0} \leq xRel \leq s_{xf} \end{cases} \quad (5.1)$$

$$RGB_{P,new} = RGB_{P,old} \cdot (1 - s_{weight}) \quad (5.2)$$

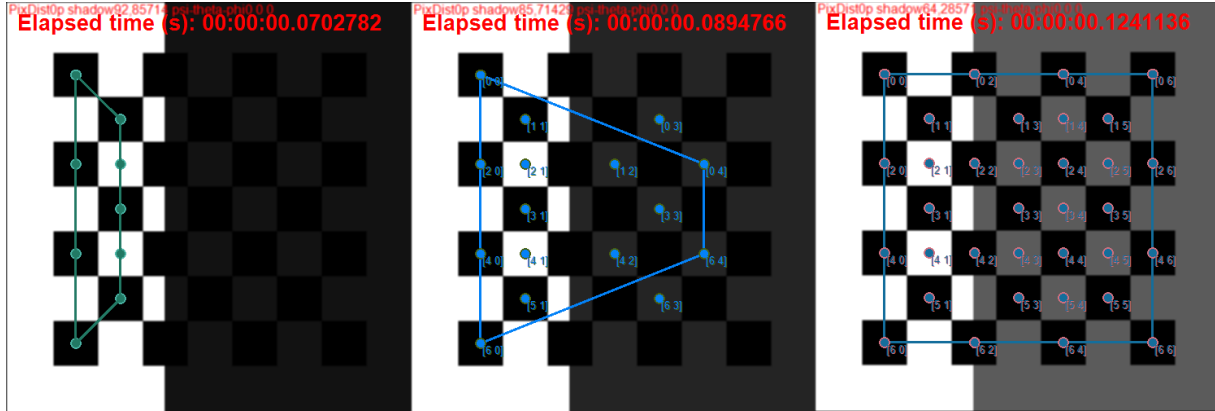


FIGURE 5.9 – Simulated hard shadow. Identification is impaired when shadow intensity exceeds threshold of 0.8.

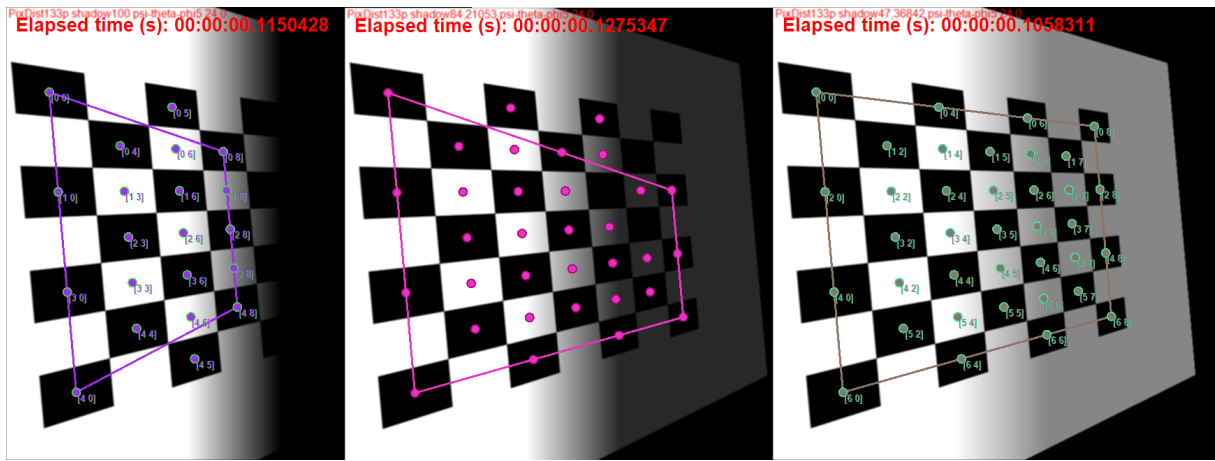


FIGURE 5.10 – Simulated soft shadow - shadow beginning and end separated by 133 pixels . Identification is impaired when shadow intensity exceeds threshold of 0.8.

The simulation allowed isolating shadow and perspective from camera factors, such as lens distortion and chromatic errors.

Simulated shadows and perspectives were run varying Euler angles from 0° to 70° , shadow intensity s_{intens} from 0 to 1 and shadow coordinates from $s_{xf} = s_{x0}$ (hard shadow) to $s_{xf} = s_{x0} + 0.4$ (soft shadow). Angles above 45° are impractical in real C&A settings because any vibration or occlusion may effectively remove the optical marker from the field of view.

Results showed that $s_{intens} > 0.8$ prevents detection of border squares and results are incorrect. Thus, checkerboard recognition will not work if the difference of luminosity factor of black squares to neighboring pixels is smaller than 0.2.

Figures 5.9 and 5.10 show the effect of increased shadow intensity. Checkerboard squares affected by shadows may have their centers slightly displaced. If shadow intensity exceeds the detection threshold, identification is incorrect.

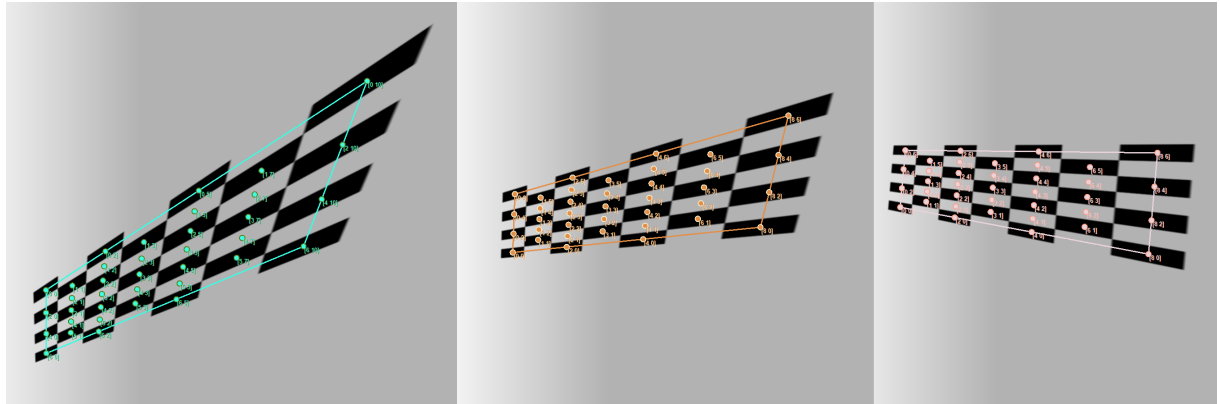


FIGURE 5.11 – Correct identification results in simulated perspective for $\phi = 70^\circ$.

If $s_{intens} \leq 0.8$ the presence of shadows and variation in perspective has no influence in checkerboard detection. There were no simulated cases where results were incorrect. Some examples are shown in Figure 5.11.

5.3.1 Experiments in Relevant Environment

In order to demonstrate robustness of the method in a relevant environment, under conditions closer to a real application, experiments were conducted at Petrobras' Research Center (CENPES - Figure 5.12) and demonstrated that, even though a simple phone camera¹ was used, it was possible to identify markers from a distance. A custom designed system, with better optics and less distortions than a consumer-level system, is expected to be able to handle even greater distances by using industrial cameras with better optical system and controllable zoom capabilities. In real applications, using high dynamic range cameras is a viable option because parts and equipments are either stationary or move slowly during C&A processes, which are performed in an interval that varies from several minutes to hours. Note that, since the dimensions of the optical markers are known, it is possible to devise a system to measure their distance and angles with respect to the camera.

In all tested settings, the obtained results were satisfactory in terms of identifying the presence of the optical markers and their position in the image. Figures 5.13 and 5.14 show that markers are identified even in the presence of shadows cast by the equipment directly on top of it. Figure 5.15 demonstrates that the methodology is robust to partial occlusion in a real setting. Figures 5.16 and 5.17 present correct OMR in curved surfaces under non uniform lighting. It is worth noting that the placement of the markers for these tests was chosen to test these limit cases. In a real application, the use of industrial cameras and placement and marker placement in uniform regions will increase system

¹13 MP Samsung Galaxy S4 without any special features



FIGURE 5.12 – Optical markers placed in simulated industrial environment at Petrobras' Research Center (CENPES). Left: Storage tank. Center: Pressure vessel. Right: Heat exchanger. Note that the identification is robust even when placed in a curved surface.

accuracy.

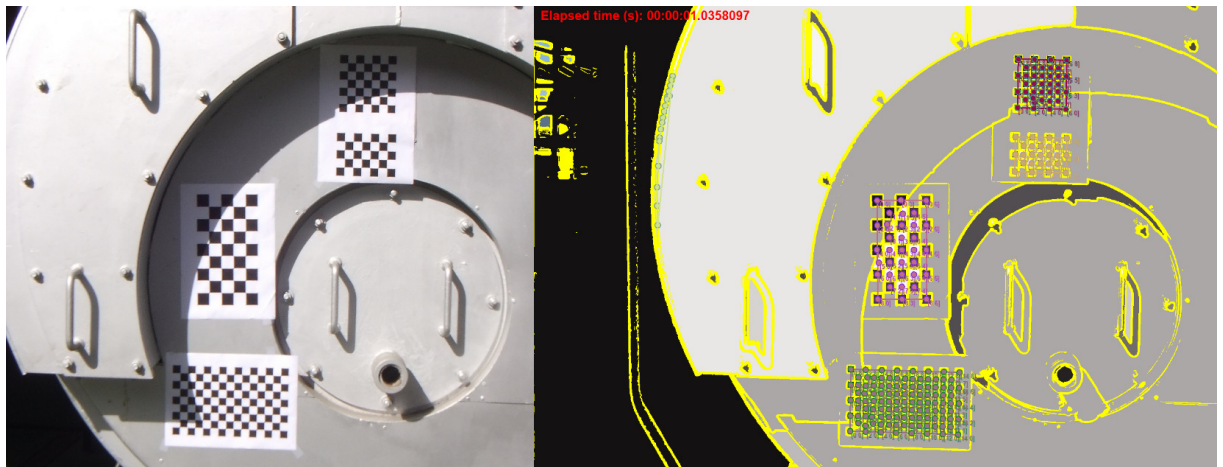


FIGURE 5.13 – Correct marker identification in a heat exchanger.

5.4 Limitations

The proposed methodology has limitations when shadows or reflexes cause extremely abrupt variation in the image, as shown in Figures 5.18 and 5.19. False negatives occurred either because of light reflexes (glare) in the scene or due to the presence of hard shadows. It is important to note that identification errors mostly stemmed from the tests carried out under very severe conditions and that the resulting identification succeeded in the majority of the cases. Light reflex is an important factor when illumination is not uniform and special ink could mitigate these effects whereas images with hard shadows could be addressed using high dynamic range techniques.

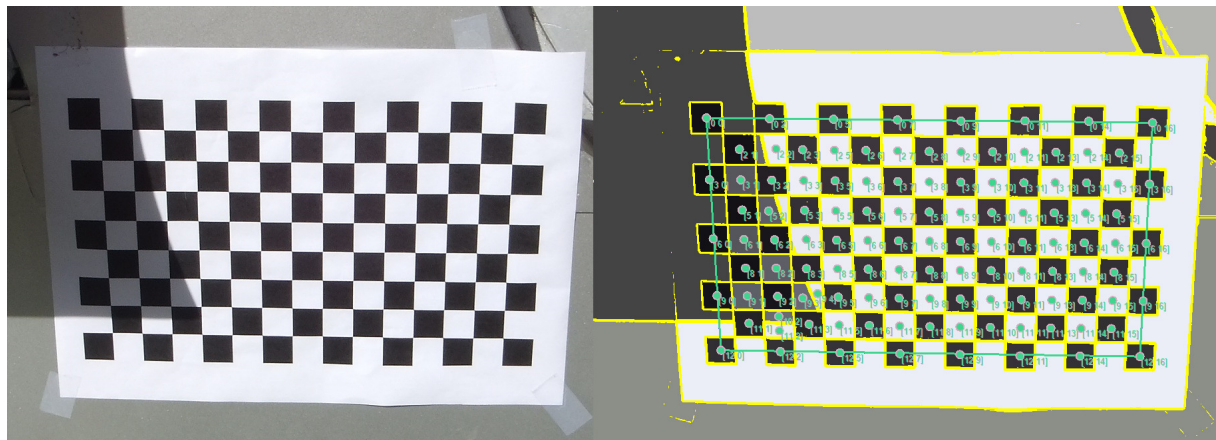


FIGURE 5.14 – Detail of identification of optical marker in the presence of shadow cast by the equipment.

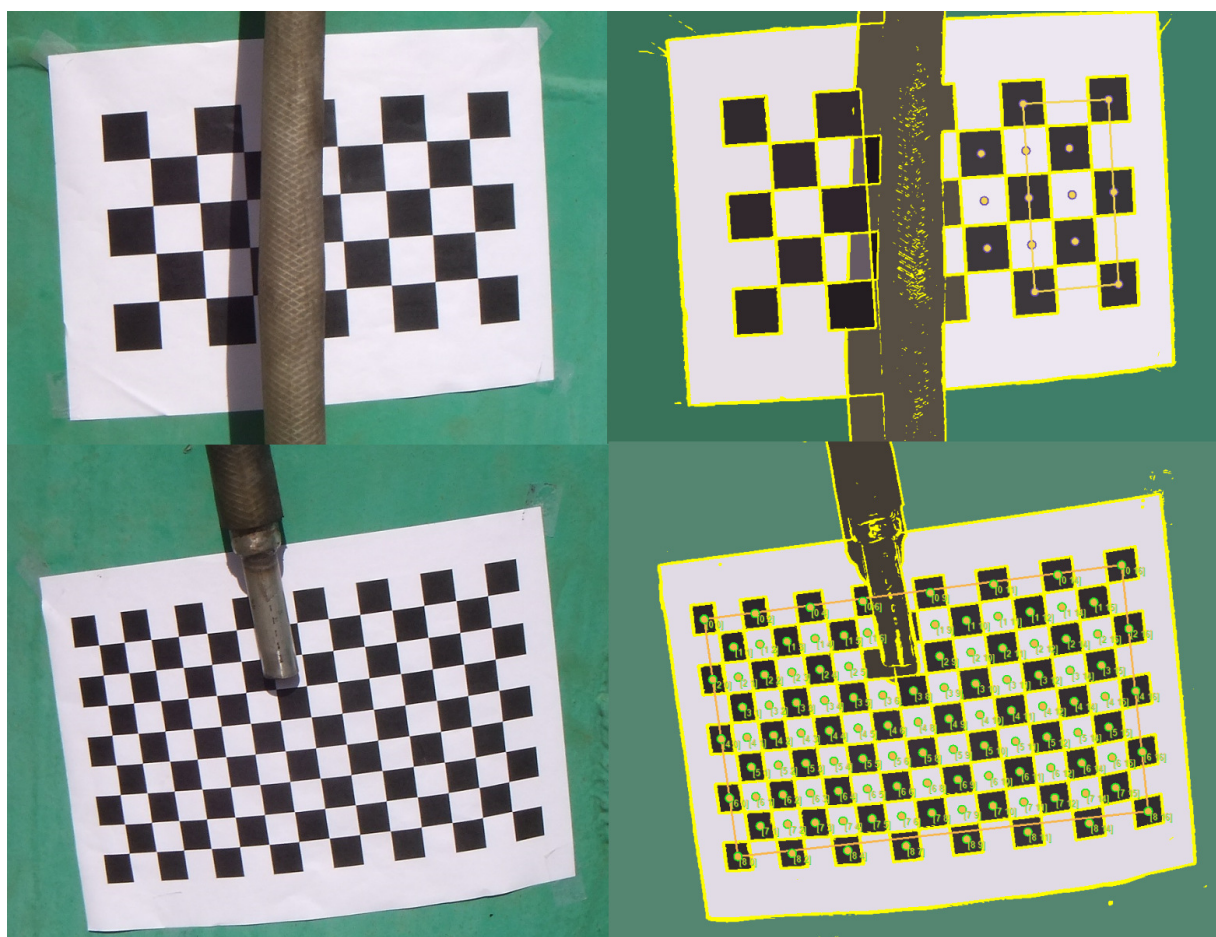


FIGURE 5.15 – Top: marker not identified due to severe occlusion. Bottom: marker recognized in the presence of partial occlusion.

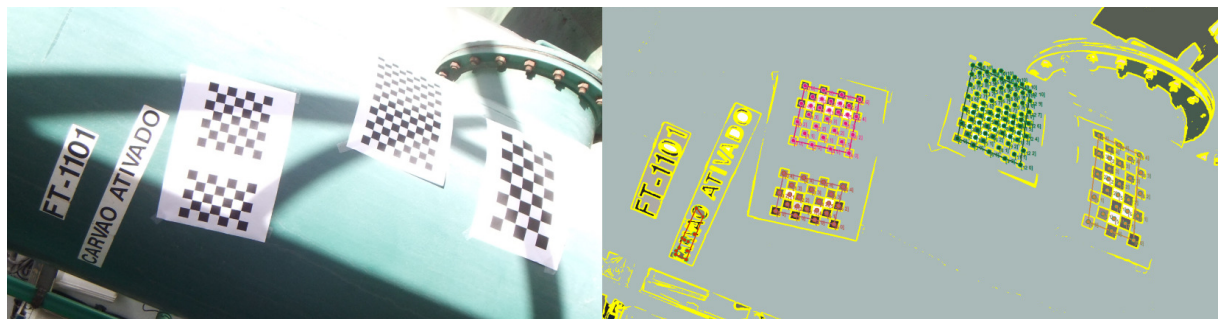


FIGURE 5.16 – Correct identification of optical markers in a curved surface, subject to shadow and exposed to light.

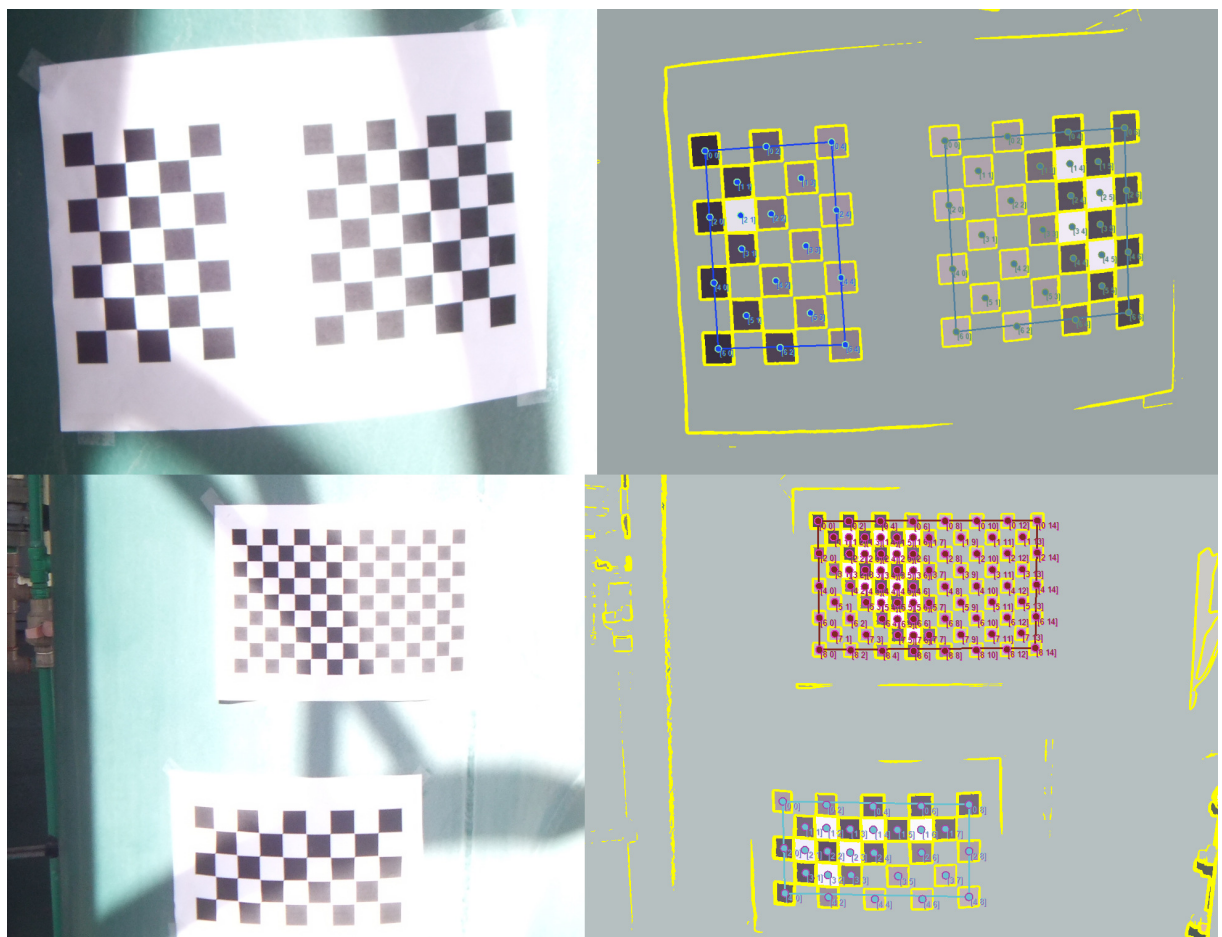


FIGURE 5.17 – Details of correct OMR when marker is exposed to light, soft shadow and object curvature.



FIGURE 5.18 – Algorithm limitations. Left: harsh light → shadow transitions impair checkerboard identification. Right: glare impairs target identification.

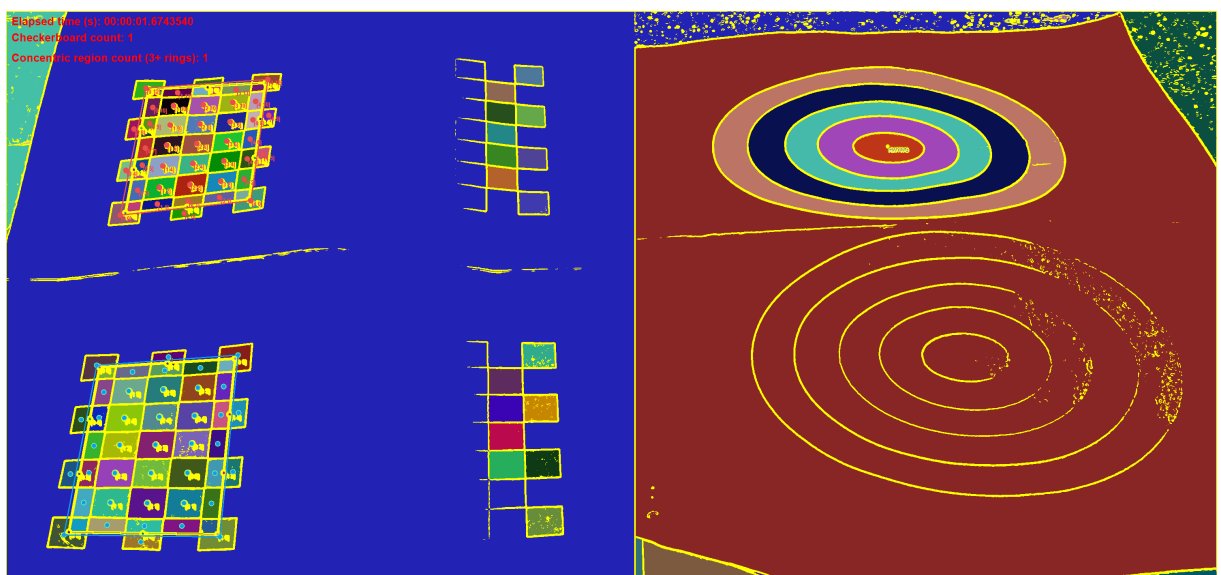


FIGURE 5.19 – False negatives color region analysis. Left: edges were not properly identified. Right: light reflex impairs edge detection.

6 Conclusion

This chapter presents a summary of the proposed methodology for robust OMR in outdoor environments, suggestions of how OMR should be implemented in field applications, results, limitations and future research.

Robust OMR is achieved using three main methods: identification of contiguous color regions, extraction of high-level region information and identification of optical marker specific characteristics. When an input image is received, all regions whose color is similar are grouped together. Region parameters, such as area and perimeter, are then computed for each region and groups of similar regions (with regards to these parameters) are computed. These groups of regions that have similar properties are then analyzed to verify if they match conditions to be classified as checkerboard or target. If the OMR is identified as checkerboard, the coordinates of each square are informed, as well as the checkerboard dimensions. In the case of targets, the output is the number and color of each concentric circle.

Specific objectives of this work were fulfilled: the results demonstrate that the proposed methodology allows OMR in outdoor environments using inexpensive printed markers which are easily replaced and robust to mechanical impact. Moreover, implementation of the proposed algorithms using heterogeneous computing enables runtimes around 1 s, an acceptable speed for field applications where positioning may take from minutes to hours.

The proposed OMR methodology applied to planar checkerboard detection allows robust identification under extremely variable lighting conditions and partial occlusion. Experiments demonstrated that, excluding hard shadow scenes, the technique is robust to variations in camera brand, lighting conditions, perspective and indoor/outdoor environments. Under normal outdoor conditions without hard shadows being projected on top of the optical markers, precision and recall is expected to be above 97%.

In real applications, it may be necessary to perform a preliminary identification of the position of the optical markers in the image. For this task, a single hidden layer feed-forward neural network can achieve 99.5% accuracy and provide initial estimates that can be used to guide the camera system to zoom in on regions of interest if necessary. The combination of optical markers for positioning and QR codes for information retrieval is

a viable option for position feedback in an automated system.

The parallel flood-filling algorithm enables the methodology to identify checkerboard and target patterns without seed points and without need for binarization, required in previous work. Criteria proposed in this work for identification of concentric regions and checkerboards provide robustness to lighting and pose. The regularity analysis task verifies neighboring region groups and uses a novel square center prediction-match algorithm that is capable of automatically detecting if the group is a valid $N \times M$ checkerboard even under partial occlusion.

To the best of the author's knowledge, this is the first methodology specifically designed for outdoor OMR. Existing OMR systems, such as ARToolKit, are extremely sensitive to occlusion and variations in lighting conditions and, unlike the proposed methodology, have poor performance in outdoor conditions.

Statistical tests with multiple images obtained from various cameras show that the implementation is robust to outdoor lighting conditions and occlusion which, to the author's knowledge, were not addressed simultaneously in any previous work.

Experiments conducted at Petrobras' Research Center (CENPES) demonstrated that the methodology is capable of performing OMR in an outdoor industrial environment. Preliminary classification of optical markers using neural networks in Haar image features can provide bounding boxes for marker candidates. This information may be used to guide the camera system to zoom in those areas and for detailed information extraction using the proposed methodology, thus allowing for optical marker identification even when they are small in the original image.

The main limitations of the OMR methodology are correct identification of region colors in target and checkerboard detection if shadow conditions are extremely severe or occlusion hinders identification of the checkerboard structure of the marker. The problem of incorrect identification of contiguous color regions when direct light or shadow is cast on top of the marker can be mitigated by using high dynamic range sensors to correct saturation. Occlusion that prevents the camera system from obtaining any image of the optical marker will prevent any type of identification. However, using multiple cameras which can obtain information from multiple poses is a possibility.

The proposed methodology should enable contractors, such as shipyards, and asset owners to reduce waste during the C&A phase of FPSOs, storage tanks and other large equipments. As of now, there is still no technology capable of satisfactory tracking objects in outdoor environments. The simplicity of deploying optical markers in the field (as opposed to RFID, for example, which requires active units or readers that must come close to the emitter) is a step forward in the direction of optimizing construction and

assembly performance¹.

6.1 Future Work Proposals

Due to time and resources constraints, it is not feasible to implement all possible applications using the developed OMR methodology. In general, for all OMR procedures in outdoor settings, it is useful to study and develop markers that are less susceptible to damage due to oxides, soot and other materials that can adhere to the marker.

In this section, implementation of three applications is proposed as future work: large object identification in outdoor environments using multiple cameras, development of new robust optical markers for outdoor applications and simultaneous optical marker detection and tracking.

6.1.1 Large object identification in outdoor environments using multiple cameras

It is possible to acquire data from multiple cameras and, through a process of triangulation and image registration, locate and track large parts in outdoor environments. Since the proposed methodology outputs pixel coordinates of the markers, if the position of calibrated cameras is known it is possible to locate plates and equipments as long as they have markers.

Shipyards would greatly benefit from this technology because of the need to track parts and the availability of suitable locations for camera positioning, as shown in Figures 6.1 and 6.2.

An initial approach to the problem, to be evaluated in the research, is as follows:

1. Determine appropriate locations for the camera system;
2. Ensure proper communication of the camera systems and the main computer;
3. Acquire images from multiple cameras;
4. Use the proposed methodology for OMR to identify optical markers in the images;
5. Use the image coordinates of the optical markers and the position of the calibrated cameras to determine spacial position of the markers;

¹During visits to shipyards in Brazil, it is possible to identify waste in the fact that large parts are displaced to wrong locations, which could be prevented by appropriate tracking and specialist systems

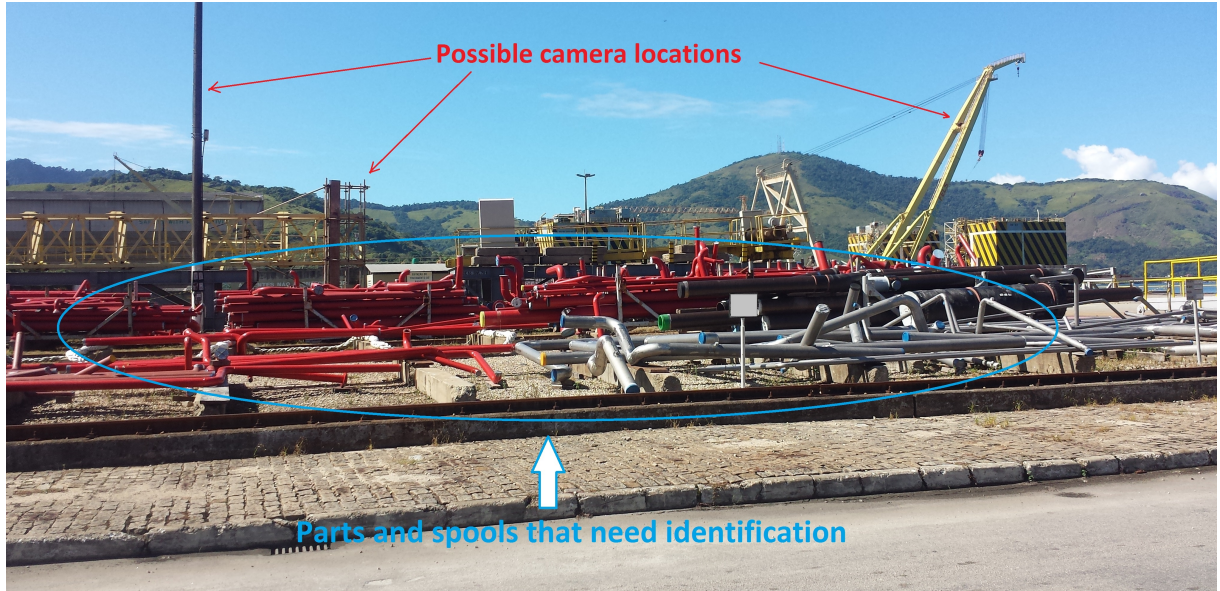


FIGURE 6.1 – Possible location of cameras for part tracking in shipyards; pipes and spools that could be identified using optical markers.

6. Devise proper coding and a database system to associate markers with their respective parts.

6.1.2 Development of new robust optical markers for outdoor applications

The proposed region grouping algorithm is versatile enough to accommodate multiple types of optical markers, other than checkerboards and targets. Application-specific parameter optimization and multiscale OMR analyses can be used to identify custom optical markers, such as checkerboards with circular dots, checkerboard inside checkerboard (as shown in Figure 6.3) or other custom shapes (Figure 6.4), whose recognition could then be done using machine learning techniques.

6.1.3 Simultaneous optical marker detection and tracking

Despite the computation offload to GPU Devices using OpenCL, it is still computationally expensive to recalculate position and coordinates of every optical marker in a camera system every frame. Instead, a tracking algorithm, such as Lucas Kanade (LU-CAS; KANADE, 1981), could be used in a faster cycle while the algorithms for the proposed OMR methodology run in a slower cycle. In fact, a vast literature exists in the field of object tracking (see (WANG *et al.*, 2017), (HU *et al.*, 2017), (DANESHYAR; NAHVI, 2017), (CHEN *et al.*, 2017), (WANG; GE, 2017)), and the challenge is one of sensor and algorithm

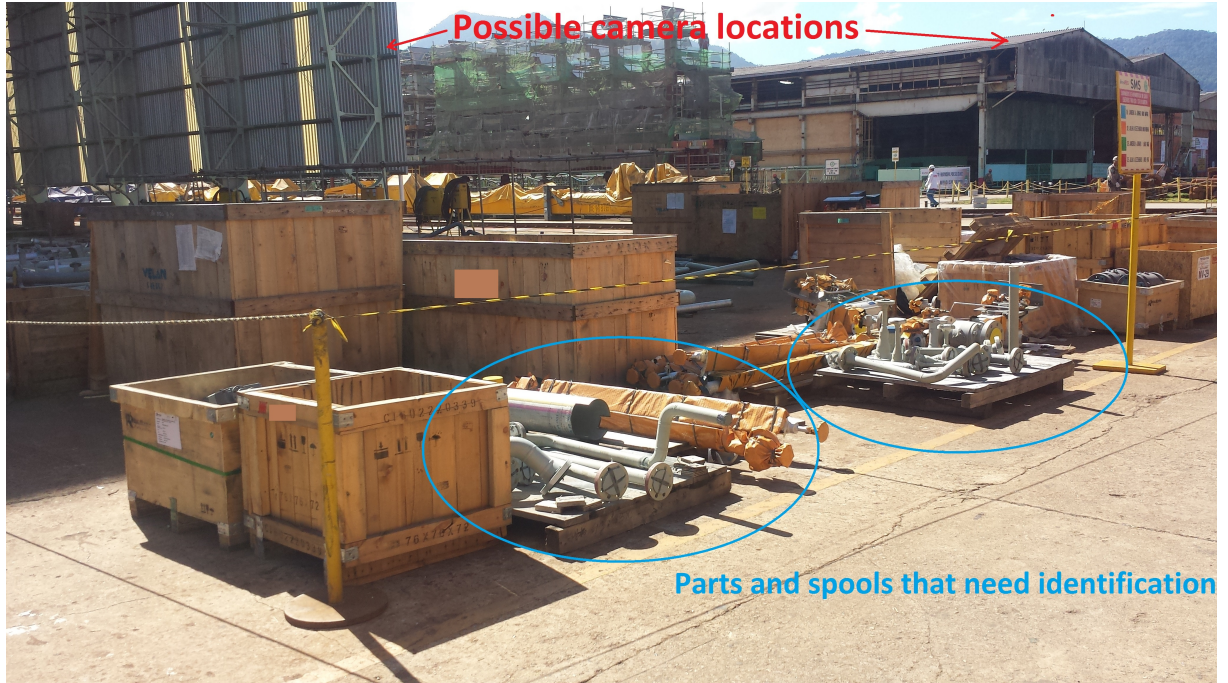


FIGURE 6.2 – Possible location of cameras for part tracking in shipyards; boxes and their contents can carry optical markers.

integration.

The simultaneous optical marker detection and tracking can be implemented using an outer (slower) identification loop, which detects optical markers, and an inner loop, which provides tracking and, if necessary, object persistency. Figure 6.5 shows a simplified scheme of this implementation, which comprises the following steps:

1. **Initialization:** Acquire image and use the proposed OMR methodology to identify marker positions;
2. **Fast cycle:** Acquire image and use chosen tracking algorithm to determine new marker positions. Current tracking methods are usually fast enough to perform this operation at high frame rates;
3. **Slow cycle:** Acquire image and use the proposed OMR methodology to identify markers. New markers should be added to the list and the position of existing ones should be updated. Application-specific algorithms need to be developed in order to handle markers that go out of sight. This “memory” can be used to make the system robust in case of temporary occlusion caused by a moving object that breaks line of sight from camera to optical marker.

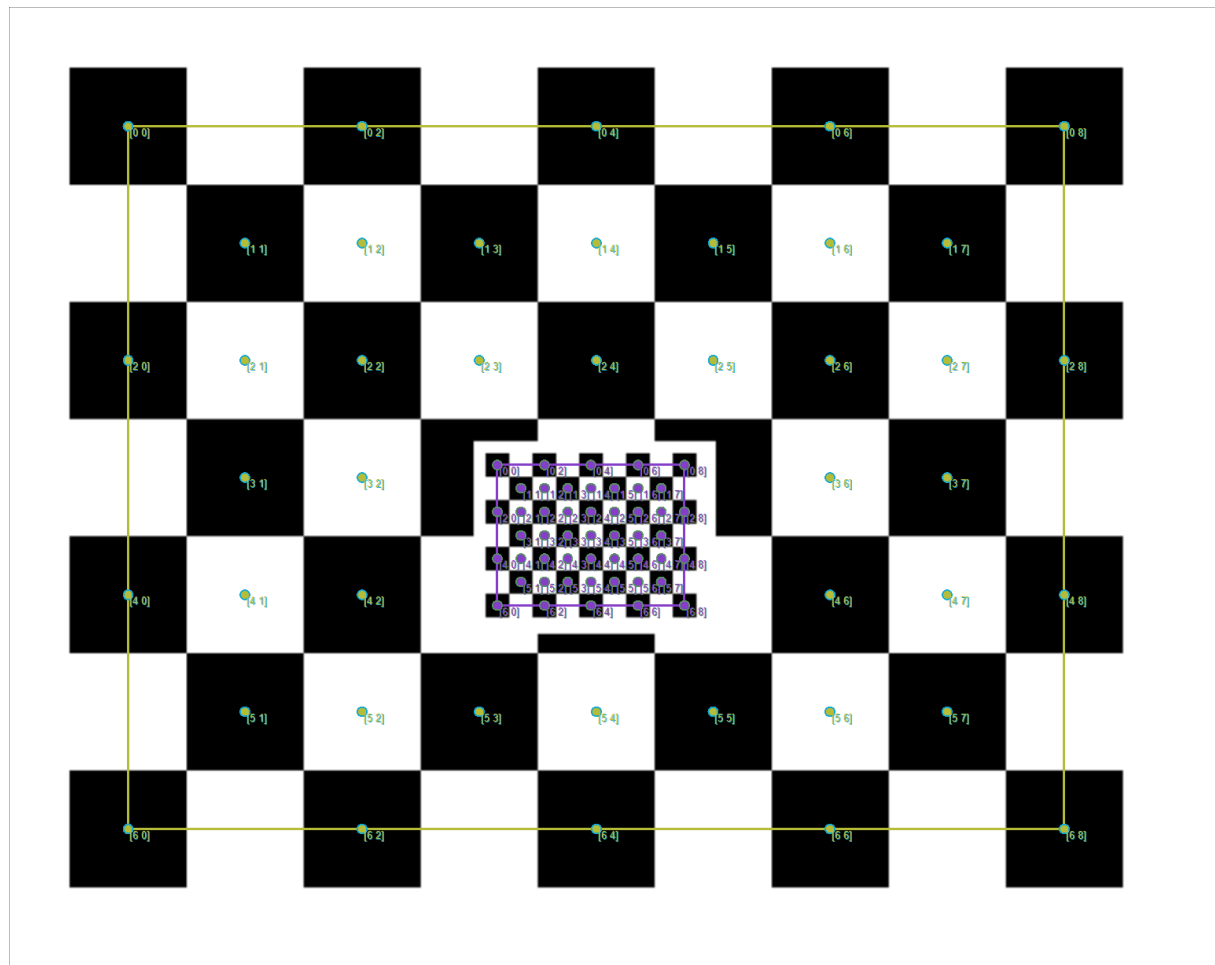


FIGURE 6.3 – Identification of checkerboard inside checkerboard. The inner checkerboard may be exchanged for other markers.



FIGURE 6.4 – Optical marker composed of random shapes and positions. The proposed region grouping algorithm identifies that the contiguous regions of the marker are similar enough to belong to the same group.

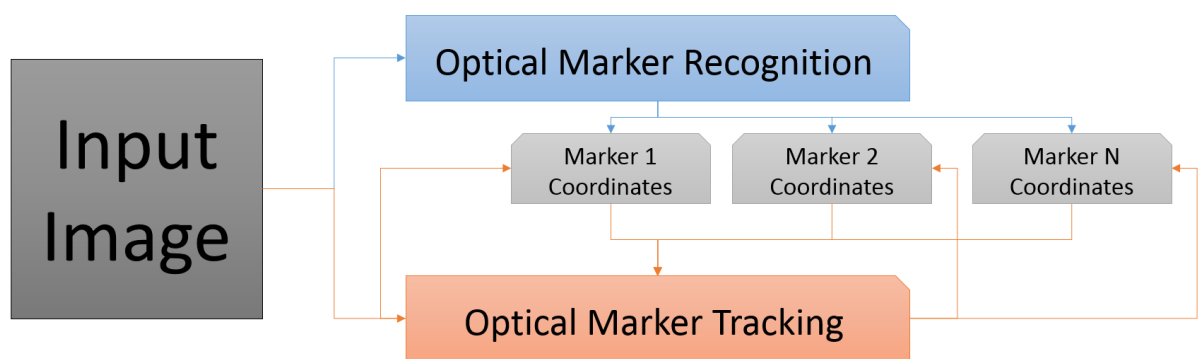


FIGURE 6.5 – Robust OMR and tracking: the combination of a slow cycle, using the proposed OMR methodology, and a fast tracking cycle will improve system performance and allow for optical marker persistency when temporarily occluded by a moving object. Blue: slow cycle. Orange: fast cycle.

References

ADVANCED MICRO DEVICES. **AMD Radeon™ R9 Series Gaming Graphics Cards with High-Bandwidth Memory.** 2016. Available at: <<http://www.amd.com/en-us/products/graphics/desktop/r9>>. Accessed 09 Sep 2016.

AL-MARAKEBY, A. Article: Multi core processors for camera based omr. **International Journal of Computer Applications**, v. 68, n. 13, p. 1–5, April 2013. Full text available.

AMAZON.COM. **Amazon.com: Online Shopping for Electronics, Apparel, Computers, Books, DVDs & more.** 2016. Available at: <<https://www.amazon.com/>>. Accessed 09 Sep 2016.

AMERICAN PETROLEUM INSTITUTE. **API Spec 5L - Specification for Line Pipe.** 2012.

AMERICAN PETROLEUM INSTITUTE. **API Standard 620 - Design and Construction of Large, Welded, Low-pressure Storage Tanks.** 12th. ed. [S.l.], 2013.

AMERICAN PETROLEUM INSTITUTE. **API Standard 650: Welded Tanks for Oil Storage.** 12th. ed. [S.l.], 2013.

AMERICAN SOCIETY OF MECHANICAL ENGINEERS. **ASME B31.4 - Pipeline Transportation Systems for Liquid Hydrocarbons and Other Liquids.** [S.l.], 2006.

AMERICAN SOCIETY OF MECHANICAL ENGINEERS. **ASME Section IX Standard: Welding and Brazing Qualifications, BPVC.** [S.l.], 2010.

AMERICAN SOCIETY OF MECHANICAL ENGINEERS. **ASME Section VIII Division 1 - Rules for Construction of Pressure Vessels.** [S.l.], 2011.

AMERICAN SOCIETY OF MECHANICAL ENGINEERS. **ASME B31.8 - Gas Transmission and Distribution Piping Systems.** [S.l.], 2012.

ANDREW, A. Another efficient algorithm for convex hulls in two dimensions. **Information Processing Letters**, v. 9, n. 5, p. 216 – 219, 1979. ISSN 0020-0190. Available at: <<http://www.sciencedirect.com/science/article/pii/0020019079900723>>.

- ASLUZEK, A. Novel machine vision methods for outdoor and built environments. **Automation in Construction**, v. 19, n. 3, p. 291 – 301, 2010. ISSN 0926-5805. 25th International Symposium on Automation and Robotics in Construction. Available at: <<http://www.sciencedirect.com/science/article/pii/S0926580509001915>>.
- ASSOCIAÇÃO BRASILEIRA DE NORMAS TÉCNICAS. **ABNT NBR 152801:2009 Dutos terrestres parte 2: Construção e Montagem**. [S.l.], 2009.
- ASSOCIAÇÃO BRASILEIRA DE NORMAS TÉCNICAS. **ABNT NBR 152801:2009 Dutos terrestres parte 1: Projeto**. [S.l.], 2011.
- AYSAL, T. C.; BARNER, K. E. Generalized mean-median filtering for robust frequency-selective applications. **IEEE Transactions on Signal Processing**, v. 55, n. 3, p. 937–948, March 2007. ISSN 1053-587X.
- BADGUJAR, H. Y. **HARD-SOFT Something More**. 2013. Available at: <<http://hemprasad.wordpress.com/category/computing-technology/parallel/gpu-cuda>>. Accessed 07 Jan 2014.
- BAGLODI, V. Edge detection comparison study and discussion of a new methodology. In: **IEEE Southeastcon 2009**. [S.l.: s.n.], 2009. p. 446–446. ISSN 1091-0050.
- BARRESI, F. F.; ALLASIA, W. Airport markings recognition for automatic taxiing. In: **Design and Architectures for Signal and Image Processing (DASIP), 2013 Conference on**. [S.l.: s.n.], 2013. p. 197–200.
- BARROS, S. M. de. **Tanques de Armazenamento**. Rio de Janeiro, 2013.
- BHADESHIA, H.; HONEYCOMBE, S. R. 10 - thermomechanical treatment of steels. In: BHADESHIA, H.; HONEYCOMBE, S. R. (Ed.). **Steels (Third Edition)**. Third edition. Oxford: Butterworth-Heinemann, 2006. p. 209 – 234. ISBN 978-0-7506-8084-4. Available at: <<http://www.sciencedirect.com/science/article/pii/B9780750680844500121>>.
- BISWAS, R.; SIL, J. An improved canny edge detection algorithm based on type-2 fuzzy sets. **Procedia Technology**, v. 4, p. 820 – 824, 2012. ISSN 2212-0173. Available at: <<http://www.sciencedirect.com/science/article/pii/S2212017312004136>>.
- BISWAS, S.; GHOSHAL, D. Blood cell detection using thresholding estimation based watershed transformation with sobel filter in frequency domain. **Procedia Computer Science**, v. 89, p. 651 – 657, 2016. ISSN 1877-0509. Twelfth International Conference on Communication Networks, ICCN 2016, August 19 to 21, 2016, Bangalore, India Twelfth International Conference on Data Mining and Warehousing, ICDMW 2016, August 19-21, 2016, Bangalore, India Twelfth International Conference on Image and Signal Processing, ICISP 2016, August 19-21, 2016, Bangalore, India. Available at: <<http://www.sciencedirect.com/science/article/pii/S1877050916310948>>.
- CANNY, J. A computational approach to edge detection. **IEEE Transactions on Pattern Analysis and Machine Intelligence**, PAMI-8, n. 6, p. 679–698, Nov 1986. ISSN 0162-8828.

- CARRION, R.; MESQUITA, E.; ANSONI, J. L. Dynamic response of a frame-foundation-soil system: a coupled bem–fem procedure and a gpu implementation. **Journal of the Brazilian Society of Mechanical Sciences and Engineering**, v. 37, n. 4, p. 1055–1063, 2015. ISSN 1806-3691. Available at: <<http://dx.doi.org/10.1007/s40430-014-0230-3>>.
- CHEN, J.; JOO, B.; III, W. W.; EDWARDS, R. Automatic offloading c++ expression templates to cuda enabled gpus. In: **Parallel and Distributed Processing Symposium Workshops PhD Forum (IPDPSW), 2012 IEEE 26th International**. [S.l.: s.n.], 2012. p. 2359–2368.
- CHEN, K.; TAO, W.; HAN, S. Visual object tracking via enhanced structural correlation filter. **Information Sciences**, v. 394 395, p. 232 – 245, 2017. ISSN 0020-0255. Available at: <<http://www.sciencedirect.com/science/article/pii/S0020025517304565>>.
- CHOI, K.-S.; OH, K.-W. Subsampling-based acceleration of simple linear iterative clustering for superpixel segmentation. **Computer Vision and Image Understanding**, v. 146, p. 1 – 8, 2016. ISSN 1077-3142. Award & Selection of Papers of {ACCV} 2014. Available at: <<http://www.sciencedirect.com/science/article/pii/S1077314216000722>>.
- CMSOFT. **OpenCL Tutorial with OpenCLTemplate and Cloo**. 2014. Available at: <<http://www.cmsoft.com.br/opencl-tutorial/>>. Accessed 09 Sep 2016.
- CORNELL. **Cornell Virtual Workshop - Memory Coalescing**. 2016. Available at: <<https://cvw.cac.cornell.edu/gpu/coalesced?AspxAutoDetectCookieSupport=1>>. Accessed 18 Oct 2016.
- DANESHYAR, S. A.; NAHVI, M. Moving objects tracking based on improved particle filter algorithm by elimination of unimportant particles. **Optik - International Journal for Light and Electron Optics**, v. 138, p. 455 – 469, 2017. ISSN 0030-4026. Available at: <<http://www.sciencedirect.com/science/article/pii/S0030402617303662>>.
- DUDA, R. O.; HART, P. E. **Pattern Classification and Scene Analysis**. New Yotk: John Willey & Sons, 1973.
- DUO-LE, F.; MING, Z. A new fast region filling algorithm based on cross searching method. In: _____. **Advances in Computer Science and Education Applications: International Conference, CSE 2011, Qingdao, China, July 9-10, 2011. Proceedings, Part II**. Berlin, Heidelberg: Springer Berlin Heidelberg, 2011. p. 380–387. ISBN 978-3-642-22456-0. Available at: <<http://dx.doi.org/10.1007/978-3-642-22456-0\55>>.
- FABIJANSKA, A.; SANKOWSKI, D. Noise adaptive switching median-based filter for impulse noise removal from extremely corrupted images. **IET Image Processing**, v. 5, n. 5, p. 472–480, August 2011. ISSN 1751-9659.
- FRANCO, E. E.; BARRERA, H. M.; LAÍN, S. 2d lid-driven cavity flow simulation using gpu-cuda with a high-order finite difference scheme. **Journal of the Brazilian Society of Mechanical Sciences and Engineering**, v. 37, n. 4, p. 1329–1338, 2015. ISSN 1806-3691. Available at: <<http://dx.doi.org/10.1007/s40430-014-0260-x>>.

- GARDNER, M.; SATHRE, P.; FENG, W. chun; MARTINEZ, G. Characterizing the challenges and evaluating the efficacy of a cuda-to-opencl translator. **Parallel Computing**, v. 39, n. 12, p. 769 – 786, 2013. ISSN 0167-8191. Programming models, systems software and tools for High-End Computing. Available at: <<http://www.sciencedirect.com/science/article/pii/S0167819113001075>>.
- GIEBEL, M.; ESSMANN, H.; PREEZ, N. D.; JOCHEM, R. Improved innovation through the integration of quality gates into the enterprise and product lifecycle roadmaps. **{CIRP} Journal of Manufacturing Science and Technology**, v. 1, n. 3, p. 199 – 205, 2009. ISSN 1755-5817. Design Synthesis. Available at: <<http://www.sciencedirect.com/science/article/pii/S1755581708000539>>.
- GUOHUI, Y.; ZHONGQIU, L.; JIAN, F.; YONG, Z.; ZEXI, Y. 2012 international conference on future energy, environment, and materials influence of quenching on-line on properties of x70 steel for sour service seamless pipe. **Energy Procedia**, v. 16, p. 444 – 450, 2012. ISSN 1876-6102. Available at: <<http://www.sciencedirect.com/science/article/pii/S1876610212000823>>.
- HALL, P. M. A practical optical character-recognition system. **Electronics and Power**, v. 14, n. 4, p. 149–153, April 1968. ISSN 0013-5127.
- HSIEH, S. L.; HSIAO, Y. J.; HUANG, Y. R. Using margin information to detect regions of interest in images. In: **Systems, Man, and Cybernetics (SMC), 2011 IEEE International Conference on**. [S.l.: s.n.], 2011. p. 3392–3396. ISSN 1062-922X.
- HU, M.; LIU, Z.; ZHANG, J.; ZHANG, G. Robust object tracking via multi-cue fusion. **Signal Processing**, v. 139, p. 86 – 95, 2017. ISSN 0165-1684. Available at: <<http://www.sciencedirect.com/science/article/pii/S0165168417301366>>.
- HUANG, G. B.; ZHOU, H.; DING, X.; ZHANG, R. Extreme learning machine for regression and multiclass classification. **IEEE Transactions on Systems, Man, and Cybernetics, Part B (Cybernetics)**, v. 42, n. 2, p. 513–529, April 2012. ISSN 1083-4419.
- HUANG, G.-B.; ZHU, Q.-Y.; SIEW, C.-K. Extreme learning machine: a new learning scheme of feedforward neural networks. In: **2004 IEEE International Joint Conference on Neural Networks (IEEE Cat. No.04CH37541)**. [S.l.: s.n.], 2004. v. 2, p. 985–990 vol.2. ISSN 1098-7576.
- JIANG, G.; QUAN, L. Detection of concentric circles for camera calibration. In: **Tenth IEEE International Conference on Computer Vision (ICCV'05) Volume 1**. [S.l.: s.n.], 2005. v. 1, p. 333–340 Vol. 1. ISSN 1550-5499.
- KANG, D.-J.; LEE, W.-H. Automatic circle pattern extraction and camera calibration using fast adaptive binarization and plane homography. **International Journal of Precision Engineering and Manufacturing**, v. 11, n. 1, p. 13–21, 2010. ISSN 2005-4602. Available at: <<http://dx.doi.org/10.1007/s12541-010-0002-7>>.
- KANG, J.-E. H. D.-J.; JEONG, M.-H. Detection of calibration patterns for camera calibration with irregular lighting and complicated backgrounds. **International Journal of Control, Automation, and Systems**, v. 6, n. 5, p. 746–754, 2008.

- KHAN, D.; ULLAH, S.; RABBI, I. Factors affecting the design and tracking of {ARToolKit} markers. **Computer Standards & Interfaces**, v. 41, p. 56 – 66, 2015. ISSN 0920-5489. Available at: <<http://www.sciencedirect.com/science/article/pii/S0920548915000227>>.
- KHRONOS GROUP. **The OpenCL Specification Version 2.0**. 2013. Available at: <<http://www.khronos.org>>. Accessed 09 Sep 2016.
- KIM, J.; LEE, S. Extracting major lines by recruiting zero-threshold canny edge links along sobel highlights. **IEEE Signal Processing Letters**, v. 22, n. 10, p. 1689–1692, Oct 2015. ISSN 1070-9908.
- LAKHANI, K.; MINOCHA, B.; GUGNANI, N. Analyzing edge detection techniques for feature extraction in dental radiographs. **Perspectives in Science**, p. –, 2016. ISSN 2213-0209. Available at: <<http://www.sciencedirect.com/science/article/pii/S2213020916301094>>.
- LEIMER, J. Design factors in the development of an optical character recognition machine. **IRE Transactions on Information Theory**, v. 8, n. 2, p. 167–171, February 1962. ISSN 0096-1000.
- LIU, X.; DOERMANN, D.; LI, H.; LEE, K. C.; OZDEMIR, H.; LIU, L. **A Novel 2D Marker Design and Application for Object Tracking and Event Detection**. Berlin, Heidelberg: Springer Berlin Heidelberg, 2008. 248–257 p. ISBN 978-3-540-89639-5. Available at: <http://dx.doi.org/10.1007/978-3-540-89639-5_24>.
- LU, H.; FENG, X.; LI, X.; ZHANG, L. Superpixel level object recognition under local learning framework. **Neurocomputing**, v. 120, p. 203 – 213, 2013. ISSN 0925-2312. Image Feature Detection and Description. Available at: <<http://www.sciencedirect.com/science/article/pii/S0925231213002993>>.
- LUCAS, B. D.; KANADE, T. An iterative image registration technique with an application to stereo vision. In: **Proceedings of the 7th International Joint Conference on Artificial Intelligence - Volume 2**. San Francisco, CA, USA: Morgan Kaufmann Publishers Inc., 1981. (IJCAI'81), p. 674–679. Available at: <<http://dl.acm.org/citation.cfm?id=1623264.1623280>>.
- MAINI, R.; AGGARWAL, H. Study and comparison of various image edge detection techniques. **International Journal of Image Processing**, v. 3, n. 1, February 2009.
- MANDUCHI, R. Mobile vision as assistive technology for the blind: An experimental study. In: _____. **Computers Helping People with Special Needs: 13th International Conference, ICCHP 2012, Linz, Austria, July 11-13, 2012, Proceedings, Part II**. Berlin, Heidelberg: Springer Berlin Heidelberg, 2012. p. 9–16. ISBN 978-3-642-31534-3. Available at: <http://dx.doi.org/10.1007/978-3-642-31534-3_2>.
- 2 - construction. In: MCALLISTER, E. (Ed.). **Pipeline Rules of Thumb Handbook (Eighth Edition)**. Eighth edition. Boston: Gulf Professional Publishing, 2014. p. 43 – 91. ISBN 978-0-12-387693-5. Available at: <<http://www.sciencedirect.com/science/article/pii/B9780123876935000024>>.

- MONTGOMERY, D. C. **Design and Analysis of Experiments.** [S.l.]: John Wiley & Sons, 2006. ISBN 0470088109.
- MOSQUEIRA, G.; APETZ, J.; SANTOS, K.; VILLANI, E.; SUTERIO, R.; TRABASSO, L. Analysis of the indoor {GPS} system as feedback for the robotic alignment of fuselages using laser radar measurements as comparison. **Robotics and Computer-Integrated Manufacturing**, v. 28, n. 6, p. 700 – 709, 2012. ISSN 0736-5845. Available at: <<http://www.sciencedirect.com/science/article/pii/S0736584512000373>>.
- MUELNER, J. E.; WANG, Z.; MARTIN, O.; JAMSHIDI, J.; MAROPOULOS, P. G. Verification of the indoor gps system, by comparison with calibrated coordinates and by angular reference. **Journal of Intelligent Manufacturing**, v. 23, n. 6, p. 2323–2331, 2012. ISSN 1572-8145. Available at: <<http://dx.doi.org/10.1007/s10845-010-0488-y>>.
- MURALIKRISHNAN, B.; PHILLIPS, S.; SAWYER, D. Laser trackers for large-scale dimensional metrology: A review. **Precision Engineering**, v. 44, p. 13 – 28, 2016. ISSN 0141-6359. Available at: <<http://www.sciencedirect.com/science/article/pii/S0141635915002202>>.
- NVIDIA. **NVIDIA OpenCL Best Practices Guide Version 1.0.** [S.l.], 2009. Available at: <http://www.nvidia.com/content/cudazone/CUDABrowser/downloads/papers/NVIDIA_OpenCL_BestPracticesGuide.pdf>. Accessed 23 Aug 2016.
- NVIDIA. **GeForce > Hardware > Desktop GPUs > GeForce GTX 780 Ti.** 2012. Available at: <<http://www.geforce.com/hardware/desktop-gpus/geforce-gtx-780-ti/specifications>>. Accessed 09 Sep 2016.
- NVIDIA. **NVIDIA’s Next Generation CUDA Compute Architecture: Kepler GK110.** 2012. Available at: <<http://www.nvidia.com/content/PDF/kepler/NVIDIA-Kepler-GK110-Architecture-Whitepaper.pdf>>. Accessed 08 Sep 2016.
- NVIDIA. **How to Access Global Memory Efficiently in CUDA C/C++ Kernels.** 2013. Available at: <<https://devblogs.nvidia.com/parallelforall/how-access-global-memory-efficiently-cuda-c-kernels/>>. Accessed 10 Oct 2016.
- OMAR, T.; NEHDI, M. L. Data acquisition technologies for construction progress tracking. **Automation in Construction**, v. 70, p. 143 – 155, 2016. ISSN 0926-5805. Available at: <<http://www.sciencedirect.com/science/article/pii/S0926580516301376>>.
- PETROBRAS. **Guia Técnico Ilustrado de Construção e Montagem (Petrobras’ Illustrated Technical Guide for C&A).** 2016. Available at: <[Petrobras Internal Network](http://Petrobras%20Internal%20Network)>. Accessed 05 Sep 2016.
- PETRÓLEO BRASILEIRO SA. **Petrobras Pre-sal: Perguntas e Respostas.** 2013. Available at: <<http://www.petrobras.com.br/pt/nossas-atividades/tecnologia-e-inovacao/>>. Accessed 13 Dec 2013.

PETRÓLEO BRASILEIRO SA. **Pré-sal**. 2016. Available at: <<http://www.petrobras.com.br/pt/nossas-atividades/areas-de-atuacao/exploracao-e-producao-de-petroleo-e-gas/pre-sal/>>. Accessed 04 Sep 2016.

PHARR, M.; HUMPHREYS, G. Chapter sixteen - light transport ii: Volume rendering. In: PHARR, M.; HUMPHREYS, G. (Ed.). **Physically Based Rendering (Second Edition)**. Second edition. Boston: Morgan Kaufmann, 2010. p. 872 – 922. ISBN 978-0-12-375079-2. Available at: <<http://www.sciencedirect.com/science/article/pii/B9780123750792500160>>.

POGOZHEV, A. V.; TSKITISHVILI, E. O.; MATROSOV, Y. I.; KLYUKVIN, M. B.; MATROSOV, M. Y.; KONOVALOV, G. N. Experience of using accelerated cooling in production of steel x70 plate for the central asia – china gas pipeline. **Metallurgist**, v. 57, n. 3, p. 215–220, 2013. ISSN 1573-8892. Available at: <<http://dx.doi.org/10.1007/s11015-013-9715-z>>.

QADRI, M. T.; ASIF, M. Automatic number plate recognition system for vehicle identification using optical character recognition. In: **2009 International Conference on Education Technology and Computer**. [S.l.: s.n.], 2009. p. 335–338. ISSN 2155-1812.

RAMANATHAN, R.; PONMATHAVAN, S.; VALLIAPPAN, N.; THANESHWARAN, L.; NAIR, A.; SOMAN, K. Optical character recognition for english and tamil using support vector machines. **Advances in Computing, Control, & Telecommunication Technologies, 2009. ACT '09. International Conference on**, p. 610–612, December 2009.

RAZALI, M. R. M.; AHMAD, N. S.; HASSAN, R.; ZAKI, Z. M.; ISMAIL, W. Sobel and canny edges segmentations for the dental age assessment. In: **Computer Assisted System in Health (CASH), 2014 International Conference on**. [S.l.: s.n.], 2014. p. 62–66.

RUFLI, M.; SCARAMUZZA, D.; SIEGWART, R. Automatic detection of checkerboards on blurred and distorted images. In: **2008 IEEE/RSJ International Conference on Intelligent Robots and Systems**. [S.l.: s.n.], 2008. p. 3121–3126. ISSN 2153-0858.

SÁNCHEZ-FERREIRA, C.; MORI, J. Y.; FARIAS, M. C. Q.; LLANOS, C. H. A real-time stereo vision system for distance measurement and underwater image restoration. **Journal of the Brazilian Society of Mechanical Sciences and Engineering**, p. 1–11, 2016. ISSN 1806-3691. Available at: <<http://dx.doi.org/10.1007/s40430-016-0596-5>>.

SANDUJA, V.; PATIAL, R. Article: Sobel edge detection using parallel architecture based on fpga. **International Journal of Applied Information Systems**, v. 3, n. 4, p. 20–24, July 2012. Published by Foundation of Computer Science, New York, USA.

SCHMITT, R.; NISCH, S.; SCHÖNBERG, A.; DEMEESTER, F.; RENDERS, S. Performance evaluation of igps for industrial applications. In: **Indoor Positioning and Indoor Navigation (IPIN), 2010 International Conference on**. [S.l.: s.n.], 2010. p. 1–8.

- SCHWENDEMANN, J.; MÜLLER, T.; KRAUTSCHNEIDER, R. Indoor navigation of machines and measuring devices with igps. In: **Indoor Positioning and Indoor Navigation (IPIN), 2010 International Conference on**. [S.l.: s.n.], 2010. p. 1–8.
- SUDATHAM, W.; MATSUMOTO, H.; TAKAHASHI, S.; TAKAMASU, K. Non-contact measurement technique for dimensional metrology using optical comb. **Measurement**, v. 78, p. 381 – 387, 2016. ISSN 0263-2241. Available at: <<http://www.sciencedirect.com/science/article/pii/S0263224115004030>>.
- TASLI, H. E.; SICRE, R.; GEVERS, T. Superpixel based mid-level image description for image recognition. **Journal of Visual Communication and Image Representation**, v. 33, p. 301 – 308, 2015. ISSN 1047-3203. Available at: <<http://www.sciencedirect.com/science/article/pii/S1047320315001911>>.
- TILOS. **Tilos Linear Project Samples**. 2016. Available at: <<http://www.tilos.org/tilos-samples.html>>. Accessed 05 Sep 2016.
- TRANSPETRO. **TRANSPETRO - Portal Internet**. 2016. Available at: <<http://www.transpetro.com.br>>. Accessed 05 Sep 2016.
- UTAMININGRUM, F.; UCHIMURA, K.; KOUTAKI, G. High density impulse noise removal based on linear mean-median filter. In: **Frontiers of Computer Vision, (FCV), 2013 19th Korea-Japan Joint Workshop on**. [S.l.: s.n.], 2013. p. 11–17.
- VERMA, K.; SINGH, B. K.; THOKE, A. An enhancement in adaptive median filter for edge preservation. **Procedia Computer Science**, v. 48, p. 29 – 36, 2015. ISSN 1877-0509. International Conference on Computer, Communication and Convergence (ICCC 2015). Available at: <<http://www.sciencedirect.com/science/article/pii/S1877050915006158>>.
- VIOLA, P.; JONES, M. Rapid object detection using a boosted cascade of simple features. In: **Computer Vision and Pattern Recognition, 2001. CVPR 2001. Proceedings of the 2001 IEEE Computer Society Conference on**. [S.l.: s.n.], 2001. v. 1, p. I-511–I-518 vol.1. ISSN 1063-6919.
- WANG, H.; GE, H. Object tracking via inverse sparse representation and convolutional networks. **Optik - International Journal for Light and Electron Optics**, v. 138, p. 68 – 79, 2017. ISSN 0030-4026. Available at: <<http://www.sciencedirect.com/science/article/pii/S0030402617302528>>.
- WANG, H.; LI, S. Z.; WANG, Y. Face recognition under varying lighting conditions using self quotient image. In: **Automatic Face and Gesture Recognition, 2004. Proceedings. Sixth IEEE International Conference on**. [S.l.: s.n.], 2004. p. 819–824.
- WANG, J.; ZHU, H.; YU, S.; FAN, C. Object tracking using color-feature guided network generalization and tailored feature fusion. **Neurocomputing**, v. 238, p. 387 – 398, 2017. ISSN 0925-2312. Available at: <<http://www.sciencedirect.com/science/article/pii/S0925231217302667>>.
- WU, S.; LI, X.; LU, X. Robust object tracking via diverse templates. In: **2016 International Conference on Computer, Information and Telecommunication Systems (CITS)**. [S.l.: s.n.], 2016. p. 1–5.

- XU, Y.; FANG, G.; LV, N.; CHEN, S.; ZOU, J. J. Computer vision technology for seam tracking in robotic {GTAW} and {GMAW}. **Robotics and Computer-Integrated Manufacturing**, v. 32, p. 25 – 36, 2015. ISSN 0736-5845. Available at: <<http://www.sciencedirect.com/science/article/pii/S0736584514000775>>.
- YING, N.; KIM, W. Use of dual euler angles to quantify the three-dimensional joint motion and its application to the ankle joint complex. **Journal of Biomechanics**, v. 35, n. 12, p. 1647 – 1657, 2002. ISSN 0021-9290. Available at: <<http://www.sciencedirect.com/science/article/pii/S0021929002002415>>.
- ZHANG, L.; VERMA, B. Class-semantic textons with superpixel neighborhoods for natural roadside vegetation classification. In: **Digital Image Computing: Techniques and Applications (DICTA), 2015 International Conference on**. [S.l.: s.n.], 2015. p. 1–8.
- ZHANG, P.; ZHUO, T.; XIE, L.; ZHANG, Y. Deformable object tracking with spatiotemporal segmentation in big vision surveillance. **Neurocomputing**, v. 204, p. 87 – 96, 2016. ISSN 0925-2312. Big Learning in Social Media AnalyticsContaining a selection of papers from the 2014 International Conference on Security, Pattern Analysis, and Cybernetics (ICSPAC2014). Available at: <<http://www.sciencedirect.com/science/article/pii/S0925231216300996>>.
- ZHANG, Z. A flexible new technique for camera calibration. **IEEE Transactions on Pattern Analysis and Machine Intelligence**, v. 22, n. 11, p. 1330–1334, Nov 2000. ISSN 0162-8828.
- ZHOU, R.; JIANG, Y.; LU, D.; ZHOU, R.; LI, Z. Development and characterization of a wear resistant bainite/martensite ductile iron by combination of alloying and a controlled cooling heat-treatment. **Wear**, v. 250, n. 1 - 12, p. 529 – 534, 2001. ISSN 0043-1648. 13th International Conference on Wear of Materials. Available at: <<http://www.sciencedirect.com/science/article/pii/S0043164801006032>>.

Appendix A - Identification Pictures and Results

A.1 Identification Pictures

Multiple pictures were taken with different cameras, in different environments and perspective settings, as described in Section 5.2. Figures A.1 to A.3 show thumbnails of sample pictures. ANOVA results showed that the sample size of 90 pictures, containing 4 checkerboards and 2 targets each, was statistically representative to determine important parameters in OMR under tested settings.

Processed images were manually analyzed to determine perspective and lighting parameters, as well as verify false positives and negatives. The methodology is expected to correctly identify 4 checkerboards and 2 targets in each picture, along with dimensions and colors.

Images were manually analyzed to determine perspective and lighting parameters, as well as verify false positives and negatives. The software generated graphics on top of the images to enable analyses. True and false positives and negatives were manually identified in each picture to generate data for ANOVA. Figures A.4 to A.7 demonstrate how performance data was extracted.

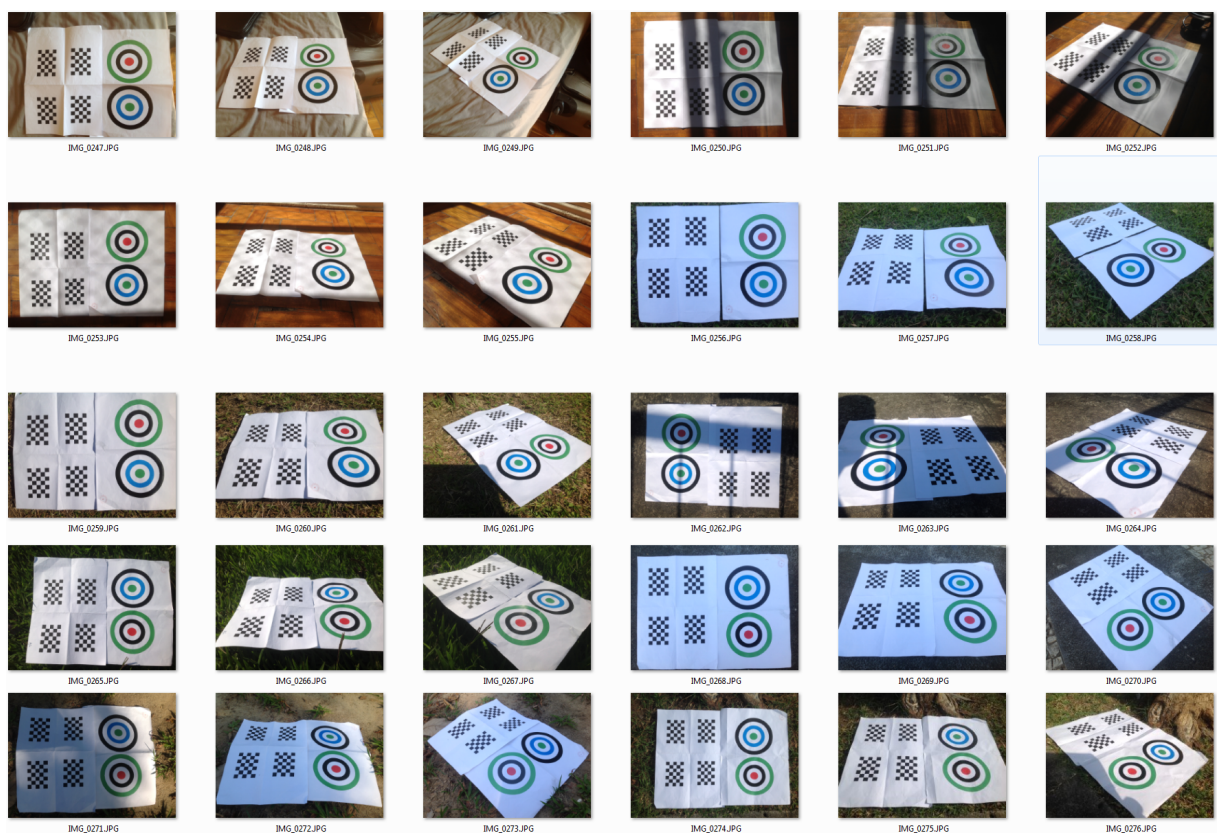


FIGURE A.1 – Test pictures thumbnails: Apple iPad 3 camera.



FIGURE A.2 – Test pictures thumbnails: Fuji W1 3D camera.

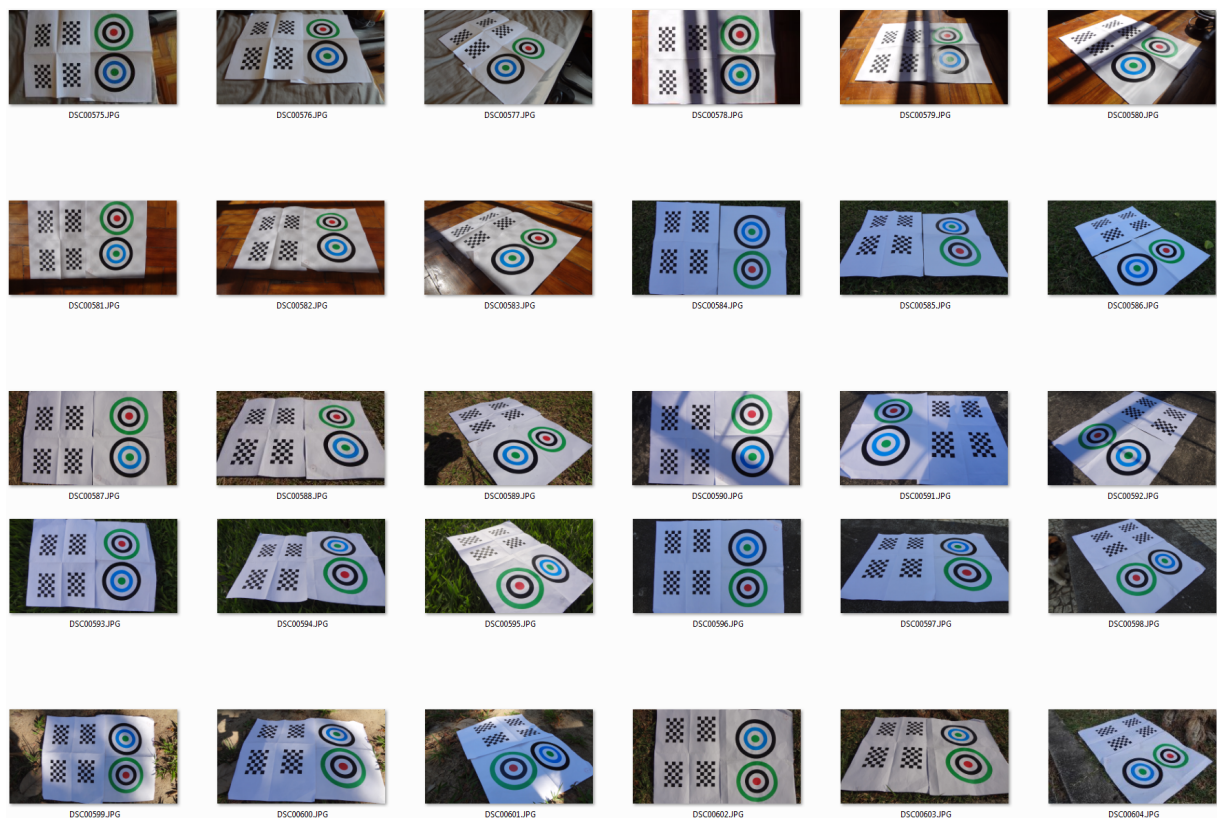


FIGURE A.3 – Test pictures thumbnails: Sony Cybershot DSC-WX7.

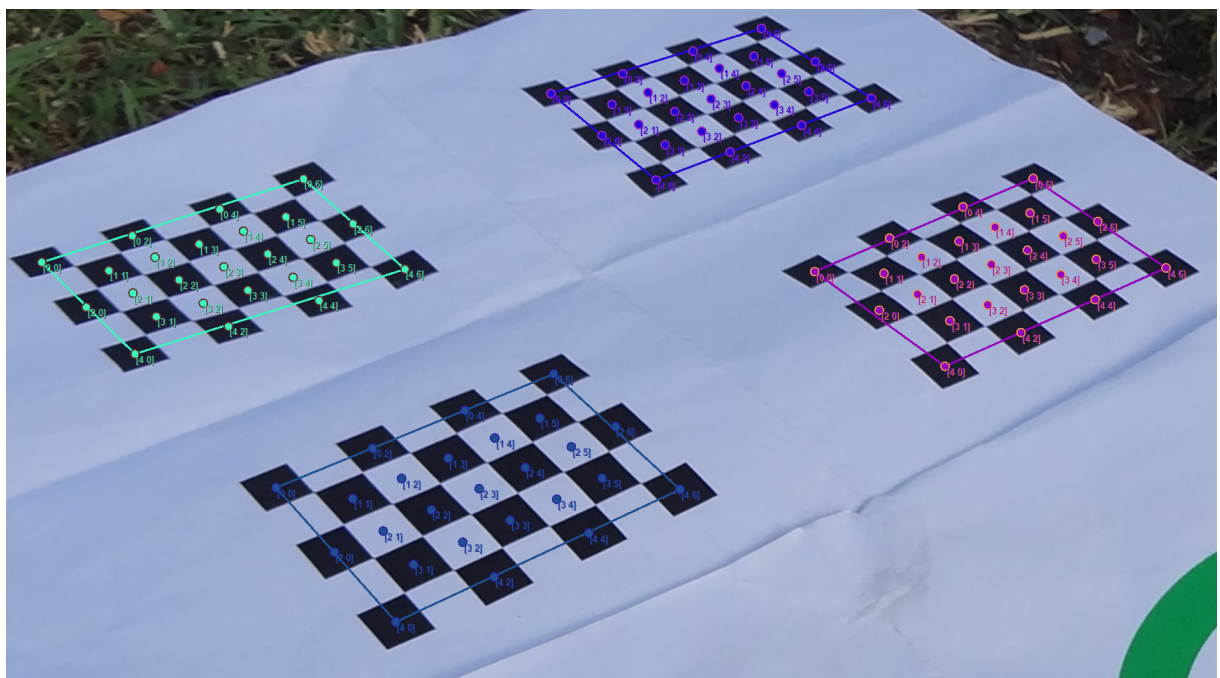


FIGURE A.4 – Detail of checkerboard true positive.



FIGURE A.5 – Detail of target true positive. Notice both target identification and color sequence labels are correct.

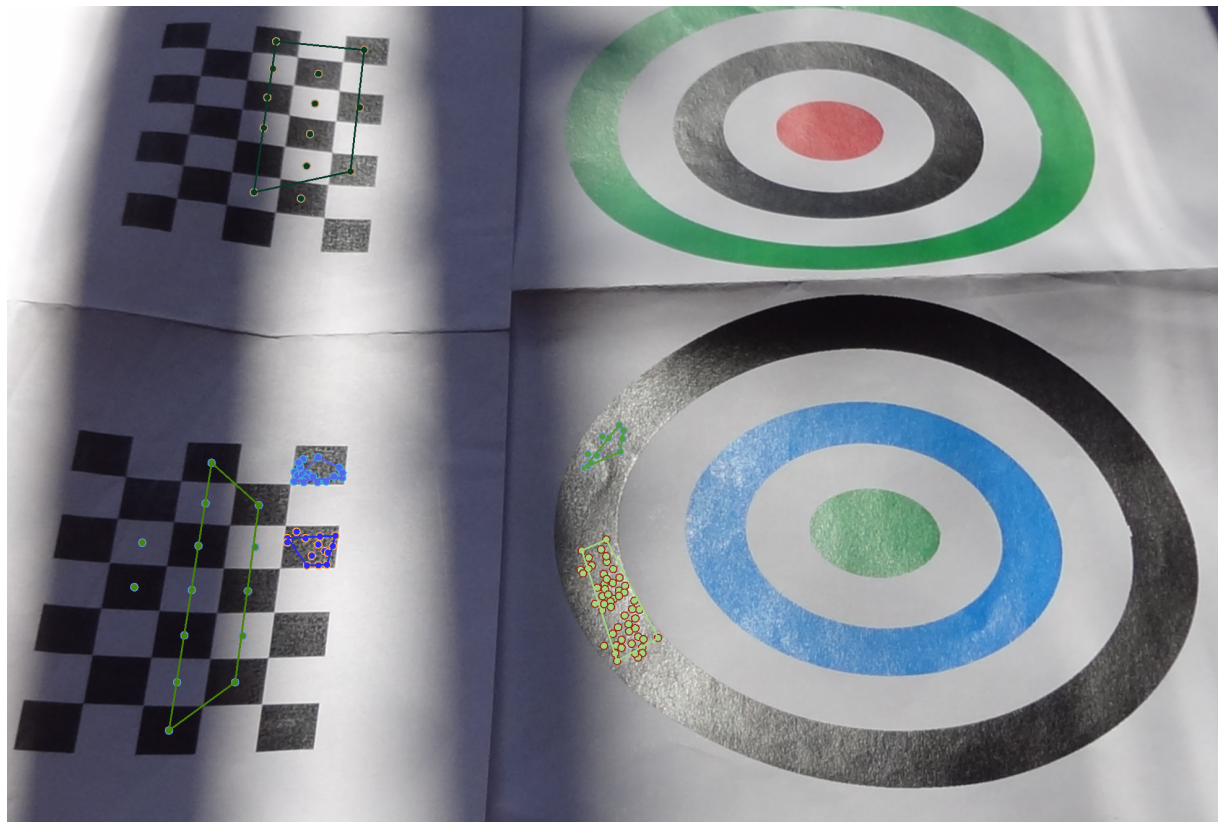


FIGURE A.6 – Detail of checkerboard and target false negative.

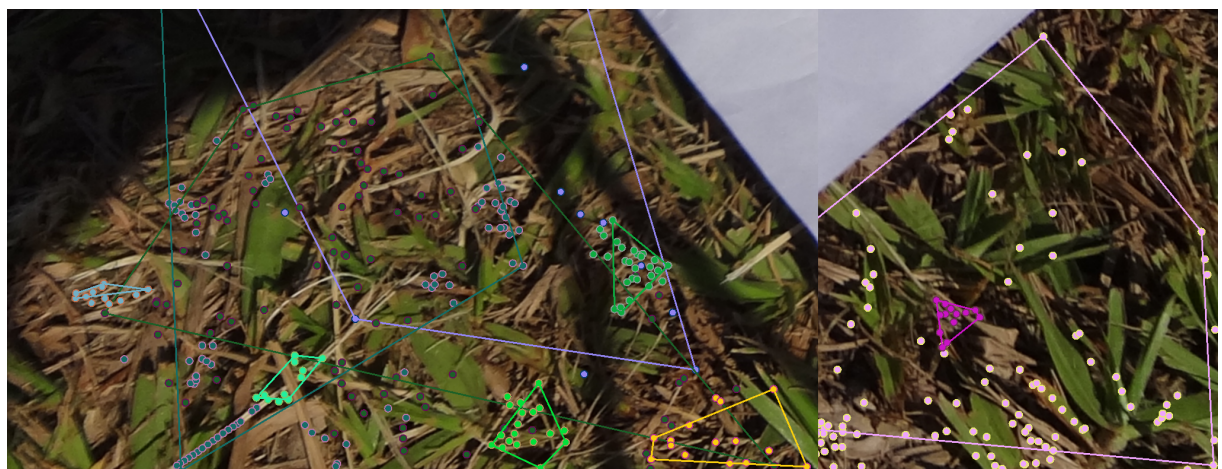


FIGURE A.7 – Detail of cluttered regions that may be identified as checkerboards. Limiting the methodology to only search for checkerboards with 5x7 number of squares solves this issue.

FOLHA DE REGISTRO DO DOCUMENTO

1. CLASSIFICAÇÃO/TIPO TD	2. DATA 12 de junho de 2017	3. DOCUMENTO No. DCTA/ITA/TD-009/2017	4. No. DE PÁGINAS 122
5. TÍTULO E SUBTÍTULO: A Methodology for Robust Optical Marker Recognition in Outdoor Environments			
6. AUTOR(ES): Douglas Coimbra de Andrade			
7. INSTITUIÇÃO(ÓES)/ÓRGÃO(S) INTERNO(S)/DIVISÃO(ÓES): Instituto Tecnológico de Aeronáutica – Divisão de Engenharia Mecânica – ITA/IEM			
8. PALAVRAS-CHAVE SUGERIDAS PELO AUTOR: Optical Mark Recognition; Computer Vision; OpenCL; Heterogeneous Computing			
9. PALAVRAS-CHAVE RESULTANTES DE INDEXAÇÃO: Sistemas ópticos; Visão por computadores; Sistemas homem-máquina; Rastreamento (posição); Computação			
10. APRESENTAÇÃO: <input checked="" type="checkbox"/> Nacional <input type="checkbox"/> Internacional ITA, São José dos Campos. Curso de Doutorado. Programa de Pós-Graduação em Engenharia Aeronáutica e Mecânica. Área de Sistemas Aeroespaciais e Mecatrônica. Orientador: Prof. Dr. Luís Gonzaga Trabasso. Defesa em 09/06/2017. Publicada em 2017.			
11. RESUMO: <p>Large industrial equipments, such as storage tanks, pipelines, and pressure vessels, are essential for the energy infrastructure of any country. Particularly in Brazil, in view of the large amounts of oil and gas expected to be extracted from the pre-salt layer, it will be necessary to build new ships and platforms and, in turn, many of these equipments. Unlike vehicle production factories, the assembly line is the one that moves and not the final product.</p> <p>Current construction and assembly (C&A) methods use mostly manual labor to identify, recognize and track objects, which results in exposure of personnel to risk. The use of robotics is expected to improve current construction processes which, for the most part, rely on positioning procedures that require operators.</p> <p>This work presents a robust methodology for optical marker recognition (OMR) in outdoor environments with regards to lighting, partial occlusion, camera brand and perspective. Optical markers are a cheap technique which, coupled with computer vision systems, can provide position feedback for robotic systems. This tool can be used to automate tracking of position and orientation of large components, such as plates, beams, valves and tubes using optical markers and camera systems. Its implementation should result in cost, time and rework reduction through better tracking and positioning of these components, as well as reduced exposure of personnel to hazardous situations.</p>			
12. GRAU DE SIGILO: <input checked="" type="checkbox"/> OSTENSIVO <input type="checkbox"/> RESERVADO <input type="checkbox"/> CONFIDENCIAL <input type="checkbox"/> SECRETO			